

Membrane Emulsification: Droplet Formation and Effects of Interfacial Tension

Promotor

Prof. dr. ir. R.M. Boom

Hoogleraar Levensmiddelenproceskunde, Wageningen Universiteit

Co-promotoren

Dr. ir. C.G.P.H. Schroën

Universitair docent, Sectie Proceskunde, Wageningen Universiteit

Dr. ir. R.G.M. van der Sman

Universitair docent, Sectie Proceskunde, Wageningen Universiteit

Promotiecommissie

Prof. dr. M.A. Cohen Stuart

Wageningen Universiteit

Dr. J.J.M. Janssen

Unilever R&D Vlaardingen

Prof. dr. ing. M. Wessling

Universiteit Twente

Prof. dr. J.M. Yeomans

University of Oxford, England

Dit onderzoek is uitgevoerd binnen de onderzoeksschool VLAG.

Sandra van der Graaf

Membrane Emulsification: Droplet Formation and Effects of Interfacial Tension

Membraanemulgeren: druppelvorming
en grensvlakspanningseffecten

Proefschrift
ter verkrijging van de graad van doctor
op gezag van de rector magnificus
van Wageningen Universiteit,
Prof. dr. M.J. Kropff,
in het openbaar te verdedigen
op vrijdag 10 februari 2006
des namiddags te vier uur in de Aula.

Sandra van der Graaf

Membrane Emulsification: Droplet Formation and Effects of Interfacial Tension

Thesis Wageningen University, The Netherlands, 2006 - with summary in Dutch

ISBN 90-8504-348-4

Contents

1	Introduction	7
2	Influence of interfacial tension on droplet formation with microsieves	17
3	Droplet formation in a T-shaped microchannel junction	39
4	Lattice Boltzmann simulations of droplet formation in a T-shaped microchannel	65
5	Diffuse interface model of surfactant adsorption onto flat and droplet interfaces	93
6	Preparation of double emulsions with membrane emulsifi- cation	111
7	Discussion	133
	Summary	145
	Samenvatting	149
	Nawoord	153
	List of publications	155
	Overview of training activities	157
	Curriculum Vitae	159

Chapter 1

Introduction

Emulsions

Emulsions are widely used for the production of food, cosmetics and pharmaceutical products. One can discern both water-in-oil (W/O) emulsions, in which the dispersed phase is water, and oil-in-water (O/W) emulsions, in which the dispersed phase is oil. Depending on the emulsification process, the diameter of the droplets varies between $0.1\ \mu\text{m}$ and $0.1\ \text{mm}$. Emulsions of this kind are normally thermodynamically unstable. This means that there is a tendency to reduce the phase interface, causing the droplets to coalesce. In contrast to dispersed systems of this kind, which are also known as macro-emulsions, thermodynamically stable emulsions, so-called micro-emulsions, do exist. The formation of micro-emulsions may occur spontaneously and the droplet diameter of micro-emulsions lies in the range of 10 to 200 nm [1]. In this thesis only macro-emulsions are considered for which the term 'emulsion' will be used. To produce 'stable' emulsions, a third component, a surfactant or emulsifier, is needed to stabilize the oil-water interface.

Besides simple emulsions, also double emulsions exist. A double emulsion is an emulsion in an emulsion. Two main types of double emulsions can be distinguished: water-in-oil-in-water (W/O/W) emulsions, in which a W/O emulsion is dispersed as droplets in an aqueous phase, and oil-in-water-in-oil (O/W/O) emulsions, in which an O/W emulsion is dispersed in an oil phase. W/O/W emulsions are more common than O/W/O emulsions. Double emulsions contain more interface and are even more thermodynamically unstable than simple emulsions. Four components are needed to produce stable double emulsions: oil, water, oil-soluble surfactant and water-soluble surfactant.

With conventional methods to produce emulsions, like rotor-stator systems and high-pressure homogenizers, large pressure gradients are applied to obtain high shear rates. Most of the energy put into the product is dissipated as heat [2]. Besides, it is difficult if not impossible to fine-tune the process to make emulsions of a specified size and with low polydispersity. Producing double emulsions is even more complicated because at high shear rates the inner droplets will coalesce with the outer phase; thus the inner phase is destroyed during the preparation of the outer emulsion.

Membrane emulsification

Since about 15 years a new method to produce emulsions is known, membrane emulsification [3 – 8]. In this method the to-be-dispersed phase is pressed through a porous membrane (or a micro-structure), and emerges at the low-pressure side as droplets. Advantages of this process, compared to traditional methods to produce emulsions, are the low energy consumption, control of droplet size and droplet size distribution and the low shear stresses that are needed.

For membrane emulsification three distinct methods of operation are used, pre-mix membrane emulsification, microchannel emulsification and the most studied form, cross-flow membrane emulsification (see figure 1.1). In pre-mix membrane emulsification [9], first a coarse pre-mix is made which is subsequently pushed through a membrane. Upon passage of the coarse droplets through the membrane they break up into finer droplets. The resulting droplet size distribution is usually somewhat wider than those obtained with cross-flow membrane emulsification, however, much higher fluxes can be obtained and also higher dispersed phase fractions.

Microchannel emulsification [10] is a novel method for producing monodisperse emulsions (even more monodisperse than with pre-mix or cross-flow membrane emulsification). A silicon microchannel plate, fabricated with micromachining technology, is used and droplets are produced by forcing the to-be-dispersed phase through the microchannels. The droplet size is precisely regulated by the geometry of the microchannel. Microchannel emulsification exploits the interfacial tension (σ_{ow}), a large force on micrometer scale, as the driving force for droplet formation [11]. The to-be-dispersed phase is forced to assume a distorted (elongated) disk-like shape on the terrace in the microchannel. This distorted shape has at least one smaller radius of curvature than a spherical shape that the droplet can take

in the well, resulting in a higher Laplace pressure and a driving force for spontaneous droplet formation. Therefore the droplets are formed without shear from continuous phase flow. Spontaneous droplet detachment can be scaled up by using a relatively thick membrane (or microdevice) with slit shaped pores, which is called straight-through microchannel emulsification [12].



Figure 1.1: Overview of different methods of membrane emulsification: pre-mix membrane emulsification (a), microchannel emulsification (b), and cross-flow membrane emulsification (c).

In cross-flow membrane emulsification the to-be-dispersed phase is pressed through the pores of a microporous membrane while the continuous phase flows along the membrane surface. Droplets grow at pores until, upon reaching a certain size, they detach. This is determined by the balance between the different forces acting on the droplet. It is important that the membrane or micro-structure is and remains wetted by the continuous phase for proper droplet formation and droplet detachment. Abrahamse *et al.* [13] showed that interconnected pores will interact strongly, and thus will further complicate the droplet formation process. In this study, we therefore studied droplet formation on a model system with just one pore. Figure 1.2 schematically shows three categories of parameters that influence cross-flow membrane emulsification: properties of the ingredients, process conditions and membrane properties. In this thesis we mainly focus on the influence of a parameter of the ingredients, namely the surfactant type and concentration (that influences the interfacial tension). In the next chapters of this thesis we will often use the shorter term 'membrane emulsification' for cross-flow membrane emulsification.

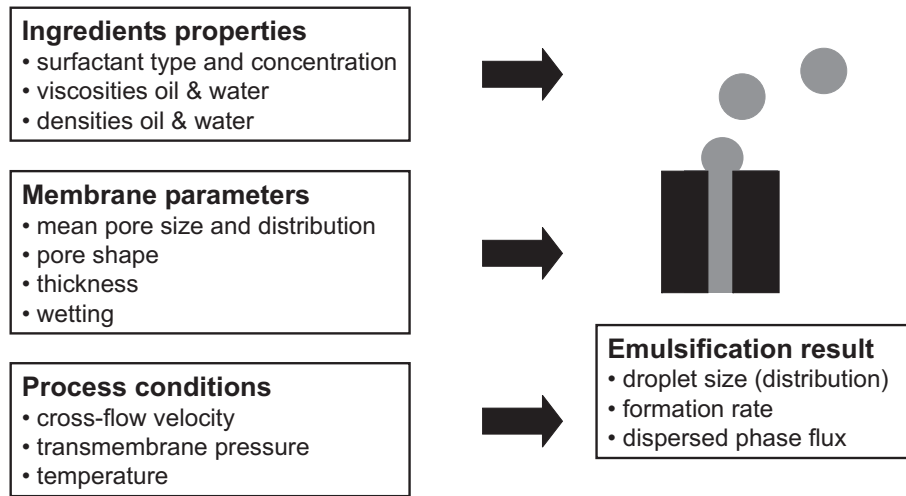


Figure 1.2: Parameters in membrane emulsification influencing the droplet formation process, adapted from [13].

Surfactants

Surfactants are essential components in an emulsion, because they stabilize the oil-water interface. Surfactants (surface active agents) consist of one or more hydrophilic head groups and one or more hydrophobic (or lipophilic) tails. Due to their amphiphilic structure, surfactants have a tendency to accumulate at interfaces, which is called adsorption [14]. Depending on the neutral, negative or positive charge of their head group, surfactants are classified as nonionic, anionic and cationic, respectively. The hydrophilic-lipophilic balance (HLB) describes the balance between the hydrophilic and hydrophobic parts of the surfactant. A low HLB value means that the surfactant is mainly soluble in oil and suitable to stabilize W/O emulsions, while a surfactant with a high HLB value is mainly soluble in water and suitable for the stabilization of O/W emulsions. Surfactants adsorb strongly at the interface and therewith lower the interfacial tension, a contracting force that works on the interface and causes a tendency to make the interface as small as possible. When the shape or size of an interface changes, the loading of surfactants on the interface changes by desorption or adsorption and therewith the value of the interfacial tension. This interfacial tension of an interface that is not in equilibrium is called the 'dynamic interfacial tension', that of an interface in equilibrium is the static value.

Interfacial tension effects and droplet formation

Interfacial tension is relevant for droplet formation from a pore, because a lower interfacial tension means a lower Laplace pressure. When the Laplace pressure is lower, a lower transmembrane pressure is needed for droplet formation.

The interfacial tension is also relevant for the final droplet size of emulsion droplets produced with membrane emulsification. Literature [15] shows that using a high surfactant concentration leads to an emulsion with small droplets and a lower concentration leads to larger droplets. This may be caused by later detachment and thus the formation of larger droplets at the membrane or by coalescence of droplets at the membrane surface or in the bulk. The Peng and Williams force and torque balance models [16] state that for the formation of small droplets in membrane emulsification two forces are important, namely the interfacial tension force which holds the droplet connected to the pore and the drag force which detaches the droplet. Droplet detachment in cross-flow membrane emulsification is thus thought to be dependent on the interfacial tension. During droplet growth the interfacial tension is not constant, because the interfacial area increases and at the same time surfactant molecules diffuse to the interface. Therefore it is difficult to determine the (dynamic) interfacial tension during fast droplet formation processes and the influence of this interfacial tension on droplet detachment and the final droplet size. According to modelling results of Rayner *et al.* [17] the transport of surfactants coupled to the expansion rate of the oil-water interface has a significant effect on the final droplet size. To be able to study this process in more detail experimental model systems are needed.

Besides experimental model systems, numerical modelling can be useful to systematically investigate the influence of different parameters on the droplet formation process and visualize the droplet formation process as was done by Abrahamse *et al.* using CFX [18], by Rayner *et al.* [19] using the Surface Evolver and by Kobayashi *et al.* [20] using CFD-ACE+. We chose for the lattice Boltzmann method with a multiphase model to simulate droplet formation. The advantage of this model is that it is suitable for modelling processes on mesoscale, it has a thermodynamic basis and can be extended to simulate surfactant dynamics.

Aim of the thesis

Experiments with model systems and simulations will help to understand the droplet formation process and the influence of surfactants on it. It is, for example, not clear yet, to what extent surfactants have time to adsorb on the interface and decrease the interfacial tension. Also, the influence of the to-be-dispersed phase flow rate, which may result in higher relative expansion rates and lower surfactant loading, on the final droplet size is not clear. Therefore, the aim of this research is to study the effects of interfacial tension and the forces during droplet formation on the final droplet size in a model system for cross-flow membrane emulsification.

Outline of the thesis

The focus of this thesis is to study droplet formation from a single pore in a cross-flow membrane emulsification system both experimentally (Chapter 2 and 3) and numerically (Chapter 4). In Chapter 2 droplet formation from a microsieve with a single circular pore is studied with a microscope connected to a high speed camera. The interfacial tension for different concentrations surfactant is estimated at high relative expansion rates that occur during droplet formation, based on interfacial tension measurements at lower relative expansion rates. Another model system for droplet formation is a T-shaped microchannel junction in a glass chip of which the results are described in Chapter 3. In this study droplet formation is investigated for different continuous phase systems (ethanol and aqueous solutions with different concentrations of surfactant) and different dispersed phase fluxes. In Chapter 4 the lattice Boltzmann method is introduced as a numerical tool to study droplet formation. For modelling droplet formation a multiphase model was implemented, which is based on a Ginzburg-Landau free-energy approach. The code is benchmarked and a parameter study is presented, in which the influence of the interfacial tension and flow rates on the final droplet size is investigated. In Chapter 5 the lattice Boltzmann model is extended with surfactant adsorption. Two-dimensional simulations of an evolving droplet and surfactant adsorption models are presented. In Chapter 6 a review about the production of double emulsions with membrane emulsification is given. Double emulsions have interesting applications in several industries, however, the production of stable double emulsion with a high encapsulation rate is difficult. Membrane emulsification seems a

promising technique to overcome this difficulty. Finally, in Chapter 7 the results are discussed and some (new) ideas about industrial application are given.

References

1. M.J. Rosen, Surfactants and Interfacial Phenomena, 1989, Wiley, New York.
2. P. Walstra, Physical Chemistry of Foods, 2003, Marcel Dekker Inc., New York·Basel.
3. T. Nakashima, M. Shimizu, M. Kukizaki, Membrane emulsification by microporous glass, *Key Eng. Mater.* 61&62 (1991) 513.
4. S.M. Joscelyne, G. Trägårdh, Membrane emulsification - a literature review, *J. Membr. Sci.* 169 (2000) 107.
5. C. Charcosset, I. Limayem, H. Fessi, The membrane emulsification process - a review, *J. Chem. Technol. Biotechnol.* 79 (2004) 209.
6. U. Lambrich, G.T. Vladisavljevic, Emulgieren mit mikrostrukturierten Systemen, *Chem.-Ing.-Tech.* 76, 4 (2004) 376.
7. A.J. Gijsbertsen-Abrahamse, A. van der Padt, R.M. Boom, Status of cross-flow membrane emulsification and outlook for industrial application, *J. Membr. Sci.* 230 (2004) 149.
8. G.T. Vladisavljevic, R.A. Williams, Recent developments in manufacturing emulsions and particulate products using membranes, *Adv. Colloid Interface Sci.* 113 (2005) 1.
9. K. Suzuki, I. Fujiki, Y. Hagura, Preparation of corn oil/water and water/corn oil emulsions using PTFE membranes, *Food Sci. Technol. Int. Tokyo* 4, 2 (1998) 164.
10. T. Kawakatsu, Y. Kikuchi, M. Nakajima, Regular-sized cell creation in microchannel emulsification by visual microprocessing method, *J. Am. Oil Chem. Soc.* 74, 3 (1997) 317.
11. S. Sugiura, M. Nakajima, S. Iwamoto, M. Seki, Interfacial tension driven monodispersed droplet formation from microfabricated channel array, *Langmuir* 17 (2001) 5562.
12. I. Kobayashi, M. Nakajima, K. Chun, Y. Kikuchi, H. Fujita, Silicon array of elongated through-holes for monodisperse emulsion droplets, *AIChE J.* 48, 8 (2002) 1639.
13. A.J. Abrahamse, R. van Lierop, R.G.M. van der Sman, A. van der Padt, R.M. Boom, Analysis of droplet formation and interactions during cross-flow membrane emulsification, *J. Membr. Sci.* 204 (2002) 125.
14. E. Dickinson, An Introduction to Food Colloids, 1992, Oxford University Press, New York.
15. V. Schröder, O. Behrend, H. Schubert, *J. Colloid Interface Sci.* 202 (1998) 334.
16. S.J. Peng, R.A. Williams, Controlled production of emulsions using a crossflow membrane. Part 1: Droplet formation from a single pore, *Trans IChemE* 76 (1998) 894.
17. M. Rayner, G. Trägårdh, C. Trägårdh, The impact of mass transfer and interfacial expansion rate on droplet size in membrane emulsification processes, *Colloids Surf. A: Physicochem. Eng. Aspects* 266, 1-3 (2005) 1.
18. A.J. Abrahamse, A. van der Padt, R.M. Boom, W.B.C. de Heij, Process fundamentals of membrane emulsification: simulation with CFD, *AIChE J.* 47, 6 (2001) 1285.

19. M. Rayner, G. Trägårdh, C. Trägårdh, P. Dejmek, Using the Surface Evolver to model droplet formation processes in membrane emulsification, *J. Colloid Interface Sci.* 279 (2004) 175.
20. I. Kobayashi, S. Mukataka, M. Nakajima, CFD simulation and analysis of emulsion droplet formation from straight-through microchannels, *Langmuir* 20 (2004) 9868.

Chapter 2

Influence of interfacial tension on droplet formation with microsieves

Abstract

Membrane emulsification is a promising and relatively new technique to produce emulsions. The purpose of this study was to better understand the influence of interfacial tension on droplet formation during membrane emulsification. Droplet formation experiments were carried out with a microengineered membrane; the droplet diameter and droplet formation time were studied as a function of the surfactant concentration in the continuous phase. These experiments confirm that the interfacial tension influences the process of droplet formation; higher surfactant concentrations lead to smaller droplets and shorter droplet formation times (until 10 ms). From drop volume tensiometer experiments we can predict the interfacial tension during droplet formation. However, the strong influence of the rate of flow of the to-be-dispersed phase on the droplet size cannot be explained by the predicted values. This large influence of the oil rate of flow is clarified by the hypothesis that snap-off is rather slow in the studied regime of very fast droplet formation.

This chapter has been published as: S. van der Graaf, C.G.P.H. Schroën, R.G.M. van der Sman, R.M. Boom, Influence of dynamic interfacial tension on droplet formation during membrane emulsification, *Journal of Colloid and Interface Science* 277 (2004) 456-463.

Introduction

The most common basic form of products in the food, cosmetics and pharmaceutical area is an emulsion, a dispersion of two immiscible phases that is stabilized by surface active components. Water-in-oil (W/O) emulsions, in which the dispersed phase is water, and oil-in-water (O/W) emulsions, in which the dispersed phase is oil, can be distinguished. Examples of emulsions are margarine, mayonnaise, sun cream, drug delivery systems, paints.

Traditional devices for producing emulsions are colloid mills, high pressure homogenizers and mixers. Since approximately 10 years ago a new method to produce emulsions has been known: membrane emulsification [1]. A recent review on the research done in this area was published by Joscelyne and Trägårdh [2]. In membrane emulsification the to-be-dispersed phase is pressed through a membrane, while the continuous phase flows across the downstream side of the membrane. Reported advantages of this process are the low energy consumption, the control of droplet size and droplet size distribution, and the low shear stresses that are needed. Parameters that influence membrane emulsification can be divided into three categories: process conditions, properties of the ingredients, and membrane properties.

Most research on membrane emulsification has been done on overall process conditions and the properties of the ingredients by evaluating the final emulsion [3]. This implies that it is not possible to distinguish between properties of the final emulsion that originate from the droplet formation process on the membrane or that are the result of other effects taking place at a later time, e.g. coalescence or further break up of the droplets by a pump [4]. The influence of surfactants on the final emulsion and the droplet break up mechanism is not totally clear. It is observed that using a high concentration of surfactant gives an emulsion with small droplets; a lower concentration leads to larger droplets [5]. This may be due either to the formation of larger droplets at the membrane, or to coalescence of droplets, which may be still attached to the membrane surface or coalesce in the bulk of the emulsion, due to a lack of stability.

Different membranes have been used for the production of emulsions, such as glass membranes [1], ceramic membranes [5] and lately also microsieves [6, 7]. A great advantage of microsieves for membrane emulsification is the uniform pore size of these microengineered membranes, which

have the potential to produce monodisperse emulsions if the droplets do not interact. These interactions were observed in prior research [6] and were found to influence the droplet formation process considerably.

It is clear that the process is influenced by a complex set of phenomena, and moreover, that there is a need to distinguish between the effects of the various phenomena. If this can be established, this will clear the way for better control of the emulsification process as a whole.

In this research we make use of Aquamarijn microsieves with one single pore. In this way it is possible to look at the process of droplet formation from a membrane without the interactions of different pores with each other. To elucidate the influence of surfactants we studied the process of droplet formation at various surfactant concentrations with a microscope connected to a high speed camera. We have further measured the dynamic interfacial tension with a drop volume tensiometer at different surfactant concentrations. The results that were thus obtained were related to the actual dynamic interfacial tension during the experiments. Based on the experimental results, a window of operation for emulsion formation can be constructed that eventually will help to optimize the entire process.

Materials and Methods

Membrane and module

We used a microengineered microsieve, kindly made available by Aquamarijn (Zutphen, The Netherlands) [7], for the droplet formation experiments. This membrane was a tailor-made chip of 4.5 x 4.5 mm made of silicon with a Si_3N_4 coating that contained a single circular pore with a diameter of 4.8 micrometer in the middle of the membrane. Just prior to the experiments, the membrane was treated with air plasma (21% O_2) to clean the surface and render it hydrophilic. The membrane was glued onto a polysulphone membrane holder with araldite glue and this holder was placed in the module. The module is shown in figure 2.1. The module has inlets for the inflow and outflow of the continuous phase. For the to-be-dispersed phase there are also two inlets. During droplet formation experiments only one entrance is used to press the dispersed phase through the membrane. Before the experiment was started the other entrance was used to remove air from the tubing and subsequently pre-wet the bottom side of the membrane with the dispersed phase. The length of the flow

channel was 15.5 cm, the width was 2.4 cm, and the height was 0.5 mm directly above the microsieve.

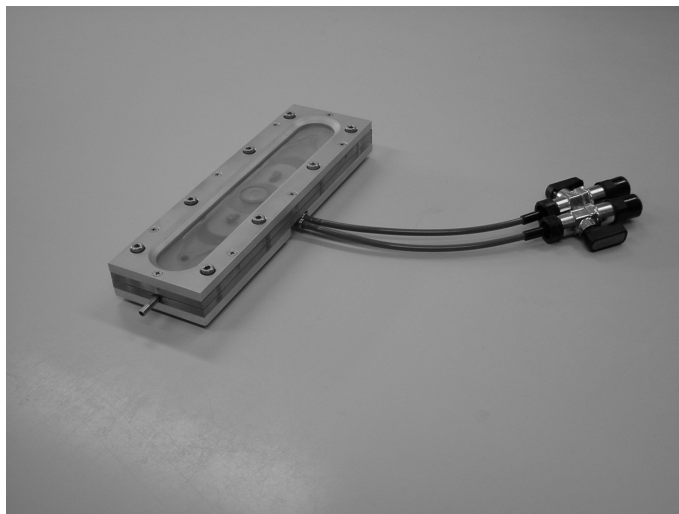


Figure 2.1: The microsieve is placed in this module. The tubing in the middle of the module is for the oil supply.

Chemicals

Tween 20 (polyoxyethylene (20) sorbitan monolaurate, Merck) was dissolved in demineralized water; this solution was used as the continuous phase. For the droplet formation experiments concentrations of 0.1, 0.3, 1, 3, 7 and 10% (w/w) Tween 20 were used. For the drop volume tensiometer experiments, concentrations in the range of 0.0037-12.2% (w/w) ($3 \cdot 10^{-5}$ - $1 \cdot 10^{-1}$ M) were used. The density of Tween 20 is $1100 \text{ kg} \cdot \text{m}^{-3}$ and the molecular weight is $1227.72 \text{ g} \cdot \text{mole}^{-1}$. N-hexadecane (Merck) was used as the dispersed phase. The density of hexadecane is $773 \text{ kg} \cdot \text{m}^{-3}$, the molecular weight $226.44 \text{ g} \cdot \text{mole}^{-1}$ and the dynamic viscosity is $3.34 \cdot 10^{-3} \text{ Pa} \cdot \text{s}$ at 20°C . We measured a value for the interfacial tension (hexadecane-water without added surfactant) of $47 \text{ mN} \cdot \text{m}^{-1}$ at 20°C .

The module and tubing were cleaned with ethanol and demineralized water prior to and between the different experiments.

Experimental setup

The experimental setup is shown in figure 2.2. Nitrogen was used to press the to-be-dispersed phase into the tubing of the module. The pressure of

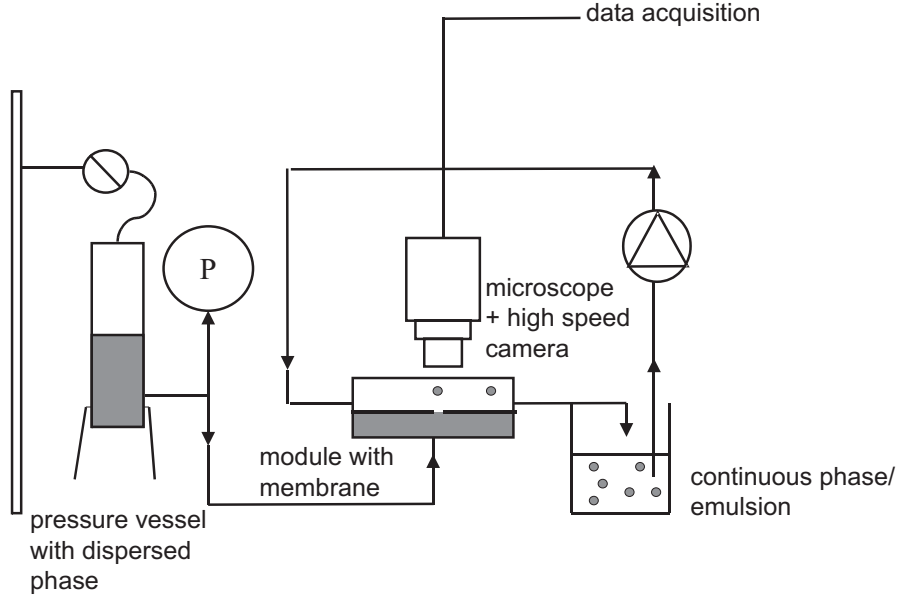


Figure 2.2: Experimental setup for the droplet formation experiments.

the dispersed phase was measured before the liquid entered the module. One series of droplet formation experiments was done at a dispersed phase pressure, p_d , of 0.67 ± 0.02 bar and the other series was done at a pressure of 1.18 ± 0.02 bar. The continuous phase was pumped through the system with a gear pump. The average velocity of the continuous phase, v_c , was $3.4 \text{ m}\cdot\text{s}^{-1}$. This velocity was constant during all experiments to keep the conditions for convective transport of surfactants toward the interface constant. The pressure in the channel above the sieve was calculated for water and has a value of 0.24 bar. With this value the pressure over the membrane, p_{trm} , was calculated: $p_{trm} = p_d - p_c$. This resulted in a transmembrane pressure of 0.43 and 0.94 bar for dispersed phase pressures of 0.67 and 1.18 bar, respectively.

For droplet formation the transmembrane pressure has to exceed at least the critical pressure. The critical Laplace pressure is given by:

$$\Delta p = \frac{2\sigma_{ow}}{r_{dr}} = \frac{2\sigma_{ow}}{r_p}, \quad (2.1)$$

with Δp the Laplace pressure, σ_{ow} the interfacial tension, r_{dr} the radius of the droplet and r_p the radius of the pore. The critical pressure is the pressure at which droplet formation starts. This means that the initial

radius of the droplet is equal to the radius of the pore, r_p . Upon exceeding the critical pressure, the droplet will grow further.

The interfacial tension is a function of the surfactant adsorption rate and kinetics on an expanding interface. Therefore, it is not possible to pinpoint one value of the critical Laplace pressure. However, it is possible to calculate the maximum value of the critical Laplace pressure from the value of an interface with no surfactants, namely $47 \text{ mN}\cdot\text{m}^{-1}$. This results in a Laplace pressure of 0.39 bar, which is well below the transmembrane pressures applied, and therewith, droplet formation is ensured in our experimental setup.

Visualization

The images of the droplet formation process were obtained with a Zeiss Axio-plan microscope at a magnification of 400x. A Roper Scientific high speed camera was connected to the microscope and the images were recorded with a frequency of 500 images per second with a resolution of 512x512 pixels. Every process condition was recorded for 1 s, and for each experiment, between 26 and 92 droplets were analyzed.

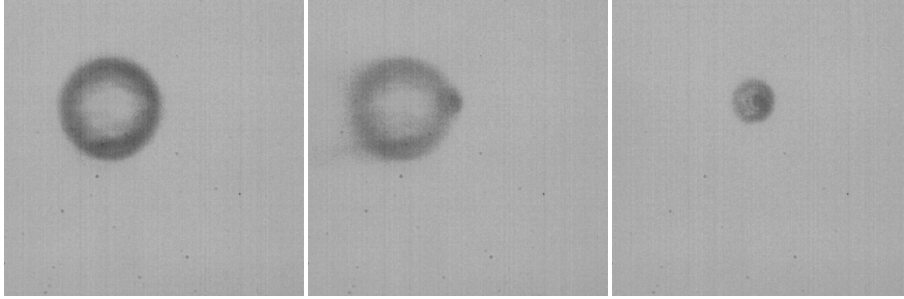
Drop volume tensiometer

A LAUDA drop volume tensiometer TVT1 was used for the measurements of the dynamic interfacial tension. The principle of the drop volume method consists of an exact determination of the volume of a droplet which detaches from a capillary. When the volume of the droplet is increased its weight increases until it reaches a critical value at which it cannot be counterbalanced by the interfacial tension and the drop detaches. This critical volume V is proportional to the interfacial tension, σ_{ow} , at the time of detachment. The force balance at the drop results in the following relation for the interfacial tension:

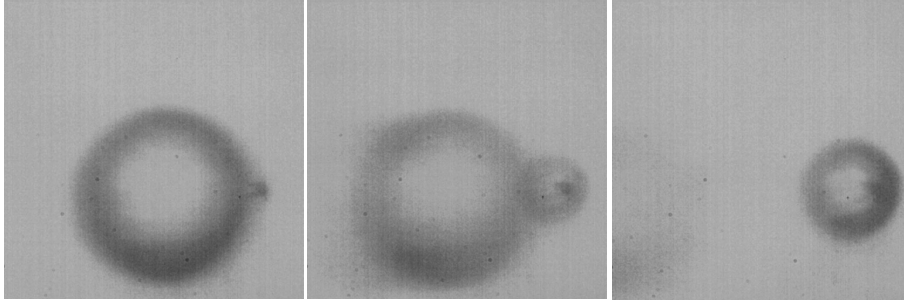
$$\sigma_{ow} = \frac{Vg\Delta\rho F}{2\pi r_{cap}}. \quad (2.2)$$

The correction factor F is a function of σ_{ow} , $\Delta\rho$, g and r_{cap} and is automatically calculated by the software of the tensiometer. For a range of surfactant concentrations, σ_{ow} can be measured as a function of different droplet volumes that relate to different droplet formation times. The radius of the capillary was 0.63 mm and it was the smallest capillary available for

this piece of equipment. The experiments that are described in this paper were done with a growing oil droplet in water, in analogy to the droplet formation experiments with the microsieve.



a.



b.

Figure 2.3: Droplet detachment and droplet formation from a pore for an oil pressure of 0.67 bar (a) and for an oil pressure of 1.18 bar (b). The pictures differ 0.002 s in time.

Results and discussion

For all images, the droplet diameters were measured and the droplet formation times were calculated. In general, the droplet diameters were much larger than the pore diameter. Figure 2.3a and 2.3b give three consecutive pictures of droplet detachment and droplet formation for experiments with 1% Tween 20 in the continuous phase and oil pressures of 0.67 bar and 1.18 bar, respectively. At the lower oil pressures, considerably smaller droplets are formed. The pictures show that just before detachment the droplet is strongly deformed; only a neck is holding the droplet connected to the pore. This observation is in accordance with simulations of droplet formation in membrane emulsification [8]. In contrary to Christov *et al.* [9] who did experiments with glass membranes at oil pressures just above the critical pressure, we did not observe droplet detachment at high surfactant concentrations without a cross-flow in the continuous phase. Apparently,

the different surface properties of the microengineered membrane and the higher oil pressures influence the detachment process enormously. (The results described below were all done with a cross-flow in the continuous phase.) No lag time was observed between the formation of droplets.

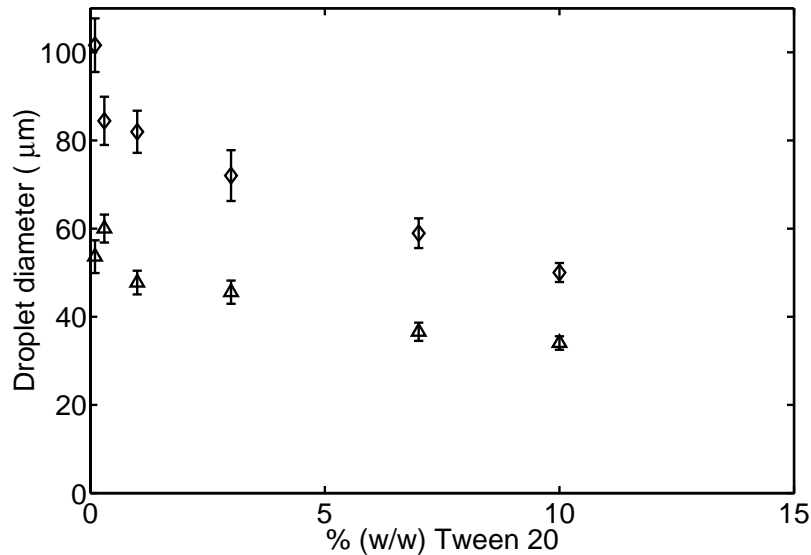


Figure 2.4: Droplet diameters of emulsion droplets as a function of concentration Tween 20 for oil pressures of 0.67 (\triangle) and 1.18 (\diamond) bar (transmembrane pressures of 0.43 and 0.94 bar, respectively).

Droplet formation experiments

Figure 2.4 gives the droplet diameter just before detachment from the membrane as a function of the surfactant concentration. It is clear that the droplet diameter decreases at higher surfactant concentration. This proves that during droplet formation, surfactants adsorb onto the interface of a growing droplet, therewith reducing the interfacial tension at detachment and consequently decreasing the volume of the droplets. The results show that larger droplets are not (only) a result of coalescence, which is expected to happen more easily when the surfactant concentration is low. Our results are in accordance with observations of Christov *et al.* [9], who saw that coalescence at the membrane surface is a rare phenomenon. The lengths of the error bars in figure 2.4 show that the small droplets that are formed at a high surfactant concentration, are more monodisperse. This is even more pronounced when considering the monodispersity of the volume of the droplets which is a third power of the radius.

Larger droplets are formed when the pressure of the to-be-dispersed phase is larger. At a concentration of 10% (w/w) Tween 20, the ratio of the droplet diameter versus the pore diameter is 7.1 and 10.4 for oil pressures of 0.67 bar and 1.18 bar, respectively. Literature [2] shows ratios of 3-12, therefore the ratios we found at high surfactant concentrations are within the range of reported results. The process conditions were not optimal for producing small droplets because the oil pressure (and also the transmembrane pressure) was quite high. A high oil pressure is required to obtain regular droplet formation at a low surfactant concentration, and therewith at high critical Laplace pressure, in order to keep the concentration range as wide as possible.

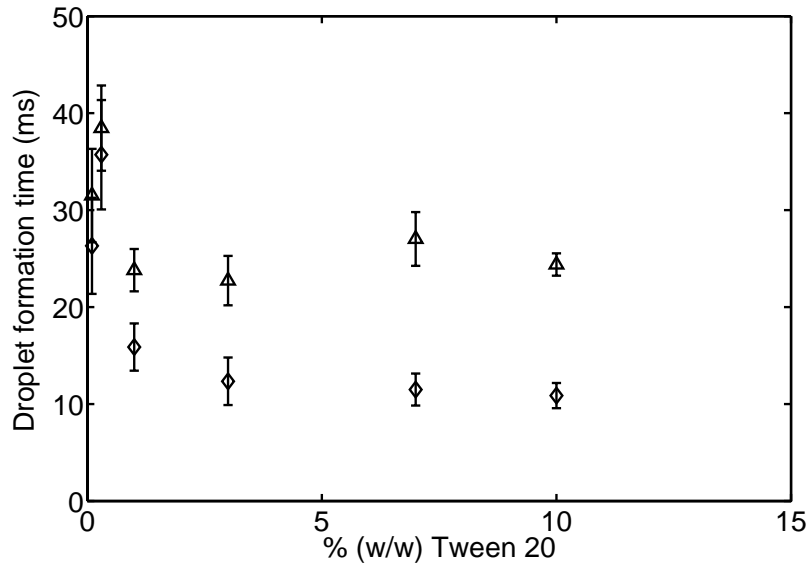


Figure 2.5: Droplet formation times of emulsion droplets as a function of concentration Tween 20 for oil pressures of 0.67 (Δ) and 1.18 (\diamond) bar (transmembrane pressures of 0.43 and 0.94 bar, respectively).

Figure 2.5 shows that the droplet formation times decrease as a function of the surfactant concentration. However, for concentrations above 1% (w/w) Tween 20 the droplet formation times do not decrease significantly. This figure also shows that the droplet formation times are dependent on the oil pressure. At higher oil pressure the droplet formation time decreases, while the droplet diameter increases (fig. 2.4). The literature [10] gives indirect estimations for average droplet formation times for high-porosity glass membranes. The estimation for a membrane with pores of 5 μm is 0.9 s, which is much longer than the droplet formation times observed in this research. In this reference, the formation times were indirectly

derived, not measured directly.

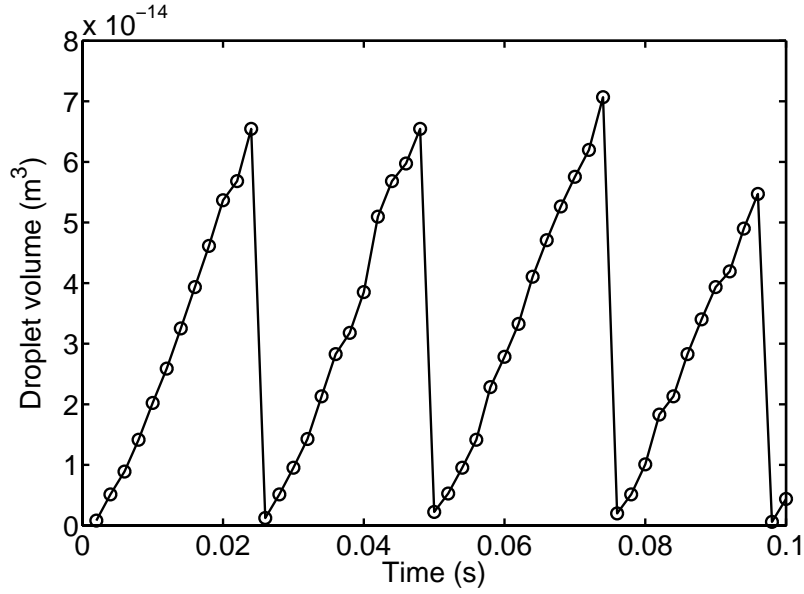


Figure 2.6: Droplet growth in time for an oil pressure of 0.67 bar and a Tween 20 concentration of 1%.

Table 2.1: The flow rates and velocities in the pore for each condition.

p_d (bar)	Tween 20 % (w/w)	Q ($10^{-12}\text{m}^3\cdot\text{s}^{-1}$)	$v_{pore}(\text{m}\cdot\text{s}^{-1})$
0.67	0.1	2.62	0.14
0.67	0.3	2.94	0.16
0.67	1	2.28	0.13
0.67	3	2.10	0.12
0.67	7	0.90	0.05
0.67	10	0.84	0.05
1.18	0.1	20.5	1.13
1.18	0.3	8.69	0.48
1.18	1	17.5	0.97
1.18	3	15.8	0.87
1.18	7	9.36	0.52
1.18	10	6.02	0.33

The average oil rate of flow can be calculated from the volume increase of the droplets and the droplet formation time. In our experiments we did not observe a lag time between droplets and the increase of the volume of the droplet in time is fairly constant, as is illustrated in figure 2.6 (1%

Tween 20, 0.67 bar). The average dispersed phase rate of flow equals in that case the volume of the droplet divided by the droplet formation time. Variations in the droplet diameter are mostly caused by the fact that the moment of droplet detachment varies somewhat. The constant rate of flow indicates that the applied oil pressures are also well above the critical Laplace pressure at the beginning of droplet formation for the applied oil pressures.

For all the experiments, the rate of flow and velocity were calculated. Table 2.1 shows that the oil rate of flow and velocity in the pore decrease as a function of the surfactant concentration, which could influence the droplet diameter. Nevertheless, the results for an oil pressure of 0.67 bar and concentrations of 0.1-3% Tween 20, for which the oil rate of flow is constant, show a decrease in droplet diameter, therewith signifying the conclusion that interfacial tension is the predominant mechanism. Please note that the effects can be partly attributed to the increase in viscosity [11] of the continuous phase at high surfactant concentration which is inherent to the system.

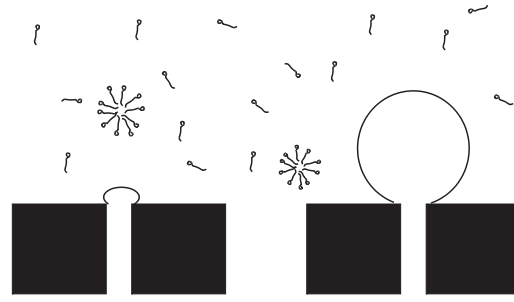
A higher rate of flow and higher velocity in the pore can be obtained at higher oil pressure, however, larger droplets will also be formed. For an industrially feasible process the rate of flow has to be high (high oil pressure) and the droplet diameter small (small oil pressure) and these are counter-acting criteria that have to be optimized. In the next section we present a tool for the prediction of the influence of the surfactant concentration on the droplet diameter.

Interfacial tension measurements

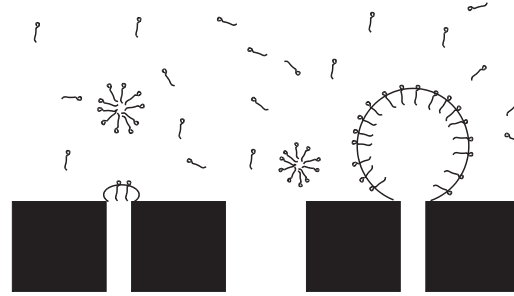
Only for systems with a constant expansion rate, such as an overflowing cylinder [12], is it possible to determine a constant dynamic interfacial tension at a certain relative expansion rate. In membrane emulsification the relative expansion rate and the dynamic interfacial tension change in time. For a growing droplet with a constant dispersed phase rate of flow (which is not only the case for a droplet volume tensiometer but also for membrane emulsification, see figure 2.6), the relative expansion rate, θ , can be calculated with (see appendix A):

$$\theta = \frac{1}{A} \frac{dA}{dt} = \frac{d \ln A}{dt} = \frac{2}{3t}. \quad (2.3)$$

This equation shows that for droplet formation the *relative* expansion rate is a function of time only (i.e. not of the rate of flow). At the initial stages the relative expansion rate is very large and decreases in time. The relative expansion rate just before detachment can be calculated using eq. 2.3, with t the time of droplet formation.



a.



b.

Figure 2.7: Relative expansion rate \gg surfactant adsorption (a) and relative expansion rate \ll surfactant adsorption (b).

The balance between the rate of convective diffusion of the surfactants to the interface and the relative expansion rate of the interface determines whether the interface stays fully covered with surfactant molecules or not [13], assuming very fast surface adsorption kinetics. Figure 2.7 shows the two extreme situations. At high relative expansion rates, diffusion is too slow to supply the expanding interface with surfactants and the interfacial tension will be equal to the interfacial tension when no surfactants are present. At low relative expansion rates, diffusion of surfactants is fast and the interfacial tension will be equal to the interfacial tension at equilibrium.

When emulsification experiments and drop volume tensiometry measurements are compared, it is expected that the relative expansion rates in both experiments determine, via the interfacial tension, at which time the droplets will break off. We will now relate the interfacial tensions that were measured for drop volume tensiometry (large droplets) to the emulsification experiments (small droplets).

Diffusion of surfactants to a flat interface differs from diffusion to a curved interface. For a spherical interface the loading is given by [14]:

$$\Gamma = 2\sqrt{\frac{Dt}{\pi}}c\left(1 + \frac{\sqrt{\pi Dt}}{2r_{dr}}\right), \quad (2.4)$$

with Γ the loading of the interface with surfactants, D the effective diffusion coefficient of the surfactant and c the surfactant concentration. The effect of a curved interface on the loading depends on the ratio between the diffusion penetration depth, $\sqrt{\pi Dt}$, and the radius of the droplet, r_{dr} . If $\sqrt{\pi Dt} \ll 2r_{dr}$ eq. 2.4 reduces to the general equation for diffusion controlled adsorption at short time scales:

$$\Gamma = 2\sqrt{\frac{Dt}{\pi}}c. \quad (2.5)$$

The results show that $\sqrt{\pi Dt} \ll 2r_{dr}$ with a diffusion coefficient of Tween 20 of $8.3 \cdot 10^{-11} \text{ m}^2 \cdot \text{s}^{-1}$ [15], and there is no influence of spherical diffusion; eq. 2.5 can be used for membrane emulsification and tensiometry. The measured interfacial tensions during tensiometry (large droplets) can be applied to the emulsification experiments (small droplets). Note that for droplets on (sub)micrometer scale spherical diffusion can not always be neglected. For droplets with a radius below approximately $1 \text{ } \mu\text{m}$, $\sqrt{\pi Dt} \ll 2r_{dr}$ is no longer valid.

By use of a log scale for the relative expansion rate it is possible to fit a linear function through the data points of the drop volume tensiometer experiments. If this function also holds for higher expansion rates, it is possible to calculate the interfacial tension in the range that is interesting for membrane emulsification. (The slopes of the lines correspond to the surface dilatation viscosity of each surfactant concentration.) This is only allowed as long as no depletion of surfactant monomers takes place. We expect that there is no depletion because the droplets are only formed from one pore and therefore, the amount of 'fresh interface' that is formed is very small. An advantage of the "simple" approach presented here is that

it does not require extensive determination of parameters (of which some can only be obtained by fitting interfacial tensions as a function of the concentration surfactant) as is the case for the more complex model presented in literature [16]. Moreover, for surfactants which are a mixture of homologous molecules (like Tween 20) and used often in industry it is even more difficult to determine these parameters. The maximum interfacial tension that can be reached is $47 \text{ mN}\cdot\text{m}^{-1}$ (for a bare hexadecane-water interface), and this is the upper limit for the window of operation. It is expected that the lines are no longer linear near $47 \text{ mN}\cdot\text{m}^{-1}$, but because we do not want to operate near this value, we did not investigate this in detail. For very low relative expansion rates a plateau is reached at approximately $5 \text{ mN}\cdot\text{m}^{-1}$, which is the measured equilibrium value of a hexadecane-water interface with 1% (w/w) Tween 20 (Wilhelmy plate method).

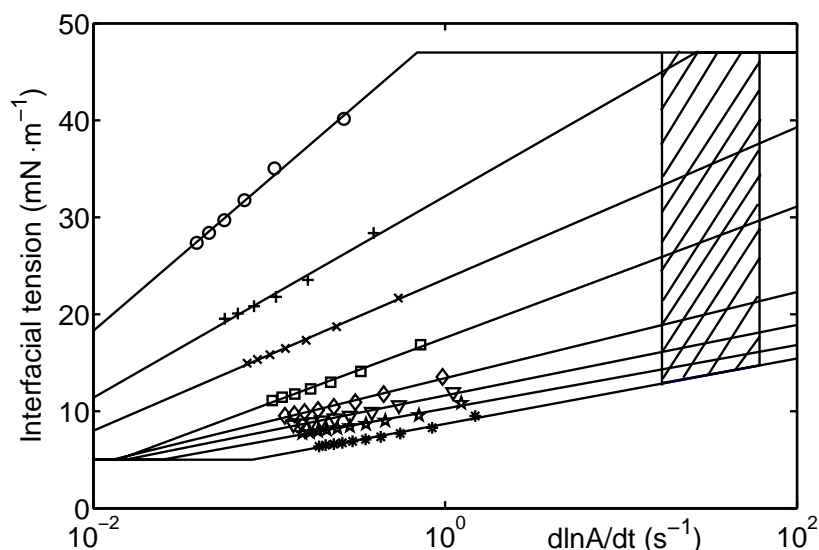


Figure 2.8: The data points and the fits of the interfacial tension of Tween 20 as a function of the relative expansion rate for 0.0037% (\circ), 0.012% ($+$), 0.037% (\times), 0.12% (\square), 0.37% (\diamond), 1.2% (∇), 3.7% (\star) and 12.3% (\ast) Tween 20. The shaded area is the window of operation in membrane emulsification, described in this paper.

Figure 2.8 shows the interfacial tension for a broad range of relative expansion rates. Tween 20 has a critical micelle concentration (CMC) of $2.8 \cdot 10^{-5} \text{ M}$ [9]. This means that all measured surfactant concentrations are above the CMC. For both low and high relative expansion rates a clear difference in interfacial tension is found. Please note that the interfacial tension in figure 2.8 corresponds to the interfacial tension at the time of

detachment. Droplet formation in membrane emulsification is very fast (up to droplet formation frequencies of 92 s^{-1}). In this range, which corresponds to relative expansion rates just before detachment in the range of $17 - 61 \text{ s}^{-1}$ (eq. 2.3), the lines predict an influence of the concentration of surfactant on the interfacial tension (figure 2.8).

We will now compare this to the results we obtained in the emulsification experiments. Peng and Williams [17] have published a model in which they assume that for droplet break up the drag force and the buoyancy force should equal the force caused by the interfacial tension via a force balance for deformed droplets or via a torque balance for spherical droplets. Van Rijn [18] showed that the force balance shows good agreement with some experimental literature results and also figure 2.3 shows that the droplets strongly deform. Therefore we concluded that the force balance is most suitable to predict the droplet size. Because the droplets are small it is safe to assume that the buoyancy force can be neglected. This results in the following equation for the prediction of the radius of the emulsion droplet:

$$r_{dr} = \sqrt{\frac{\sigma_{ow} r_p}{5.1 \tau_{wall}}}. \quad (2.6)$$

The radius of the droplet is related to the interfacial tension via a square root relationship.

Although the concentrations in figure 2.8 are slightly different than the concentrations used in the droplet formation experiments with a membrane it is expected that the fits give a good indication of the actual dynamic interfacial tension during emulsification. Table 2.2 gives the calculated interfacial tensions at the time of droplet detachment. The predicted interfacial tensions are almost identical for oil pressures of 0.67 and 1.18 bar, because the actual relative expansion rates do not differ that much. This is in contrast to the experimental results, which show a large influence of the oil pressure on the droplet diameter. When the droplet snap-off mechanism would be fast compared to the flow of the to-be-dispersed phase, we would expect that the absolute velocity of this phase does not have any influence on the droplet size. Clearly this is not the case and most probably, this snap-off time is rather slow in this regime of droplet formation; in the range of milliseconds at least. Scheele and Meister [19] also observed in high speed movies that a considerable amount of liquid flowed into a droplet during the process of droplet break up, therewith supporting our assumption that the snap-off time is rather long. Besides, Schröder et al.

[5] show results in which the ratio between the maximum droplet size and the minimum droplet size at a constant wall shear stress is much higher (about 10) than the ratio that is expected (about $\sqrt{27/3.4} = 2.8$), based on the possible range of values of the interfacial tension which is 3.4 - 27 mN·m⁻¹ for this specific article. This confirms the idea that the effect of snap-off comes into play. However, this large ratio could also be both a consequence of varying droplet sizes at droplet detachment due to a different σ_{ow} and a result of coalescence. Therefore more research is needed to predict the exact influence of dynamic interfacial tension, oil pressure and snap-off time on the droplet size.

Table 2.2: Prediction of dynamic interfacial tension.

p_d (bar)	Tween 20 % (w/w)	t_{form} (s)	θ (s ⁻¹)	σ (mN·m ⁻¹)
0.67	0.1	0.0315	21	26.6
0.67	0.3	0.0385	17	18.9
0.67	1	0.0238	28	16.9
0.67	3	0.0227	29	15.1
0.67	10	0.0244	27	12.5
1.18	0.1	0.0263	25	27.1
1.18	0.3	0.0357	19	19.1
1.18	1	0.0159	42	17.5
1.18	3	0.0123	54	15.9
1.18	10	0.0109	63	14.7

Conclusion

Droplet formation in membrane emulsification is a very fast process with droplet formation times in the range of tens of milliseconds. Still, there is an influence of the surfactant concentration on droplet formation: higher surfactant concentrations lead to smaller droplets. The relatively large droplets that are formed at low surfactant concentrations are a direct result of a high interfacial tension during droplet formation and not (only) a result of coalescence. It was also shown that higher oil pressures and a higher surfactant concentration lead to smaller droplet formation times. With a drop volume tensiometer the interfacial tension was measured as a function of the relative expansion rates. Extrapolation of these measured values leads to a prediction for the interfacial tension at the high relative expansion rates that occur in membrane emulsification. This interfacial

tension, which is dependent on surfactant concentration and surfactant type, can be used to predict the trend of the droplet diameter.

Although it is obvious that a high interfacial tension leads to a large droplet, the exact relation between the interfacial tension and the droplet diameter at detachment is not clear. A possible explanation is that the time needed for snap-off is not negligible and causes a pronounced influence of the oil pressure (and rate of flow) on the droplet size. This time should be higher than several milliseconds, but smaller than approximately 10-15 milliseconds.

Until now, all tensiometers have applied relative expansion rates that are orders of magnitude smaller than those relevant for emulsification processes. Further optimization of this method for predicting the interfacial tension during membrane emulsification could lead to a measuring instrument based on membrane emulsification to predict the interfacial tension at (very) high expansion rates.

Acknowledgement

The authors thank Dr. Martin Bos for making it possible to do drop volume tensiometer measurements and Dr. Cees van Rijn from Aquamarijn for the microsieves. This research was supported by the European Community, project QLRT-2000-01228.

Nomenclature

A	interfacial area (m^2)
c	concentration ($\text{mole}\cdot\text{m}^{-3}$)
D	diffusion coefficient ($\text{m}^2\cdot\text{s}^{-1}$)
g	gravity constant ($\text{m}\cdot\text{s}^{-2}$)
p_c	continuous phase pressure (bar)
p_d	dispersed phase pressure (bar)
p_{trm}	transmembrane pressure (bar)
Q	oil rate of flow ($\text{m}^3\cdot\text{s}^{-1}$)
r_{cap}	radius of the capillary (m)
r_{dr}	radius of the droplet (m)
r_p	radius of the pore (m)
t	time (s)
t_{form}	droplet formation time (s^{-1})
v_c	velocity of the continuous phase ($\text{m}\cdot\text{s}^{-1}$)
v_{pore}	velocity in the pore ($\text{m}\cdot\text{s}^{-1}$)
V	volume of the droplet (m^3)

Greek letters

Γ	loading of an interface ($\text{mole}\cdot\text{m}^{-2}$)
θ	relative expansion rate (s^{-1})
σ_{ow}	interfacial tension of the oil-water interface ($\text{N}\cdot\text{m}^{-1}$)
τ_{wall}	wall shear stress (Pa)

Appendix A: Derivation of equation for relative expansion rate

We assume that the rate of flow is a constant in time and the volume of a droplet, V_{dr} , is dependent on the flux, Q , and the time, t :

$$V_{dr}(t) = Qt = \frac{4}{3}\pi r_{dr}^3, \quad (2.7)$$

$$r_{dr}(t)^3 = \frac{3}{4\pi}Qt, \quad (2.8)$$

$$r_{dr}(t) = \left(\frac{3}{4\pi}Qt\right)^{1/3}, \quad (2.9)$$

$$A_{dr}(t) = 4\pi(r_{dr}(t))^2 = 4\pi\left(\frac{3}{4\pi}Qt\right)^{2/3} = 4\pi\left(\frac{3}{4\pi}\right)^{2/3}Q^{2/3}t^{2/3}, \quad (2.10)$$

$$\frac{dA}{dt} = \frac{dA}{dV} \frac{dV}{dt} = \frac{8\pi r_{dr}}{4\pi r_{dr}^2} \frac{dV_{dr}(t)}{dt} = \frac{2}{r_{dr}(t)}Q, \quad (2.11)$$

$$\frac{dA}{dt} = \frac{2}{\left(\frac{3}{4\pi}Qt\right)^{1/3}}Q = 2\left(\frac{4\pi}{3}\right)^{1/3}Q^{2/3}t^{-1/3}, \quad (2.12)$$

$$\frac{d\ln A}{dt} = \frac{1}{A} \frac{dA}{dt} = \frac{2\left(\frac{4\pi}{3}\right)^{1/3}Q^{2/3}t^{-1/3}}{4\pi\left(\frac{3}{4\pi}\right)^{2/3}Q^{2/3}t^{2/3}} = \frac{2}{3t}. \quad (2.13)$$

References

1. T. Nakashima, M. Shimizu, M. Kukizaki, Membrane emulsification by microporous glass, *Key Eng. Mat.* 61&62 (1991) 513.
2. S.M. Joscelyne, G. Trägårdh, Membrane emulsification - a literature review, *J. Membr. Sci.* 169 (2000) 107.
3. V. Schröder, Herstellen von Öl-in-Wasser-Emulsionen mit mikroporösen Membranen, Ph.D. thesis, University Karlsruhe, 1999.
4. R. Katoh, Y. Asano, A. Furuya, K. Sotoyama, M. Tomita, S. Okonogi, A method of preventing dispersed droplets from crushing using a membrane emulsification system, *Journal of the Japanese society for food science and technology* 44, 3 (1997) 233.
5. V. Schröder, O. Behrend, H. Schubert, Effect of dynamic interfacial tension on the emulsification process using microporous, ceramic membranes, *J. Colloid Interface Sci.* 202 (1998) 334.
6. A.J. Abrahamse, R. van Lierop, R.G.M. van der Sman, A. van der Padt, R.M. Boom, Analysis of droplet formation and interactions during cross-flow membrane emulsification *J. Membr. Sci.* 204 (2002) 125.
7. C.J.M. van Rijn, M.C. Elwenspoek, Micro filtration membrane sieve with silicon micro machining for industrial and biomedical applications, *Proceedings of the IEEE* 83 (1995) 83.
8. A.J. Abrahamse, A. van der Padt, R.M. Boom, W.B.C. de Heij, Process fundamentals of membrane emulsification: simulation with CFD, *AIChE J.* 47 6 (2001) 1285.
9. N.C. Christov, D.N. Ganchev, N.D. Vassileva, N.D. Denkov, K.D. Danov, P.A. Kralchevsky, Capillary mechanisms in membrane emulsification: oil-in-water emulsions stabilized by Tween 20 and milk proteins, *Colloids Surfaces A: Physicochem. Eng. Aspects* 209 (2002) 83.
10. G.T. Vladislavjevic, H. Schubert, Preparation and analysis of oil-in-water emulsions with a narrow droplet size distribution using Shirasu-porous-glass (SPG) membranes, *Desalination* 144 (2002) 167.
11. G. Kedvessy, E. Regdon-Kiss, Versuche zum studium der micellenbildung solubilisierten mittel, *Pharmazie* 18, 2 (1963) 131.
12. D.J.M. Bergink-Martens, H.J. Bos, A. Prins, B.C. Schulte, Surface dilatation and fluid-dynamical behavior of Newtonian liquids in an overflowing cylinder, *J. Colloid Interface Sci.* 138, 1 (1990) 1.
13. E.H. Lucassen-Reynders, K.A. Kuipers, The role of interfacial properties in emulsification, *Colloids and Surfaces* 65 (1992) 175.
14. P. Joos, Dynamic surface phenomena, 1999, VSP, Utrecht, p. 142.
15. M. Rayner, G. Trägårdh, Transfer of surfactants to an expanding oil water interface during membrane emulsification, *Proceedings LiFT symposium Gothenburg* (2003) 68.
16. F. van Voorst Vader, Th.F. Erkens, M. van den Tempel, Measurement of dilatational surface properties, *Trans. Faraday Soc.* 60 (1964) 1170.

17. S.J. Peng, R.A. Williams, Controlled production of emulsions using a crossflow membrane. Part I: Droplet formation from a single pore, *Trans IChemE* 76 (1998) 894.
18. C.J.M. van Rijn, Nano and Micro Engineered Membrane Technology, 2004, Elsevier Science, Amsterdam.
19. G.F. Scheele, B.J. Meister, Drop formation at low velocities in liquid-liquid systems: Part 1. Prediction of drop volume, *AIChE J.* 14, 1 (1968) 9.

Chapter 3

Droplet formation in a T-shaped microchannel junction

Abstract

Droplet formation was studied in a glass microchip with a small channel containing to-be-dispersed phase perpendicular to a large channel with a cross-flowing continuous phase. This resembles the situation during cross-flow membrane emulsification. In this model system, droplets are formed at a T-junction of these two rectangular channels; the droplet formation and detachment process is studied from aside with a microscope connected to a high speed camera. Monodisperse hexadecane droplets were formed in aqueous solutions with various concentrations of ethanol, SDS and Tween 20. Just before detachment, the neck diameter was measured and a critical neck diameter of $4\text{ }\mu\text{m}$ was found, which is in the same range as the depth of the channel ($5\text{ }\mu\text{m}$). After detachment, the droplet diameter was determined for the various aqueous solutions. The droplet diameter increased as a function of the oil flow rate. Use of surfactants (SDS, Tween 20) resulted in the formation of smaller droplets than in systems without surfactants. A simple model is proposed to describe the droplet formation process, inspired on the idea that the necking process is a dynamic process that takes a certain time, which explains the influence of both the oil flow rate and the properties of the fluid phases on the final droplet size. Fitting the experimental data with the model results in a necking time of about 11 ms.

This chapter has been published as: S. van der Graaf, M.L.J. Steegmans, R.G.M. van der Sman, C.G.P.H. Schroën, R.M. Boom, Droplet formation in a T-shaped microchannel junction: A model system for membrane emulsification, *Colloids and Surfaces A: Physicochemical and Engineering Aspects* 266 (2005) 106-116.

Introduction

Emulsions are widely used in the production of food, cosmetics and pharmaceutical products. Water-in-oil (W/O) emulsions, in which the dispersed phase is water, and oil-in-water (O/W) emulsions, in which the dispersed phase is oil, can be distinguished. A relatively new method to produce monodisperse emulsions is membrane emulsification [1], in which the to-be-dispersed phase is pushed through a membrane and the droplets formed at the membrane surface are detached by the cross-flowing continuous phase. Monodispersity of emulsions has a positive influence on product properties like shelf-life, mouth feeling, appearance and stability. Especially for the production of double emulsions and encapsulates mild and controlled methods such as membrane emulsification are promising [2]. Lately, also other techniques to produce highly monodisperse droplets have been introduced, like microchannel emulsification [3] in which micro-fabricated channels are used to make droplets. Umbanhowar *et al.* [4] developed a technique in which the to-be-dispersed phase is introduced into a coflowing, surfactant-laden continuous phase via a capillary. In addition flow focusing microdevices [5] to produce droplets of varying size and microfluidic devices with a geometry that facilitates break up of larger droplets into smaller droplets [6] have recently been developed.

A lot of research on membrane emulsification has been done on overall process conditions by evaluating the final emulsion [7]. In those investigations it is not really possible to unravel the mechanism of droplet formation and detachment. For example, the influence of surfactants, (dynamic) interfacial tension and to-be-dispersed phase flow rate on the droplet formation and detachment process, and therewith the final droplet size, is not totally clear. Understanding the droplet formation process in detail enables us to explore the possibilities and limits of membrane emulsification for various applications.

In this research, we look at droplet formation in microchannels that have dimensions comparable to the dimension of a typical pore used in cross-flow membrane emulsification. In this way, it is possible to microscopically study the droplet formation and study the detachment process and shape of the droplet in detail, which has not been reported in earlier work [8 – 11]. We specifically study the influence of the properties of the aqueous phase (static interfacial tension, the influence of the dynamics of the interfacial tension, phase viscosity and density) on the process of droplet formation

and investigate the mechanisms at hand. The results are related to the membrane emulsification process.

Materials and Methods

Chemicals

Anhydrous hexadecane (Sigma), $C_{16}H_{34}$, was used as to-be-dispersed phase. De-ionised water was used as continuous phase. Various concentrations of surfactants and ethanol were added to the continuous phase to change the interfacial tension. Rinse ethanol (98% (w/w)) was dissolved in de-ionised water to make 2.5, 5, 10 and 49% (w/w) ethanol solutions. Sodium dodecyl sulfate (SDS, Sigma) solutions of 0.25 and 1 % (w/w) and Tween 20 (polyoxyethylene (20) sorbitan monolaurate, Merck) solutions of 0.001, 0.01, 0.1 and 1% (w/w) were prepared.

Density, viscosity and interfacial tension measurements

The densities of de-ionised water and the various aqueous ethanol, SDS, and Tween 20 solutions were determined using a volumetric flask. The difference in weight was used to calculate the density. The obtained values were compared to values in literature for known concentrations.

The viscosity of the different aqueous phases was determined using an Ubbelohde viscosimeter. The Ubbelohde viscosimeter was calibrated by determining the flow time of de-ionised water in duplicate. All measurements were performed in duplicate and the error in the determined flow times was less than 1 %. The Ubbelohde was cleaned with an Alconox solution of approximately 3% (w/w) and flushed three times with de-ionised water.

The interfacial tension at a hexadecane-aqueous phase interface was determined as a function of time using dynamic drop shape tensiometry [12]. After a hexadecane droplet had been formed on the tip of the U-shaped needle, which took 1-2 s, the interfacial tension measurement started. The droplet shape was analysed and the interfacial tension was calculated by the software using the Laplace equation. The various ethanol, SDS, and Tween 20 water solutions were measured component by component and in order of increasing concentration. In between duplicate measurements, the tip of the needle was rinsed with an excess of de-ionised water and dried

with the tip of a tissue. In between the components, syringe and bended needle were cleaned with chloroform, flushed with a liter of de-ionised water, and blow dried with air. For all droplet formation experiments (see next section), the same batch of chemicals was used as for the determination of the density, viscosity and interfacial tension.

Droplet formation experiments

Droplet formation was studied in microchannel glass chips (Micronit microfluidics bv., the Netherlands). The microchannel glass chips consist of a lower glass plate, in which channels with a depth of 5 μm are etched, and a thinner top plate with inlets for the fluid phase, which is pressed against the lower plate to close off the channels. The hexadecane and aqueous phases are introduced into the chip via separate channels; they meet at a T-shaped junction in the middle of the chip, where droplets can be formed. Figure 3.1 shows a schematic top view of a T-junction in the chip with its dimensions. The width of the hexadecane channel (24 μm) and the aqueous channel (303 μm) are chosen such to be relevant for membrane emulsification. The microchip was placed into a chip holder (Micronit microfluidics bv.). Hexadecane and aqueous phase were introduced into the chip through glass capillaries connected to syringes (Hamilton, gastight luer lock syringe) in syringe pumps (Harvard apparatus 11 Plus).

The droplet formation process was recorded using a Zeiss upright microscope, type Quanticell 900, connected to a CCD high speed camera (Redlake Motion Pro). The frame rate was set at 500 - 1600 frames per second, depending on the frequency of droplet formation. A shutter speed in the range of 1000 - 8000 s^{-1} was used. The flow rate of the continuous aqueous phase was always in the range 8-12 $\mu\text{l}\cdot\text{min}^{-1}$. For most droplet formation experiments, the applied continuous phase flow rate was 10 $\mu\text{l}\cdot\text{min}^{-1}$, which corresponds to a velocity of 0.11 $\text{m}\cdot\text{s}^{-1}$ in the large channel of the glass chip. The applied flow rate was checked by measuring the weight of fluid passing through the large channel in time and the found values matched exactly with the applied continuous flow rate. The applied oil flow rate was not always the same as the flow rate calculated from the sizes and number of formed droplets (especially not at high applied flow rates). We assume that the calculated flow rate is most reliable, and therefore use this value, which was in the range 0.003-0.06 $\mu\text{l}\cdot\text{min}^{-1}$ and corresponds to a velocity in the glass chip in the range $4.2\cdot 10^{-4}$ - $8.3\cdot 10^{-3}$ $\text{m}\cdot\text{s}^{-1}$.

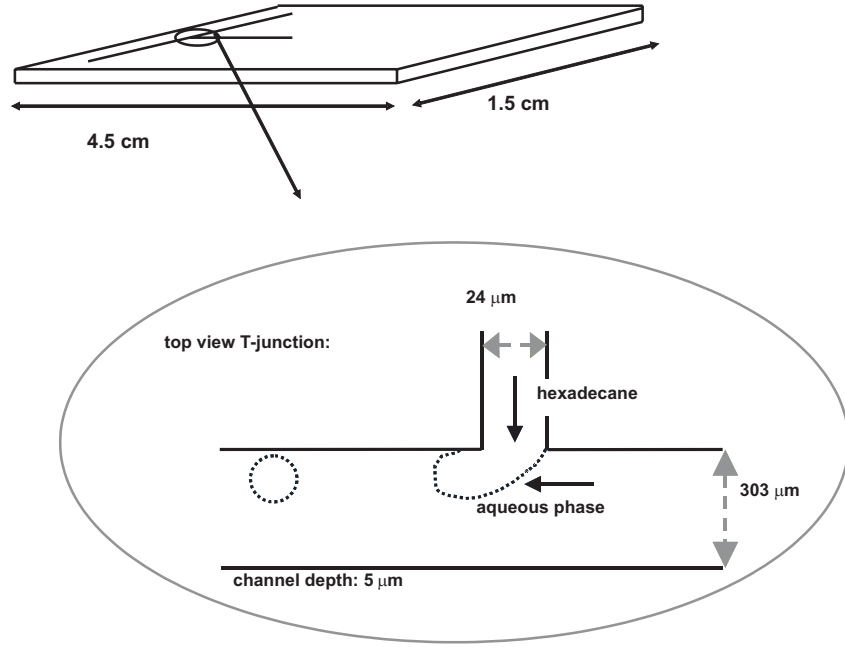


Figure 3.1: Schematic topview of the T-junction with its dimensions.

For each process condition, at least 20 droplets were analysed. Prior to recording, the glass chip was subjected to the process conditions for 10 min in order to allow for stable conditions inside the chip. After detachment of a droplet, the horizontal (D_h) and vertical (D_v) diameter of the droplet were determined by image analysis. The oil flow rate in the microchannel was calculated using the droplet formation recordings. The droplets are not exactly circular, but somewhat deformed due to friction and fluid flow of the continuous phase through the channel. The ratio of D_h and D_v was found to have a constant value of 0.9 and the droplets are 10° tilted in the direction of the flow; however, the resulting error in D_v is small (in the order of 1%), and therefore not taken into account in determining the oil flow rate.

Just before detachment, 4 characteristic measures of the droplet were determined. D_{neck} is the diameter of the neck parallel to the left wall of the hexadecane channel. $L_{penetration}$ is the penetration length of aqueous phase into the hexadecane channel. L_{detach} is the length between the left wall of the hexadecane channel and the furthest point of the droplet in contact with the wall of the chip. The fourth parameter is D_{detach} , which is the diameter of the thickest part of the forming droplet, when it is still attached to the wall (see figure 3.2). All four characteristics were determined in the

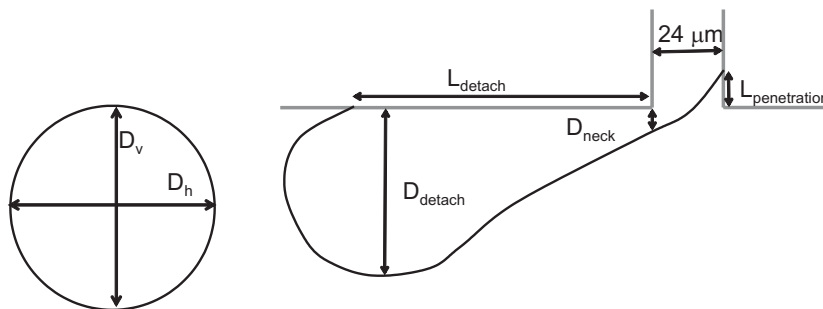


Figure 3.2: Schematic drawing of a droplet with the definition of the horizontal (D_h) and vertical (D_v) diameter and just before detachment with the definition of the neck diameter (D_{neck}), penetration length ($L_{penetration}$), detachment length (L_{detach}) and the droplet diameter of the attached droplet (D_{detach}).

last frame before detachment of the droplet.

Results and Discussion

Density, viscosity and interfacial tension measurements

We measured some properties (density, viscosity and interfacial tension) of the different aqueous phases to be able to take the influence of these properties on the droplet formation experiments into account. Table 3.1 gives an overview of the results. Please note that the interfacial tension given in table 3.1 is the equilibrium interfacial tension.

For the solutions with different concentrations of SDS and Tween 20, the density and viscosity are not very different from pure water, and therefore these differences are not expected to lead to differences in the results obtained with the microchip. The addition of ethanol not only decreased the interfacial tension as was our intention (see also [13] for surface tension values of ethanol-water mixtures with air), but also increased the dynamic viscosity significantly and decreased the density somewhat. This should be taken into account when interpreting the results. The values reported here are in accordance with literature results for density [14] and dynamic viscosity [15] measurements of ethanol-water mixtures. Addition of ethanol to the water phase leads to an instantaneous decrease of the interfacial tension while addition of a surfactant leads to a decrease in time depending on the diffusion rate and adsorption time that is needed for the adsorption of surfactants to the interface. Thus, we expect to see the effects of the dynamics in the interfacial tension by comparing these two systems.

Table 3.1: Measured density, dynamic viscosity and equilibrium interfacial tension of de-ionised water, aqueous ethanol, SDS and Tween 20 solutions at room temperature (22.5 ± 1.0 °C). The density values of ethanol were compared with literature [14] and similarity was found (error < 1%). The viscosity and interfacial tension measurements were done in duplicate and errors < 1% were found.

solution	ρ [g·l ⁻¹]	η [mPa·s]	σ_{eq} [mN·m ⁻¹]
de-ionised water	992	1.00	44.0
2.5% (w/w) ethanol	988	1.10	40.4
5% (w/w) ethanol	988	1.21	36.3
10% (w/w) ethanol	980	1.44	29.5
49% (w/w) ethanol	912	2.65	9.5
0.25% (w/w) SDS	992	1.00	9.0
1% (w/w) SDS	992	1.08	8.2
0.001% (w/w) Tween 20	992	1.00	6.6
0.01% (w/w) Tween 20	992	1.00	5.2
0.1% (w/w) Tween 20	992	1.03	5.4
1% (w/w) Tween 20	992	1.07	4.8

Droplet formation

Figure 3.3 shows hexadecane droplets formed in water. Droplet formation starts with a half disc of hexadecane formed at the pore opening. In time, the droplet grows and is deformed in the direction of the aqueous phase flow (right to left). A neck is formed which holds the droplet connected to the pore while the continuous water phase intrudes into the pore. Finally, the droplet detaches at the left side of the pore opening.

In contrast with hexadecane droplets in water, droplet formation in aqueous ethanol solutions starts at a distance from the pore opening as can be seen in figure 3.4. Droplet formation in SDS solutions always starts at the pore opening as was the case for water. With Tween 20 droplet formation mostly starts at the pore opening, but incidentally (and more often at high concentrations), the droplets do not snap off at the left wall of the pore opening but near the droplet, as was also observed for the ethanol solutions (results SDS and Tween 20 not shown). This switch in snap off location is comparable to CFD calculations for different wall contact angles [16]. Therefore, different wetting conditions (also caused by different interfacial tensions) may be the reason for this behaviour.

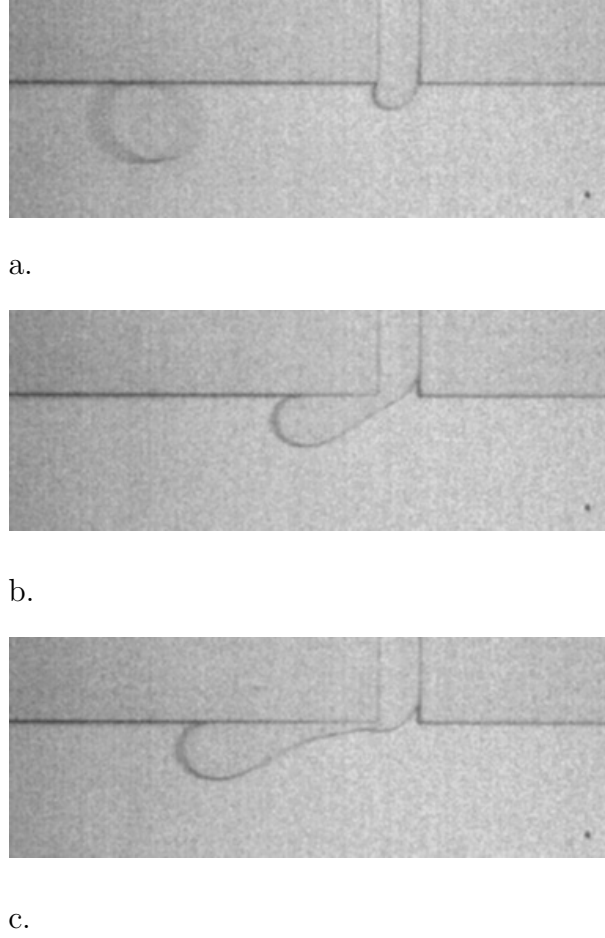
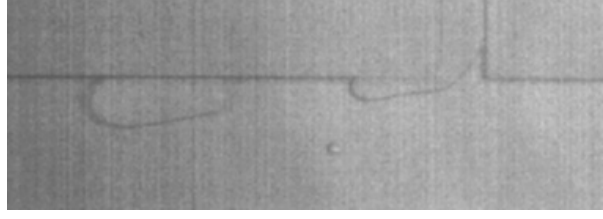


Figure 3.3: Hexadecane droplets formed in de-ionised water, continuous phase flow rate $10 \mu\text{l}\cdot\text{min}^{-1}$ and oil flow rate $0.04 \mu\text{l}\cdot\text{min}^{-1}$. The previous droplet has just detached at $t=0$ s (a), the droplet grows, $t=0.006$ s (b) and at $t=0.01$ s (c) the new droplet is going to detach.

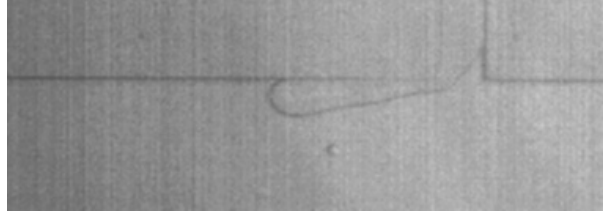
Different regimes for droplet break up were observed. At a continuous phase flow rate of $10 \mu\text{l}\cdot\text{min}^{-1}$, an oil flow rate higher than $0.06 \mu\text{l}\cdot\text{min}^{-1}$ led to a jet of oil phase. Around this 'critical dispersed phase velocity' a transition regime is visible in which sometimes droplets, and sometimes jets are formed. Different regimes in droplet formation experiments and transitions between these experiments in microchips have also been reported by others [17, 18]. In the following paragraphs, we will only focus on results from the droplet formation regime.

Droplet detachment characteristics

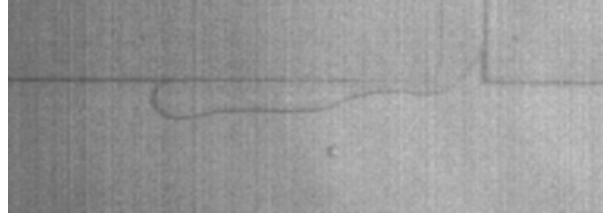
Table 3.2 gives a summary of two characteristics of droplet detachment: the neck diameter and the penetration length. Please note that the average is shown for different oil flow rates and different concentrations of ethanol



a.



b.



c.

Figure 3.4: Hexadecane droplets formed in 10% ethanol, continuous phase flow rate $10 \mu\text{l}\cdot\text{min}^{-1}$ and oil flow rate $0.035 \mu\text{l}\cdot\text{min}^{-1}$. The previous droplet has just detached at $t=0$ s (a), the droplet grows, $t=0.006$ s (b) and at $t=0.01$ s (c) the new droplet is going to detach.

or surfactant. According to Schröder *et al.* [19], the neck diameter is important for the detachment process in membrane emulsification, because the force that is mainly responsible for holding the droplet connected to the pore (F_σ , the interfacial tension force) is dependent on the neck diameter. A critical neck diameter of $4 \mu\text{m}$ (error $0.8 \mu\text{m}$) was found for all process conditions and seems independent of the process conditions. It is not coincidental that the critical neck diameter is in the same range as the depth of the microchannel ($5 \mu\text{m}$). Analysis of the Laplace pressures in the flat part of the neck and in the droplet, connected to the pore by the neck, shows that snap-off can only occur when the neck becomes smaller than the depth of the channel (see appendix A).

Table 3.2: Average neck diameter and penetration length for de-ionised water, aqueous ethanol, SDS and Tween 20 solutions. The error in determining the values with image analysis is $0.8 \mu\text{m}$.

solution	neck diameter [μm]	penetration length [μm]
de-ionised water	4.1	13.7
ethanol	3.9	19.6
SDS	3.7	13.1
Tween 20	4.1	8.0

It was observed that there is always penetration of aqueous phase into the hexadecane channel. The penetration length just before detachment was smallest for Tween 20 with an average of $8 \mu\text{m}$ and largest for the ethanol solutions with an average of $20 \mu\text{m}$. The penetration length for SDS and de-ionised water is in between these values. In the work of Nisisako *et al.* [20], this behaviour could also be observed for droplet formation in a microchip with vegetable oil as the continuous phase and water as the to-be-dispersed phase. The shape of a droplet and intrusion of continuous phase into the pore was also found computationally in lattice Boltzmann simulations [21] of droplet formation in a glass chip.

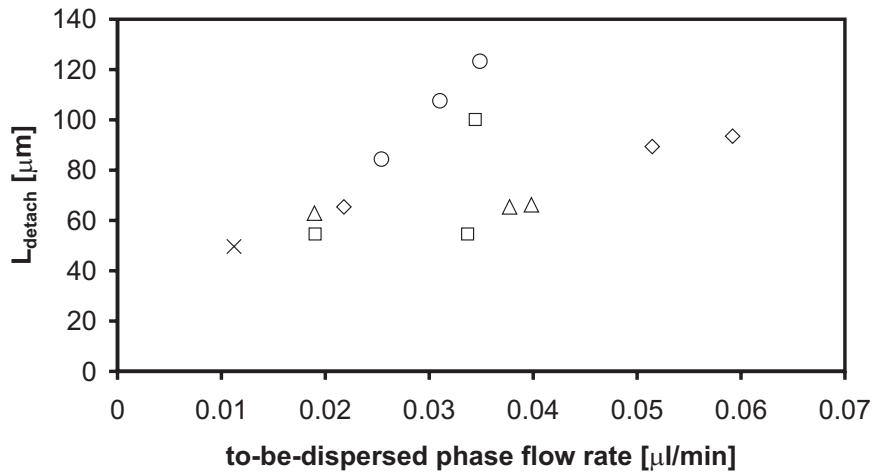


Figure 3.5: L_{detach} as a function of the oil flow rate for 0 % (\times), 0.001 % (\square), 0.01% (\triangle), 0.1% (\diamond) and 1% (\circ) Tween 20 at a constant continuous phase flow rate of $10 \mu\text{l}\cdot\text{min}^{-1}$.

The detachment process with ethanol-water mixtures seems to be different from what is observed with the other systems causing large detachment

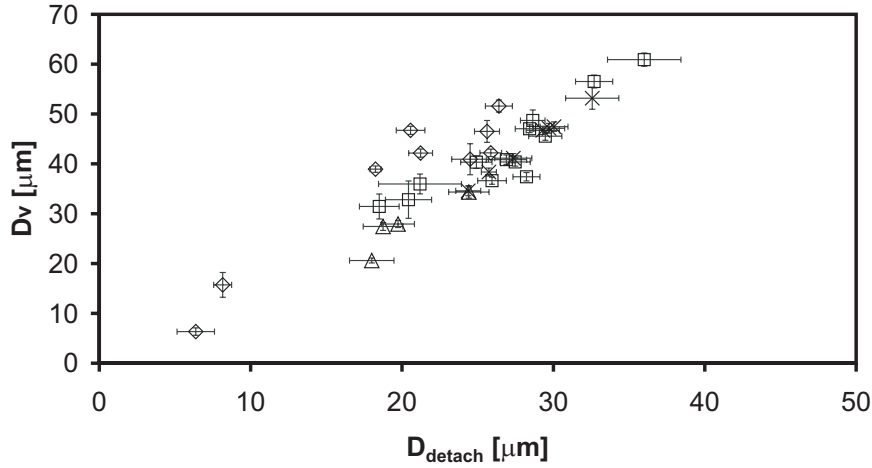


Figure 3.6: D_v as a function of D_{detach} for de-ionised water (\times), ethanol (\diamond), Tween 20 (\square) and SDS (\triangle) solutions at a constant continuous phase flow rate of $10 \mu\text{l}\cdot\text{min}^{-1}$. Error bars indicate 95% reliability interval.

lengths (around $100\text{-}150 \mu\text{m}$). For SDS, the detachment length is smallest (around $30\text{-}50 \mu\text{m}$). The detachment length of Tween 20 and de-ionised water is in between. For most solutions, the detachment length increases as a function of the oil flow rate as can be seen in figure 3.5 for Tween 20.

When plotting the droplet diameter D_v versus the diameter prior to droplet detachment (D_{detach}), a linear relation is found for all four aqueous solutions (figure 3.6). From this figure, we can conclude that D_{detach} just before detachment is a good indication for the final droplet size.

Influence of oil flow rate

The droplet diameter was investigated at various continuous and to-be-dispersed phase flow rates. Figure 3.7 shows an increase in D_v as a function of the oil flow rate for three different continuous phase flow rates. Because there are no surfactants in the system, the interfacial tension can be safely assumed to be that of a hexadecane-water interface. This means that the size of the droplets is only an effect of both flow rates and the system geometry. At a continuous phase flow rate of $8 \mu\text{l}\cdot\text{min}^{-1}$, larger droplets are formed and at a continuous phase flow rate of $12 \mu\text{l}\cdot\text{min}^{-1}$ smaller droplets are the result. This is in correspondence with the force (or torque) balance model which predicts that a higher continuous phase flow rate, and thus a larger drag force, detaches droplets earlier and causes smaller droplets.

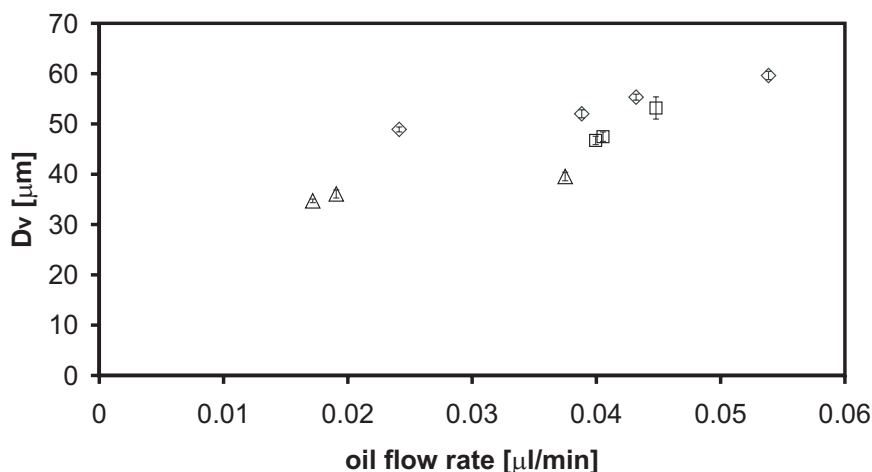


Figure 3.7: D_v as a function of the oil flow rate for droplet formation in de-ionised water at a continuous phase flow rate of 8 (\diamond), 10 (\square) and 12 (\triangle) $\mu\text{l}\cdot\text{min}^{-1}$. Error bars on the y-axis indicate 95% reliability interval.

Figure 3.8 shows D_v as a function of the oil flow rate for experiments with aqueous solutions with 0, 2.5, 5, 10 and 49% ethanol. For the solutions with 0, 2.5, 5 and 10% ethanol, there is no significant influence of the addition of the ethanol on the droplet diameter. Droplets formed in a 49% ethanol solution are considerably smaller than droplets formed in the other solutions. This is caused by both the decreased interfacial tension as the increased viscosity, which can be expressed in terms of a capillary number ($\text{Ca} = v_{\text{cont}} \cdot \eta / \sigma$). For the 49% ethanol, the capillary number has a value of 0.03, while for the other points, the capillary number is much lower (0.002-0.005). Following the theory of droplet detachment in membrane emulsification, a low interfacial tension leads to a lower force that holds the droplet connected to the pore. At the same time the drag force, which is dependent on the viscosity of the continuous phase, is increased, and thus the droplet detaches more easily (at a higher capillary number). For both the 49% points and the other points, an increase as a function of the oil flow rate is visible, which is in line with figure 3.7.

Figure 3.9 a and b give the results of D_v as a function of the oil flow rate for 0, 0.001, 0.01, 0.1 and 1% Tween 20 and 0, 0.25 and 1% SDS, respectively. For both figures, D_v increases as a function of the oil flow rate. The solution with the highest concentration of Tween 20 (1%) seems to give smaller D_v values than the other Tween 20 solutions of which the concentration surfactant does not yet seem to influence the droplet

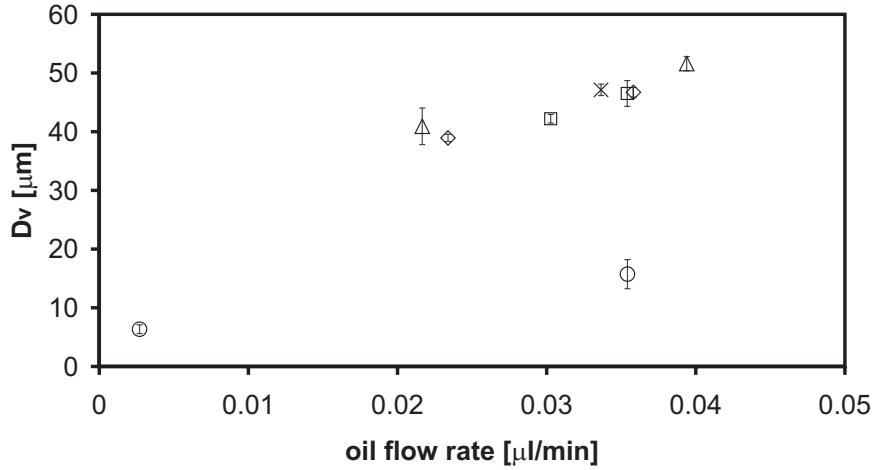
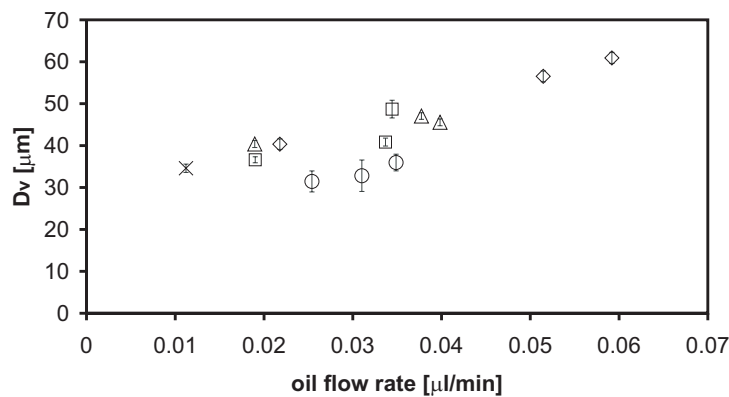


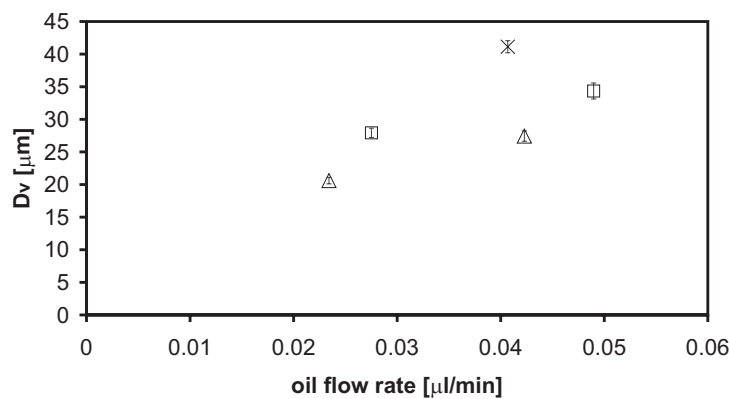
Figure 3.8: D_v as a function of the oil flow rate of aqueous ethanol solutions with 0 % (\times), 2.5 % (\square), 5% (\triangle), 10% (\diamond) and 49% (\circ) ethanol at a constant continuous phase flow rate of $10 \mu\text{l}\cdot\text{min}^{-1}$. Error bars on the y-axis indicate 95% reliability interval.

diameter. Apparently, only at a very high concentration of Tween 20, about a factor 140 above the CMC of $0.07 \text{ g}\cdot\text{l}^{-1}$ (see table 3.3), there is an influence of a decreased interfacial tension on the droplet size. A possible reason for the small influence of the lower surfactant concentration on the droplet size is the fact that droplet formation is very fast. Only at very high Tween 20 concentrations, a considerable amount of surfactant adsorbs. Figure 3.9a also shows that for 1% Tween 20, the variability is larger. The droplet formation movies show that for 1% Tween 20 droplets do not detach at the pore, which is common for Tween 20. Instead, droplets detach somewhat away from the pore and not always at exactly the same place. This is a likely cause of the larger error bars.

Figure 3.9b shows the influence of the surfactant concentration on D_v for SDS as well. Both the 0.25% and the 1% SDS give smaller D_v 's than de-ionized water without surfactants. SDS has a CMC of $2.4 \text{ g}\cdot\text{l}^{-1}$, which corresponds to 0.24%, so the used SDS concentrations are just above the CMC. A possible reason why for SDS, surfactant concentrations just above the CMC have an influence and Tween 20 not, is that SDS is a much smaller molecule and will diffuse faster to the interface. Table 3.3 gives the properties of both surfactants and confirms that the diffusion coefficient of SDS is larger than for Tween 20.



a.



b.

Figure 3.9: D_v as a function of the oil flow rate of 0 % (\times), 0.001 % (\square), 0.01% (\triangle), 0.1% (\diamond) and 1% (\circ) Tween 20 (a); 0 % (\times), 0.25 % (\square) and 1% (\triangle) SDS (b) solutions at a constant continuous phase flow rate of $10 \mu\text{l}\cdot\text{min}^{-1}$. Error bars on the y-axis indicate 95% reliability interval.

Table 3.3: Molecular formula, molecular weight (M_w), diffusion coefficient (D) and critical micel concentration (CMC) of the surfactants Tween 20 and SDS.

surfactant	molecular formula	M_w [g·mole ⁻¹]	D [m ² ·s ⁻¹]	CMC [g·l ⁻¹]
Tween 20	C ₅₈ H ₁₁₄ O ₂₆	1227.7	$8.3 \cdot 10^{-11}$ [22]	0.07 [23]
SDS	C ₁₂ H ₂₅ OSO ₃ Na	288.4	$3 \cdot 10^{-10}$ [24] ¹	2.4 [7]

The influence of the oil flow rate is at least as important as the concentration surfactant or alcohol for the droplet size. Only for 49% ethanol, the measured droplet size is considerably lower; this is a combined effect of both a decreased interfacial tension and an increased viscosity. The in-

¹According to Walstra [24] for small molecules D is in the order of $3 \cdot 10^{-10} \text{ m}^2\cdot\text{s}^{-1}$.

fluence of the oil flow rate is interesting in view of the well-known Peng and Williams force and torque balance models that state that in membrane emulsification only two forces are important, namely the interfacial tension force which holds the droplet connected to the pore and the drag force which detaches the droplet. The oil flow rate does not come into play. Schröder *et al.* [19] show that there is a regime, dependent on a.o. pore size, concentration and type surfactant, where the oil flow rate (or transmembrane pressure) does not influence the droplet size and in this regime the Peng and Williams models seem to be able to predict the final droplet sizes. They also show that there is a regime where the droplet size increases as a function of the oil flow rate. Usually, this is explained by the idea that the interfacial tension force becomes larger because of depletion of surfactants due to a fast growing droplet [25]. As a consequence, the interfacial tension force, which holds the droplet connected to the pore increases and droplets detach at a later stage, and thus become larger. The results in figure 3.7-3.9 clearly show that this cannot be the only reason in our system. Figure 3.7 shows that there is a definite influence of the oil flow rate on the droplet size while the surfactant concentration seems to be of less importance. This suggests that also in membrane emulsification there is a direct influence of the oil flow rate (i.e. not only an indirect influence via depletion of surfactant).

Droplet formation time

Figure 3.10 gives the average droplet formation time as a function of the oil flow rate for aqueous ethanol solutions. Again, the 49% ethanol points are different from the other points and have much smaller droplet formation times. For the other points, a decrease in droplet formation time as a function of oil flow rate is visible, which seems to converge to a constant value of about 13 ms at high oil flow rates. The average droplet formation time as a function of the oil flow rate for Tween 20 and SDS is given in figure 3.11. Figure 3.11a shows also a decrease in droplet formation time as a function of the oil flow rate and also seems to go to a constant value comparable to the value found with the ethanol systems at high oil flow rates. The 1% points (\circ) have a smaller droplet formation time than the other points and this confirms our hypothesis that only for 1% Tween 20 (considerable) surfactant adsorption took place. For SDS (figure 3.11b) the droplet formation time is considerably lower than for de-ionised water

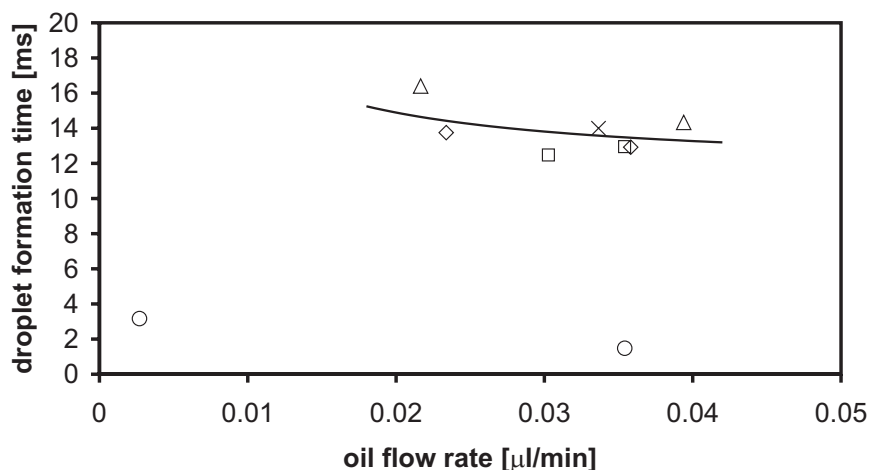
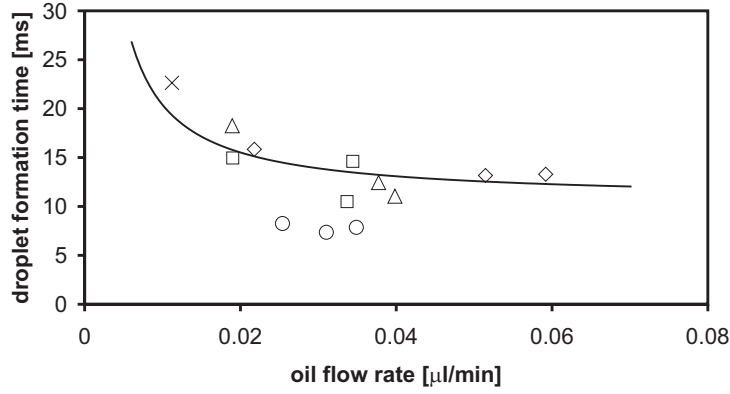


Figure 3.10: Average droplet formation time as a function of aqueous ethanol solutions with 0 % (\times), 2.5 % (\square), 5% (\triangle), 10% (\diamond) and 49% (\circ) ethanol at a constant continuous phase flow rate of $10 \mu\text{l}\cdot\text{min}^{-1}$. For the fit, the 49% ethanol points (\circ) were not taken into account. The error in the average droplet formation time is $< 1\%$ (the individual droplet formation times were not determined).

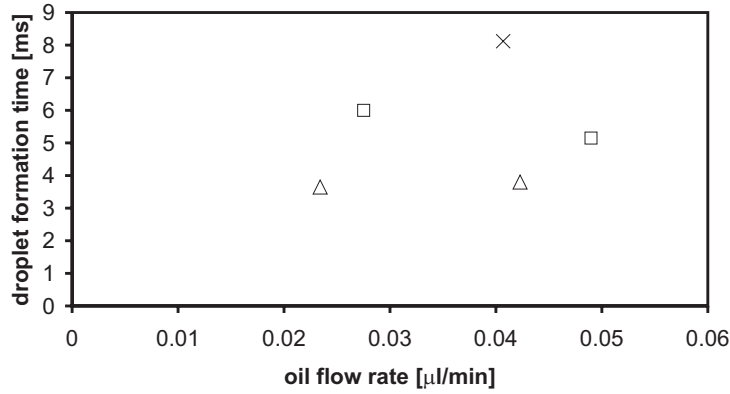
and most droplet formation times of ethanol and Tween 20 (figure 3.10 and 3.11a). This confirms the idea that droplets detach earlier, because there is adsorption of surfactants both for 0.25 and 1% SDS.

The droplet formation times given in figure 3.11 can be used to calculate the relative expansion rate of a droplet (see Appendix B) and therewith estimate the (average) dynamic interfacial tension just before detachment (for further explanation we refer to [11]). Although the equilibrium interfacial tension for the different concentrations Tween 20 is comparable (see table 3.1), estimation of the dynamic interfacial tension for 1% Tween 20 gives by far a much lower value (approximately $15 \text{ mN}\cdot\text{m}^{-1}$) than the interfacial tension of a bare hexadecane-water interface and the estimations of other Tween 20 concentrations (all in the range $30\text{-}44 \text{ mN}\cdot\text{m}^{-1}$), which justifies not taking the 1% Tween 20 points into account in fitting the data.

It is to be expected on the basis of the force and torque balance models that a droplet first has to become larger than a certain size (V_{crit}), at which the drag force exerted by the continuous phase balances the interfacial tension force. From this moment (t_{crit}), the droplet can start to detach. We hypothesize here, that this detachment process is not infinitely fast, but requires a certain time (t_{neck}), which may be dependent on the system. The idea that necking takes some time can explain the influence of the oil



a.



b.

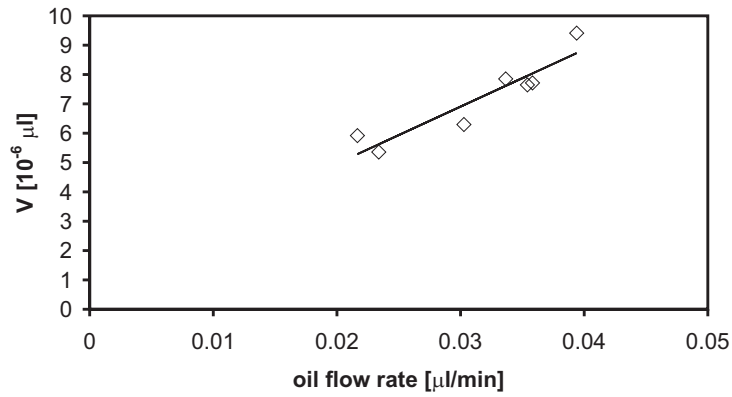
Figure 3.11: Average droplet formation time as a function of the oil flow rate of 0 % (\times), 0.001 % (\square), 0.01% (\triangle), 0.1% (\diamond) and 1% (\circ) Tween 20 (a); 0 % (\times), 0.25 % (\square) and 1% (\triangle) SDS (b) solutions at a constant continuous phase flow rate of $10 \mu\text{l}\cdot\text{min}^{-1}$. For the fit in figure 3.11a the 1% Tween 20 points (\circ) were not taken into account. The error in the average droplet formation time is $< 1\%$ (the individual droplet formation times were not determined).

flow rate on the droplet size even in the absence of surfactants. This was also put forward by Umbanhowar *et al.* [4], who studied droplet formation at a (three-dimensional) capillary. Also literature about droplet formation in microgravity assume both an expansion and a detachment stage [26]. Equation 3.1 gives the final volume of the droplet (V) with ϕ_v the oil flow rate during both droplet formation and the necking process ($\phi_{neck} = \phi_v$ is assumed, because we applied a constant oil flow rate) :

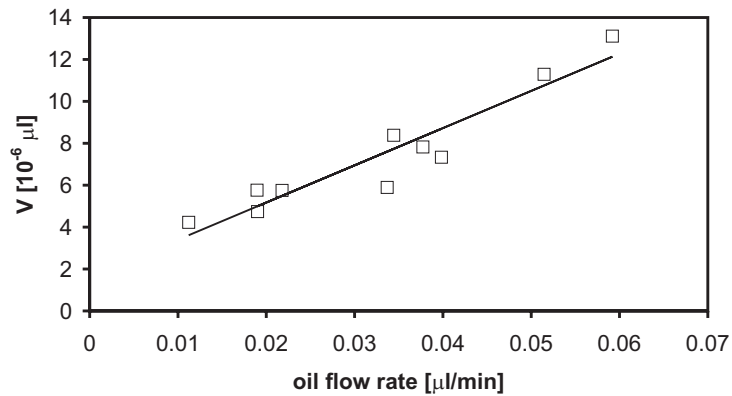
$$V = \phi_v \cdot (t_{crit} + t_{neck}) = V_{crit} + t_{neck} \cdot \phi_v. \quad (3.1)$$

Plotting the droplet formation time which is the sum of t_{crit} , which decreases as the oil flow rate increases, and the constant value t_{neck} as a func-

tion of the flow rate gives the fits in figure 3.10 and 3.11a ($t = t_{crit} + t_{neck} = \frac{V_{crit}}{\phi_v} + t_{neck}$ with fitting parameters, V_{crit} and t_{neck} , derived below). The 49% ethanol points and the 1% Tween 20 points were not taken into account in the fits in figure 3.10 and 3.11a respectively, because these systems showed different behaviour. At low flow rates, the droplet formation time is mostly determined by t_{crit} while at higher flow rates the droplet formation time approaches the value of t_{neck} . In case of different fluid phase properties (e.g. interfacial tension, viscosities), V_{crit} (and thus D_{crit}) have different values. This explains the small values for the 49% ethanol system, the SDS and 1% Tween 20 systems. Of course, a smaller V_{crit} corresponds to a smaller t_{crit} , and thus a smaller total droplet formation time. We fitted the Tween



a.



b.

Figure 3.12: Droplet volume as a function of the oil flow rate for ethanol (a) and Tween 20 (b) and their fits: $y = 1.08 + 194 \cdot x$ for ethanol and $y = 1.62 + 178 \cdot x$ for Tween 20.

20 data (without the 1% data points) and the ethanol data (without the 49% points) and assumed that the different concentrations Tween 20 and ethanol did not have an influence on the value of V_{crit} (this assumption is

based on the results of the droplet diameters which show no influence on the droplet size). Figure 3.12 shows the droplet volumes for both ethanol (a) and Tween 20 (b) as a function of the oil flow rate and their fits which are in good agreement with the measured data. For ethanol, the fit gives a t_{neck} of 11.7 ms and a V_{crit} of $1.08 \cdot 10^{-6}$ μl , which corresponds to a critical diameter, D_{crit} , of 16.6 μm . For Tween 20, a t_{neck} of 10.7 ms and a V_{crit} of $1.62 \cdot 10^{-6}$ μl are found. This value corresponds to a D_{crit} of 20.3 μm . Both fits show a t_{neck} of about 11 ms, which means that for hexadecane droplets formed in aqueous solutions with little surfactant or ethanol (comparable with de-ionised water) the necking process takes about 11 ms.

Conclusions

Monodisperse droplets can be produced in a T-junction of rectangular channels in a glass microchip and act as a quasi two-dimensional model system for cross-flow membrane emulsification. In this glass chip droplet formation can be observed from aside and the influence of different parameters can be studied by following the droplet formation process.

It was found that in these systems, snap-off could only occur when the thickness of the oil phase neck is smaller than the channel height; this was also observed experimentally.

Droplet formation and detachment of hexadecane droplets in aqueous ethanol solutions is different than droplet formation in other solutions. Experiments with an aqueous solution containing 49% ethanol showed clearly a different behaviour due to the lowered interfacial tension and increased viscosity of this solution.

Only in aqueous solutions with SDS and 1% Tween 20 considerable adsorption of surfactant was found to significantly influence the droplet formation process and smaller droplets were formed in shorter droplet formation times. Droplet formation in the other aqueous solutions is comparable to droplet formation in de-ionised water, which indicates that droplet formation was faster than surfactant adsorption. One of the most important parameters determining droplet size was the oil flow rate. This cannot be explained by the (static) force or torque balance model and clearly shows the strong and direct influence of fluid dynamics on the process, apart from the influence via the dynamic interfacial tension.

The droplet size could be described by a model that assumes that the final droplet size consists of both a critical volume determined by a force

or torque balance and a contribution to the volume caused by a certain necking time. The oil flow rate during the necking process contributes to the final droplet size and this explains the influence of the oil flow rate on the final droplet size. The experimental results can be fitted by the model; the necking time was thus found to be 11 ms.

Acknowledgement

This research was supported by the European Community, project QLRT-2000-01228. The authors thank Jan Benjamins for the fruitful discussions and his help with the drop shape tensiometry measurements.

Nomenclature

A	interfacial area (m^2)
D	diffusion coefficient ($\text{m}^2 \cdot \text{s}^{-1}$)
D_c	depth of the channel (m)
D_{crit}	critical droplet diameter determined by force or torque balance (m)
D_{detach}	diameter of droplet attached to wall (m)
D_h	horizontal diameter of droplet (m)
D_{neck}	diameter of the neck (m)
D_v	vertical diameter of droplet (m)
L_{detach}	length from left wall pore to end of droplet (m)
$L_{penetration}$	penetration length (m)
M_w	molecular weight ($\text{g} \cdot \text{mol}^{-1}$)
$R_{1,2}$	radii of curvature (m)
R_c	half of the channel depth (m)
R_d	radius of a droplet (m)
R_{dr}	radius of a deformed droplet connected to the pore via a neck (m)
R_{neck}	radius of the neck (m)
R_{nz}	radius of the neck perpendicular to the depth of the channel (m)
v_{cont}	continuous phase velocity ($\text{m} \cdot \text{s}^{-1}$)
V	(final) droplet volume (l or m^3)
V_{crit}	critical droplet volume determined by force or torque balance (l or m^3)
t	(droplet formation) time (s)
t_{crit}	critical droplet formation time (s)
t_{neck}	necking time (s)

Greek letters

$\Delta P_{Laplace}$	Laplace pressure (Pa)
η	dynamic viscosity ($\text{Pa} \cdot \text{s}$)
ρ	density ($\text{g} \cdot \text{l}^{-1}$)
ϕ_{neck}	oil flow rate during necking ($\text{l} \cdot \text{min}^{-1}$ or $\text{m}^3 \cdot \text{s}^{-1}$)
ϕ_v	oil flow rate ($\text{l} \cdot \text{min}^{-1}$ or $\text{m}^3 \cdot \text{s}^{-1}$)
σ	interfacial tension ($\text{N} \cdot \text{m}^{-1}$)
σ_{eq}	equilibrium interfacial tension ($\text{N} \cdot \text{m}^{-1}$)

Appendix A: Analysis of the Laplace pressures

The Laplace pressure is written as:

$$\Delta P_{Laplace} = \sigma \left(\frac{1}{R_1} + \frac{1}{R_2} \right). \quad (3.2)$$

We assume that the interfacial tension is the same for the whole droplet and that only the radii of curvature determine the differences in Laplace pressure in the droplet. Figure 3.13 shows the relevant radii of curvature.

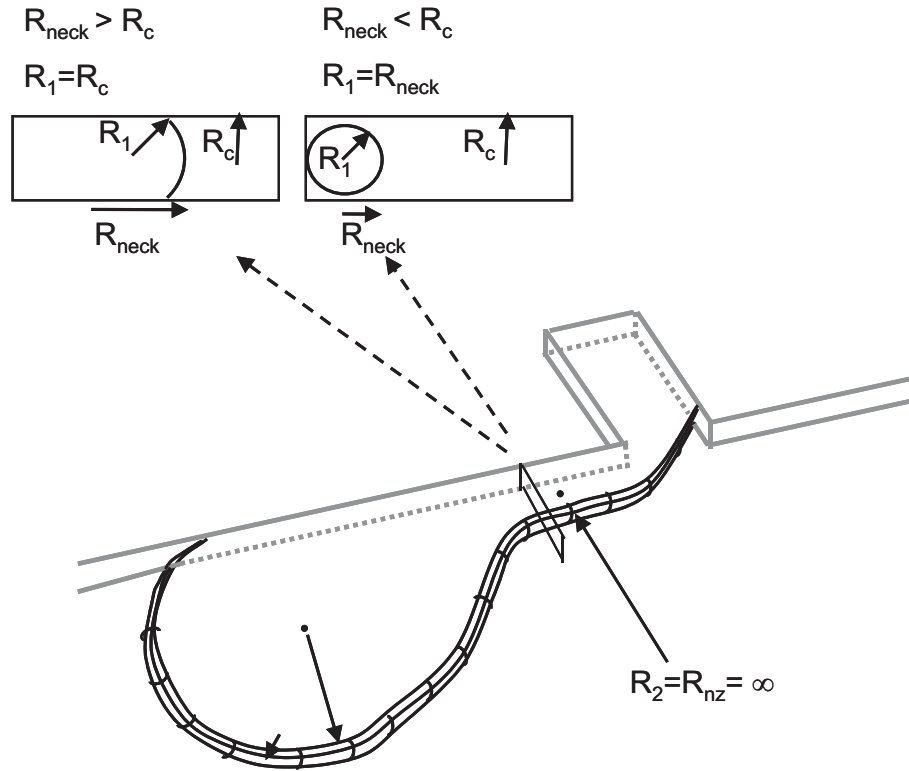


Figure 3.13: Schematic overview of the relevant radii of curvature.

Before detachment, $R_{neck} > R_c$ (=half of the channel depth), which means that $\Delta P_{Laplace}$ in the neck is not determined by R_{neck} but by R_c . The other radius of curvature in the neck parallel to the direction of flow, R_{nz} , is almost infinite because the oil-aqueous interface is quite flat before detachment (see also figure 3.3-3.4). $\Delta P_{Laplace}$ in the neck becomes:

$$\Delta P_{Laplace,neck} = \sigma \left(\frac{1}{R_c} + \frac{1}{R_{nz}} \right). \quad (3.3)$$

In the droplet (connected to the pore by the neck) the Laplace pressure is

determined by R_c and by R_{dr} , which is half of D_{detach} :

$$\Delta P_{Laplace,droplet} = \sigma \left(\frac{1}{R_c} + \frac{1}{R_{dr}} \right), \quad (3.4)$$

$$\Delta P_{Laplace,neck} - \Delta P_{Laplace,droplet} = \sigma \left(\frac{1}{R_{nz}} - \frac{1}{R_{dr}} \right) \approx -\frac{\sigma}{R_{dr}}. \quad (3.5)$$

Because $R_{nz} \gg R_{dr}$, $\Delta P_{Laplace,neck} < \Delta P_{Laplace,droplet}$ and the neck is stabilized by a driving force for fluid flow from the droplet to the neck as long as the neck is squeezed in between top and bottom ($R_{neck} > R_c$). When $R_{neck} < R_c$, the Laplace pressure in the neck is no longer determined by R_c :

$$\Delta P_{Laplace,neck} = \sigma \left(\frac{1}{R_{neck}} + \frac{1}{R_{nz}} \right). \quad (3.6)$$

At a certain moment $\Delta P_{Laplace,neck} = \Delta P_{Laplace,droplet}$, the neck is no longer stabilized and snap-off can take place:

$$\sigma \left(\frac{1}{R_{neck}} + \frac{1}{R_{nz}} \right) = \sigma \left(\frac{1}{R_c} + \frac{1}{R_{dr}} \right), \quad (3.7)$$

$$\frac{1}{R_{neck}} \approx \left(\frac{1}{R_c} + \frac{1}{R_{dr}} \right). \quad (3.8)$$

With $R_c = 2.5 \mu\text{m}$ and depending on the value of R_{dr} (10-20 μm) and the wetting properties in the channel, R_{neck} will have a value around 2 μm and the theoretically determined critical neck diameter will have a value around 4 μm , which is in correspondence with our experimental results.

Appendix B: Derivation of relative expansion rate in a glass chip

We assume that the volume of a droplet, V , is dependent on the flow rate, ϕ_v , and the time, t . We approximate the interface, A , as a slice of a cylinder with depth D_c , radius R_d and assume there is no influence of the deformation and neck formation on the relative expansion rate.

$$V = \phi_v t = D_c \pi R_d^2, \quad (3.9)$$

$$R_d = \sqrt{\frac{\phi_v t}{D_c \pi}}, \quad (3.10)$$

$$A = 2D_c \pi R_d, \quad (3.11)$$

$$\frac{dA}{dt} = \frac{dA}{dV} \frac{dV}{dt} = \frac{2D_c \pi}{2D_c \pi R_d} \phi_v = \frac{\phi_v}{R_d} = \frac{\phi_v}{\phi_v^{1/2} t^{1/2} D_c^{-1/2} \pi^{-1/2}}, \quad (3.12)$$

$$\frac{1}{A} = \frac{1}{2D_c \pi R_d} = \frac{1}{2D_c \pi \phi_v^{1/2} t^{1/2} D_c^{-1/2} \pi^{-1/2}}, \quad (3.13)$$

$$\frac{d \ln A}{dt} = \frac{1}{A} \frac{dA}{dt} = \frac{1}{2D_c \pi \phi_v^{1/2} t^{1/2} D_c^{-1/2} \pi^{-1/2}} \frac{\phi_v}{\phi_v^{1/2} t^{1/2} D_c^{-1/2} \pi^{-1/2}}, \quad (3.14)$$

$$\frac{d \ln A}{dt} = \frac{1}{2t}. \quad (3.15)$$

References

1. T. Nakashima, M. Shimizu, M. Kukizaki, Membrane emulsification by microporous glass, *Key Eng. Mat.* 61&62 (1991) 513.
2. S. Okushima, T. Nisisako, T. Torii, T. Higuchi, Controlled production of monodisperse double emulsions by two-step droplet breakup in microfluidic devices, *Langmuir* 20, 23 (2004) 9905.
3. S. Sugiura, M. Nakajima, J. Tong, H. Nabetani, M. Seki, Preparation of monodispersed solid lipid microspheres using a microchannel emulsification technique, *J. Colloid Interface Sci.* 227 (2000) 95.
4. P.B. Umbanhowar, V. Prasad, D.A. Weitz, Monodisperse emulsion generation via drop break off in a coflowing stream, *Langmuir* 16, 2 (2000) 347.
5. S.L. Anna, N. Bontoux, H.A. Stone, Formation of dispersions using "flow focusing" in microchannels, *Appl. Phys. Lett.* 82, 3 (2003) 364.
6. D.R. Link, S.L. Anna, D.A. Weitz, H.A. Stone, Geometrically mediated breakup of drops in microfluidic devices, *Phys. Rev. Lett.* 92, 5 (2004) 054503-1.
7. V. Schröder, Herstellen von Öl-in-Wasser-Emulsionen mit mikroporösen Membranen, Ph.D. thesis, University Karlsruhe, 1999.
8. A.J. Abrahamse, R. van Lierop, R.G.M. van der Sman, A. van der Padt, R.M. Boom, Analysis of droplet formation and interactions during cross-flow membrane emulsification, *J. Membr. Sci.* 204, 1-2 (2002) 125.
9. M. Yasuno, M. Nakajima, S. Iwamoto, T. Maruyama, S. Sugiura, I. Kobayashi, A. Shono, K. Satoh, Visualization and characterization of SPG membrane emulsification, *J. Membr. Sci.* 210, 1 (2002) 29.
10. N.C. Christov, D.N. Ganchev, N.D. Vassileva, N.D. Denkov, K.D. Danov, P.A. Kralchevsky, Capillary mechanisms in membrane emulsification: oil-in-water emulsions stabilized by Tween 20 and milk proteins, *Colloids Surfaces A: Physicochem. Eng. Aspects* 209 (2002) 83.
11. S. van der Graaf, C.G.P.H. Schroën, R.G.M. van der Sman, R.M. Boom, Influence of dynamic interfacial tension on droplet formation during membrane emulsification, *J. Colloid Interface Sci.* 277, 2 (2004) 456.
12. S. Labourdenne, N. Gaudry-Rolland, S. Letellier, M. Lin, A. Cagna, G. Esposito, R. Verger and C. Rivière, The oil-drop tensiometer: potential applications for studying the kinetics of (phospho)lipase action, *Chem. Phys. Lipids* 71 (1994) 163.
13. R.C. Weast, M.J. Astle (Eds.), CRC Handbook of Chemistry and Physics: a ready-reference book of chemical and physical data, 59th edition, 1978-1979, CRC press, Florida, p. F-45.
14. E.J.W. Wensink, A.C. Hoffmann, P.J. van Maaren, D. van der Spoel, Dynamic properties of water/alcohol mixtures studied by computer simulation, *J. Chem. Phys.* 119, 14 (2003) 7308.
15. L.P.B.M. Janssen, M.M.C.G. Warmoeskerken, Transport phenomena data companion, 1987, Edward Arnold, London and Delftse Uitgevers Maatschappij, Delft.

16. A.J. Gijsbertsen-Abrahamse, A. van der Padt, R.M. Boom, Status of cross-flow membrane emulsification and outlook for industrial application, *J. Membr. Sci.* 230 (2004) 149.
17. T. Nisisako, T. Torii, T. Higuchi, Novel microreactors for functional polymer beads, *Chem. Eng. J.* 101, 1-3 (2004) 23.
18. V. Cristini, Y.-C. Tan, Theory and numerical simulation of droplet dynamics in complex flows - a review, *Lab Chip* 4, 4 (2004) 257.
19. V. Schröder, O. Behrend, H. Schubert, Effect of dynamic interfacial tension on the emulsification process using microporous, ceramic membranes, *J. Colloid Interface Sci.* 202, 2 (1998) 334.
20. T. Nisisako, T. Torii, T. Higuchi, Droplet formation in a microchannel network, *Lab Chip* 2, 1 (2002) 24.
21. S. van der Graaf, T. Nisisako, C.G.P.H. Schroën, R.G.M. van der Sman, R.M. Boom, Lattice Boltzmann simulations of droplet formation in a T-shaped microchannel, submitted (2005).
22. M. Rayner, G. Trägårdh, Transfer of surfactants to an expanding oil water interface during membrane emulsification, *Proceedings LiFT symposium Gothenburg* (2003) 68.
23. K. Shimizu, M. Iwatsuru, Measurement of the distribution parameter in solubilized systems. 2. Measurement of the distribution parameter of alkylparabens and alkyl gallates in ionic and nonionic surfactant solutions, *Chem. Pharm. Bull.* 36, 2 (1988) 726.
24. P. Walstra, Physical Chemistry of Foods, 2003, Marcel Dekker Inc., New York-Basel, p. 348.
25. V. Schröder, H. Schubert, Production of emulsions using microporous, ceramic membranes, *Colloids Surfaces A: Physicochem. Eng. Aspects* 152 (1999) 103.
26. I. Kim, Y. Kamotani, S. Ostrach, Modeling bubble and drop formation in flowing liquids in microgravity, *AIChE J.* 40, 1 (1994) 19.

Chapter 4

Lattice Boltzmann simulations of droplet formation in a T-shaped microchannel

Abstract

We investigated the formation of a droplet from a single pore in a glass chip, which is a model system for droplet formation in membrane emulsification. Droplet formation was simulated with the lattice Boltzmann method, a method suitable for modeling on mesoscale. We validated the lattice Boltzmann code with several benchmarks like the flow profile in a rectangular channel, droplet deformation between two shearing plates and a sessile drop on a plate with different wetting conditions. In all cases, the modelling results were in good agreement with the benchmark. Comparison of experimental droplet formation in a microchannel glass chip showed good quantitative agreement with the modelling results. With this code, droplet formation simulations with various interfacial tensions and various flow rates were performed. All resulting droplet sizes could be correlated quantitatively with the capillary number and the fluxes in the system.

This chapter has been submitted as: S. van der Graaf, T. Nisisako, C.G.P.H. Schroën, R.G.M. van der Sman, R.M. Boom, Lattice Boltzmann simulations of droplet formation in a T-shaped microchannel.

Introduction

Emulsions consist of droplets of one liquid dispersed in an other liquid. They are widely used as food, cosmetic and pharmaceutical products. Many underlying mechanisms for emulsion droplet formation are still poorly understood, in spite of the fact that droplet size and droplet size distribution are generally regarded as important product properties [1]. Some relatively new experimental techniques for the production of monodisperse emulsions have been reported, like membrane emulsification [2], (straight-through) microchannel emulsification [3, 4], flow focusing and microfluidic devices [5, 6].

Some numerical studies with various calculation methods have been reported on droplet formation. Abrahamse *et al.* [7] simulated the process of droplet break up in cross-flow membrane emulsification using CFX with the VOF method and Ohta *et al.* [8] used a VOF method to study the formation of a single droplet at an orifice in a pulsed sieve-plate column. Quite recently, both Kobayashi *et al.* [9] and Rayner *et al.* [10] simulated droplet formation from straight-through microchannels using a CFD software package (CFD-ACE+) with the so-called piecewise linear interface construction (PLIC) method and the Surface Evolver, respectively. For a recent review about numerical simulations of droplet dynamics in complex flows we refer to Cristini and Tan [11].

Although the mentioned CFD packages give a general idea of droplet break up, not all phenomena are modelled on a solid physical basis, which can result in ambiguous results, as is the case for modelling contact line dynamics [12]. Therefore, in this study, the lattice Boltzmann method is used which is positioned in between the continuum level described by the Navier-Stokes equation and the microscopic (molecular) level. Lattice Boltzmann is a relatively new simulation technique that is based on hypothetical particles (packages of fluid) that move and collide on a lattice according to the kinetic gas theory. The method is suitable for modelling processes on mesoscale and above that, it is possible to extend it to a multiphase model [13] that has a physical, thermodynamic basis such that components as surfactants and polymers can be incorporated [14, 15]. Another advantage is that with the lattice Boltzmann methodology it is not necessary to track the interface explicitly; the interface arises naturally from the thermodynamic basis of the method. A typical mesoscopic phenomenon that can be described by lattice Boltzmann is thus droplet formation at small length

scales in confined geometries. For such a system with mobile contact interfaces in small channels, a correct description of all interfaces (including wetting) is important [16].

The objective of this study is to achieve a better understanding of droplet formation from a pore in a T-shaped microchannel. We evaluate the influence of various parameters on droplet formation with the lattice Boltzmann method and compare results of the simulations with experimental results of droplet formation in a T-shaped microchannel. We first discuss the theoretical background of the lattice Boltzmann method, including the implementation of the multiphase model and the wetting boundary conditions. Then, some benchmarks of the code are presented: the flow through the channel is compared to the analytical relation of single phase flow through a channel with the same geometry, the deformation of a droplet in linear shear is investigated and further the wetting boundary conditions are tested. In the next section, simulations of droplet formation in a T-junction are presented and the results of the simulations are compared with experimental results. Finally, a parameter study is presented in which the influence of the interfacial tension and flow rates on the final droplet size is investigated. These results are then compiled into one scaling rule.

Lattice Boltzmann simulations of droplets

Several models are known in literature to describe multiphase systems with the lattice Boltzmann approach, for example the model based on interparticle potentials and the model based on free energy.

The model using interparticle potentials to model multiphase flows in lattice Boltzmann was first proposed by Shan and Chen [17]. Droplet deformation and break up was described with this model in 2D for a liquid-liquid system [18]. With the same code (the *FlowLab* code) coalescence of bubbles was described in 2D [19]. In another article [20] the displacement of a two-dimensional, immiscible droplet subject to gravitational forces in a channel was studied. One of the major drawbacks of this method is the fact that the interfacial tension in this model is actually a numerical artefact and its value is fixed after one chooses the value of the strength of the interparticle potential. This creates difficulties in applications in which the interfacial tension is variable, because the value cannot be set independently [21].

The model based on a Ginzburg-Landau free energy approach for phase transition was developed by Swift and co-workers [13, 22]. Based on this, Desplat *et al.* [23] developed a complete multiphase 3D code which is quite flexible. Theissen and Gompper [24] used an elaborated Ginzburg-Landau free energy functional for a ternary system (oil, water and surfactants) in which spontaneous emulsification took place. Lamura *et al.* [14, 15] extended the code to a ternary system with surfactants as well. An advantage of the Ginzburg-Landau free energy approach is that the diffuse interface evolves through the mesh due to chemical potential gradients. The interface does not have to be tracked separately. However the interface is diffuse; i.e. the transition of one phase to another is not abrupt but somewhat gradual. As a physical interface is quite sharp, the diffuse interface is a numerical artefact. This has to be taken into account in the interpretation of the results. For modelling droplet formation and detachment, as presented in this article, we have developed a multiphase 3D code based on this Ginzburg-Landau free energy approach for a continuous water phase, a dispersed oil phase and a solid phase that represents the microchannel.

Model

The simulations are based on the lattice Boltzmann scheme developed by Swift *et al.* [13]. This scheme is based on a free energy functional which is explained below.

Lattice Boltzmann scheme

In this method the dynamics are defined by the velocity distribution functions $f_i(\mathbf{x}, t)$ to model the total density, ρ , and $g_i(\mathbf{x}, t)$ to model the order parameter, ϕ , defined at each lattice site \mathbf{x} at each time t . The distribution functions evolve during a timestep Δt according to the lattice Boltzmann equation:

$$f_i(\mathbf{x} + \mathbf{c}_i \Delta t, t + \Delta t) - f_i(\mathbf{x}, t) = -\frac{1}{\tau} [f_i(\mathbf{x}, t) - f_i^{eq}(\mathbf{x}, t)], \quad (4.1)$$

$$g_i(\mathbf{x} + \mathbf{c}_i \Delta t, t + \Delta t) - g_i(\mathbf{x}, t) = -\frac{1}{\tau_\phi} [g_i(\mathbf{x}, t) - g_i^{eq}(\mathbf{x}, t)], \quad (4.2)$$

where $f_i^{eq}(\mathbf{x}, t)$ and $g_i^{eq}(\mathbf{x}, t)$ are local equilibrium distributions, τ and τ_ϕ independent relaxation parameters and \mathbf{c}_i is the velocity vector. We mostly

work with nineteen velocity vectors in three dimensions (D_3Q_{19} lattice), i.e. a zero velocity vector ($i = 0$), the nearest ($i = 1..6$) and next-nearest ($i = 7..18$) vectors on a cubic lattice (some benchmark studies were done in a two dimensional lattice). The distribution functions are related to the total density, ρ , to the mean fluid velocity, \mathbf{u} , and to the scaled density difference, the order parameter ϕ , through:

$$\rho = \sum_i f_i, \quad \rho u = \sum_i f_i \mathbf{c}_i, \quad \phi = \sum_i g_i. \quad (4.3)$$

These quantities are locally conserved in any collision process. The higher order moments of the local equilibrium distribution functions should satisfy:

$$\sum_i f_i^{eq} c_{i,\alpha} c_{i,\beta} = P_{\alpha\beta} + \rho u_\alpha u_\beta, \quad (4.4)$$

$$\sum_i f_i^{eq} c_{i,\alpha} c_{i,\beta} c_{i,\gamma} = \rho c_s^2 (u_\alpha \delta_{\beta\gamma} + u_\beta \delta_{\alpha\gamma} + u_\gamma \delta_{\alpha\beta}), \quad (4.5)$$

$$\sum_i g_i^{eq} c_{i,\alpha} = \phi u_\alpha, \quad (4.6)$$

$$\sum_i g_i^{eq} c_{i,\alpha} c_{i,\beta} = \Gamma \mu \delta_{\alpha\beta} + \phi u_\alpha u_\beta, \quad (4.7)$$

where Γ is a coefficient related to the mobility of the fluid, c_s the speed of sound, $\delta_{\alpha\beta}$ the Kronecker delta ($\delta_{\alpha\beta}=1$ for $\alpha = \beta$ and $\delta_{\alpha\beta}=0$ for $\alpha \neq \beta$) and $P_{\alpha\beta}$ is the complete pressure tensor (see next section).

The local equilibrium distribution functions can be expressed as:

$$f_i^{eq} = A_k + B_k u_\alpha c_{i,\alpha} + C_k u^2 + D_k u_\alpha u_\beta c_{i,\alpha} c_{i,\beta} + G_{k\alpha\beta} c_{i,\alpha} c_{i,\beta}, \quad (4.8)$$

$$g_i^{eq} = H_k + K_k u_\alpha c_{i,\alpha} + J_k u^2 + Q_k u_\alpha u_\beta c_{i,\alpha} c_{i,\beta}. \quad (4.9)$$

The values of A , B , D , D , G , H , K , J , and Q have different values for the nearest ($i = 1..6$, $k = 1$ for D_3Q_{19}) and next-nearest ($i = 7..18$, $k = 2$ for D_3Q_{19}) vectors; the values are given in Appendix A. The value for the equilibrium distribution function of the zero velocity vector ($i = 0$) can be calculated via $\sum_i f_i^{eq} = \sum_i f_i = \rho$ and $\sum_i g_i^{eq} = \sum_i g_i = \phi$ by subtraction of the other equilibrium distribution functions from ρ or ϕ .

Free energy model

The free energy functional generally used in studies on a binary system is:

$$F = \int dx \left\{ c_s^2 \rho \ln \rho - \frac{A}{2} \phi^2 + \frac{B}{4} \phi^4 + \frac{\kappa}{2} (\nabla \phi)^2 \right\}, \quad (4.10)$$

where ϕ is again the order parameter which describes the normalized difference in density of the two fluids. The term c_s^2 , a term comparable to kT , corresponds with $\frac{c^2}{3}$ to obtain isotropic viscosity. The thermodynamic properties of the fluids follow directly from the free energy. The functional derivative of equation 4.10 gives the chemical potential difference between the two fluids:

$$\Delta\mu = \frac{\delta F}{\delta \phi} = -A\phi + B\phi^3 - \kappa \nabla^2 \phi, \quad (4.11)$$

with the definition for the derivative of $F = \int f(\phi, \nabla \phi) dx$, which is the functional of a function, $\phi(x)$, and the derivative of this function, $\nabla \phi(x)$:

$$\frac{\delta F}{\delta \phi} = \frac{\partial f}{\partial \phi} - \frac{\partial}{\partial x} \left[\frac{\partial f}{\partial \nabla \phi} \right]. \quad (4.12)$$

Also the pressure can be derived from equation 4.10. The scalar part, p_0 , of the pressure tensor is given by:

$$\begin{aligned} p_0 &= \phi \frac{\delta F}{\delta \phi} + \rho \frac{\delta F}{\delta \rho} - f(\rho, \phi) \\ &= c_s^2 \rho - \frac{A}{2} \phi^2 + \frac{3B}{4} \phi^4 - \kappa \phi (\nabla^2 \phi) - \frac{\kappa}{2} (\nabla \phi)^2. \end{aligned} \quad (4.13)$$

In this equation $f(\rho, \phi)$ is the free energy density, which is the integrand of equation 4.10. The last term of the complete pressure tensor (Korteweg-DeVries tensor), $P_{\alpha\beta}$, can be derived via the Gibbs-Duhem relation:

$$\nabla P_{\alpha\beta} = \phi \nabla \mu, \quad (4.14)$$

and now the complete pressure tensor becomes:

$$P_{\alpha\beta} = p_0 \delta_{\alpha\beta} + \kappa \partial_\alpha \phi \partial_\beta \phi. \quad (4.15)$$

The equilibrium order parameter in the bulk of the two fluids, $\phi = \pm \phi_0$, follows from equation 4.11 by setting $\nabla \phi = 0$:

$$\phi_0 = \pm \left(\frac{A}{B} \right)^{1/2}. \quad (4.16)$$

The parameters B and κ are always positive. When the value of A is positive phase separation occurs; when A is negative there is no phase separation. In this paper a positive value of A is used, because we want to model two immiscible phases, oil and water. The value of κ corresponds with the interfacial properties of the interface between the two fluids. A dimensionless measure for the interface thickness is given by the grid Cahn number (Ch^*):

$$Ch^* = \frac{\zeta}{\Delta x}, \quad (4.17)$$

in which ζ is defined with $\zeta = \sqrt{\frac{2\kappa}{A}}$. The profile of the order parameter at a planar oil-water interface in a quiescent fluid for an infinite system is given by [25]:

$$\phi(x) = \phi_0 \tanh(x/\zeta), \quad (4.18)$$

with $\pm\phi_0$ the value of the order parameter in the (water or oil) bulk phase. The interfacial tension σ for this interface is calculated from:

$$\sigma = \int_{-\infty}^{+\infty} \kappa \partial_x \phi^2 dx^2. \quad (4.19)$$

Substitution of the profile equation (4.18) in the integral equation (4.19), and subsequent integration gives the classical result for the interfacial tension:

$$\sigma_{ow} = \frac{4\kappa\phi_0^2}{3\zeta}. \quad (4.20)$$

In this paper we assumed equal densities for the oil and water phase. To allow for unequal kinematic viscosities for the two phases, we used a harmonic mean [26]:

$$\frac{\phi_0}{\nu(\phi)} = \frac{\phi_0 - \phi}{2\nu_1} + \frac{\phi_0 + \phi}{2\nu_2}, \quad (4.21)$$

with $\nu_{1,2}$ is the viscosity of water (1) or oil (2).

Wetting boundary conditions

The implemented wetting boundary conditions are comparable to those of Iwahara *et al.* [27], who used the boundary conditions for a solid wall in a vapour-liquid system in a D_2Q_9 lattice. In this work wetting boundary conditions were implemented in a liquid-liquid system in a D_2Q_9 and a D_3Q_{19} lattice. To incorporate wetting, a surface term dependent on the imposed wetting properties of the surface, is added to the free energy,

following Cahn [28] and Jerry and Nauman [29]. This approach was used before by Desplat *et al.* [23] and Briant *et al.* [30] to simulate wetting of a surface, however, our implementation is slightly different; the boundaries of the system are placed halfway between the lattice sites. For the walls or other solid obstacles that have specific wetting properties, we assign a certain value of the order parameter, ϕ , to the solid lattice site next to the wall. We use 19-point finite difference stencils for the calculation of the $\nabla^2\phi$ term in the chemical potential in equation 4.11. In these calculations for the fluid lattice sites next to the wall, we use the value of the order parameter assigned to the wall (ϕ_{wall}), resulting in a special case of the Cahn boundary condition [28]. In this way, the value of the chemical potential becomes dependent on the properties of the solid lattice sites nearby. If the value of the order parameter assigned to the solid lattice sites is equal to that of oil, the oil nearby these lattice sites will spread on the surface and the water phase will not spread on this surface. Vice versa, if the value of the order parameter assigned to the solid lattice sites is equal to that of water, water will spread on the surface and oil will not. For neutral wetting, the order parameter of the solid lattice sites is exactly in between the order parameter of the oil phase and the water phase ($\phi_{wall} = 0$).

Wetting properties are usually characterized with the contact angle of a solution on a surface. Young's law gives the relation between a contact angle and interfacial tensions. For a droplet of oil on a surface, surrounded by water, the contact angle is:

$$\cos(\theta) = \frac{\sigma_{w,wall} - \sigma_{o,wall}}{\sigma_{ow}}, \quad (4.22)$$

with $\sigma_{w,wall}$ the interfacial tension of water with the surface, $\sigma_{o,wall}$ the interfacial tension of oil with the surface and σ_{ow} the interfacial tension of the oil-water interface. The interfacial tension of the oil-water interface is already given by equation 4.20 and the interfacial tensions of the water or oil phase with the wall can be derived as well from equation 4.19 by calculating the integral from the wall at x_{wall} till infinity. For the oil phase at a planar wall with $\phi_{oil} = +\phi_0$ at $x \gg x_{wall}$ the integral becomes:

$$\sigma_{o,wall} = \int_{x_{wall}}^{+\infty} \kappa \partial_x \phi^2 dx^2, \quad (4.23)$$

with $\phi_0 \tanh(x_{wall}/\zeta) = \phi_{wall}$. This gives for the oil phase:

$$\sigma_{o,wall} = \frac{\kappa\phi_0^2}{\zeta} \left(2/3 - (\phi_{wall}/\phi_0 - \frac{1}{3}(\phi_{wall}/\phi_0)^3) \right). \quad (4.24)$$

For the water phase at a planar wall with $\phi_{water} = -\phi_0$ at $x \gg x_{wall}$:

$$\sigma_{w,wall} = \frac{\kappa\phi_0^2}{\zeta} \left(2/3 - (-\phi_{wall}/\phi_0 + \frac{1}{3}(\phi_{wall}/\phi_0)^3) \right). \quad (4.25)$$

Young's law (equation 4.22) gives the relation between $\tilde{\phi} = \phi_{wall}/\phi_0$ and the contact angle:

$$\cos(\theta) = 3/2\tilde{\phi}(1 - \frac{1}{3}\tilde{\phi}^2). \quad (4.26)$$

It is remarkable that the contact angle is nearly linear with ϕ_{wall} (see also figure 4.5). In contrast to the model of Briant *et al.* [30] this approach can be applied more easily to sharp corners, which are essential for T-shaped channels.

Validation of code

Flow in a rectangular channel

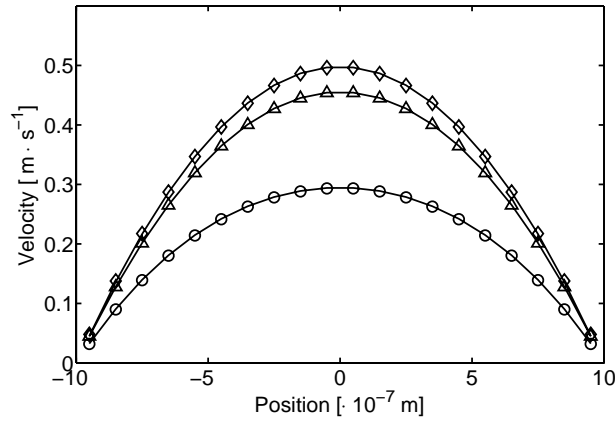
Single phase behaviour is verified with flow in a rectangular channel. Fully developed flow in a long channel with a flat rectangular cross section, like a glass chip, of width $2b$ and height $2c$ (walls at $x = \pm b$ and $z = \pm c$) has a specific flow profile depending on the values of b and c . The general solution for flow in a tube of rectangular cross section is given below [31, 32]:

$$v_y(x, z) = v_0 \left[1 - \left(\frac{z}{c} \right)^2 + 4 \sum_{k=1}^{\infty} \frac{(-1)^k}{\alpha_k^3} \frac{\cosh(\frac{\alpha_k x}{c})}{\cosh(\frac{\alpha_k b}{c})} \cos(\frac{\alpha_k z}{c}) \right], \quad (4.27)$$

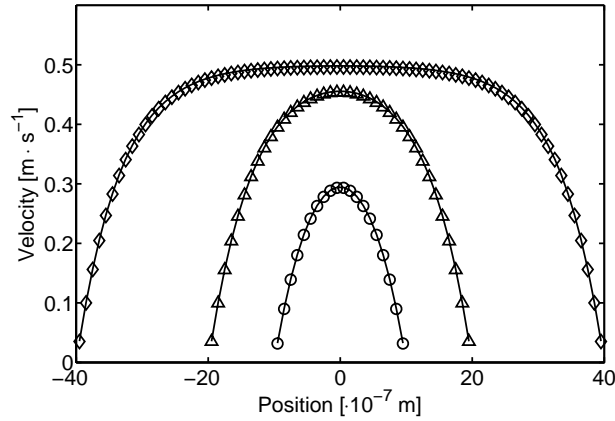
with

$$v_0 = \frac{(2c)^2 \Delta P}{8\eta L}, \quad \alpha_k = (2k-1)\frac{\pi}{2}, \quad k = 1, 2, \dots \quad (4.28)$$

with η the dynamic viscosity, ΔP the pressure drop over the channel, and L the length of the channel. We compared the (equilibrium) flow profile of lattice Boltzmann simulations for typical values of water flowing through rectangular microchannels with the analytical solution. In figure 4.1 the validation results of simulations with $\eta=0.001$ Pa·s, $\frac{\Delta P}{L}$ of 10^9 Pa·m⁻¹ and



a.



b.

Figure 4.1: Simulation results of flow profile in a channel of 20x20 (\circ), 20x40 (\triangle) and 20x80 (\diamond) lattice cells as function of the position along the short side of the channel (a) and as a function of the position along the long side of the channel (b). The solid lines give the analytical result.

$\Delta x = \Delta y = 1 \cdot 10^{-7} \text{ m}$ and aspect ratio of 1, 2 and 4 are given. The figure shows that the simulation results are in excellent agreement with the analytical solution.

Taylor deformation

Taylor deformation simulations were performed to investigate the droplet deformation behaviour of the two phase code. A droplet was placed in between two shearing plates to obtain linear shear at the Stokes regime (low Reynolds number) and the droplet deformation was studied as a function of the shear rate (expressed as capillary number) at a constant Peclet number. The Peclet number is defined as the ratio between the diffuse time scale

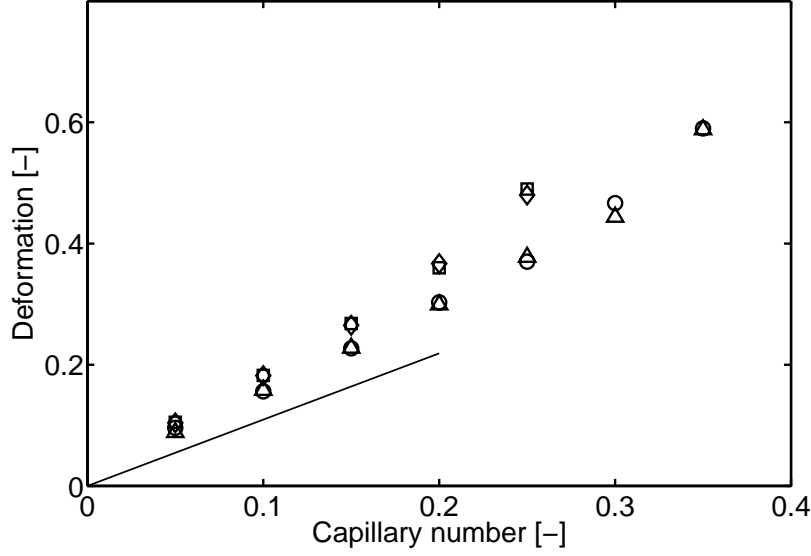


Figure 4.2: Deformation parameter as a function of the capillary number at $Re=0.05$. The solid line gives the theoretical Taylor relation for a system with shearing plates that are infinitely far apart (this is a different situation than the numerical system). Values are given for Cahn=1, box=40x80x40 (\diamond), Cahn=2, box=40x80x40 (\triangle), Cahn=1, box=40x160x40 (\square) and Cahn=2, box=40x160x40 (\circ) at a strain of 10.

and the convective time scale [33]. The definitions of the Reynolds number (Re), capillary number (Ca), and Peclet number (Pe) are given below:

$$Re = \frac{\dot{\gamma} r^2 \rho}{\eta}, \quad (4.29)$$

$$Ca = \frac{\dot{\gamma} r \eta}{\sigma_{ow}}, \quad (4.30)$$

$$Pe = \frac{\dot{\gamma} r \zeta}{D \Gamma}. \quad (4.31)$$

In these equations $\dot{\gamma}$ is the shear rate, the velocity of the moving upper wall divided by the channel height, r the radius of the droplet, ρ the density, η the dynamic viscosity, σ_{ow} the interfacial tension, ζ the width of the interface, D the diffusivity, and Γ a parameter related to mobility (see also eq. 4.7). The densities are the same for both fluids. We varied the capillary number, the size of the box and the grid Cahn number. Simulations were done with $Ch^*=1$ and $Ch^*=2$, at $Re = 0.05$, $Pe = 10$, $\lambda = \eta_d/\eta_c = 1$, and for a droplet with a radius of 10 lattice cells in a system of 40x80x40 or 40x160x40 lattice cells. The simulations were run for a strain ($=\dot{\gamma}t$)

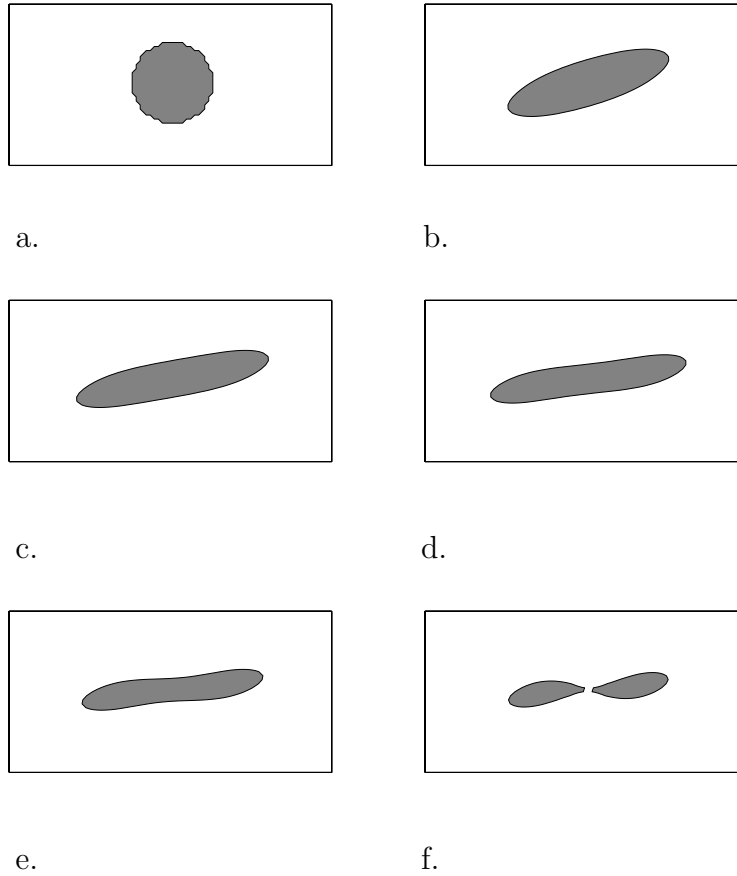


Figure 4.3: Droplet in a shear field at $Ca=0.4$, $Ch^*=2$ and break up into two droplets at a strain of 0 (a), 5 (b), 10 (c), 15 (d), 20 (e) and 25 (f).

of 10. After some time, steady state was reached and the droplet had assumed an elliptic shape. This elliptic shape is usually characterized with the deformation parameter (D_f):

$$D_f = \frac{L - B}{L + B}, \quad (4.32)$$

with L the major and B the minor axis of the ellipse. For a drop in the Stokes regime and for low capillary numbers ($Ca < 0.2$) with plates that are infinitely far away (unbounded shear flow) a theoretical relation is known [34, 35]:

$$D_f = \frac{19\lambda + 16}{16\lambda + 16} Ca. \quad (4.33)$$

Figure 4.2 gives the deformation parameter as a function of the capillary number. The figure shows that with the lattice Boltzmann simulations higher deformation values are found than the theoretical relation. This is most likely caused by the limited distance between the shearing plates [36]. The influence of the length of the channel was of minor importance.

Simulations done with $Ch^*=2$ were closer to the theoretical line than simulations done with $Ch^*=1$. Clearly, numerical parameters like Ch^* influence the results considerably and have to be chosen with care. For $Ch^*=1$ the droplet breaks up at $Ca=0.3$ and the droplet deformation only goes to an equilibrium till $Ca=0.25$. For $Ch^*=2$ the droplet breaks up at the critical capillary number $Ca=0.4$ [36] as can be seen in figure 4.3 (for this simulation a strain of 25 was used). Because the droplets break up at the right critical capillary number, we expect that simulations with droplet detachment in microchannels can describe droplet detachment and the resulting droplet sizes appropriately. From the results we can conclude that for simulations with a broader interface ($Ch^*=2$) the physical behaviour is better than with a smaller interface ($Ch^*=1$) and are expected to be suitable for describing droplet break up. Probably, the gradients in the order parameter are too sharp for $Ch^*=1$.

Sessile drop simulations

To assess our formulation of wetting boundary conditions we performed simulations in a 2-dimensional lattice (D_2Q_9) of 240×240 cells. A large lattice was chosen to be able to measure the contact angle of the sessile droplet on surfaces with different wetting properties. At the beginning of the simulations, the 'droplet' was defined as a square of 40×40 cells on a surface and the simulations were run till the shape of the droplet did not change anymore and equilibrium had been reached. We denote the droplet as the oil phase and therefore has hydrophobic properties and the surrounding fluid is water and has hydrophilic properties. By choosing certain values for A , B and κ it was possible to vary the interfacial tension (see eq. 4.20). The contact angle was measured by fitting the arc of a circle to the cross-section of the sessile drop and determining the contact angle of this arc with the surface, using the least squares method.

Figure 4.4 shows sessile droplets in equilibrium on a surface with different wettabilities, which means with a different ϕ_{wall} . It can be seen quite easily that the method is successful in a qualitative way (please note that the densities of the two fluids were chosen equal). Figure 4.5 shows the contact angle as a function of the fraction of the order parameter of the surface for $Ch^*=2.0$ and $\sigma=0.01$. The result is indeed an almost linear relation between the order parameter and the contact angle and shows good agreement with the theoretical line. For very hydrophobic (ϕ_{wall} almost the

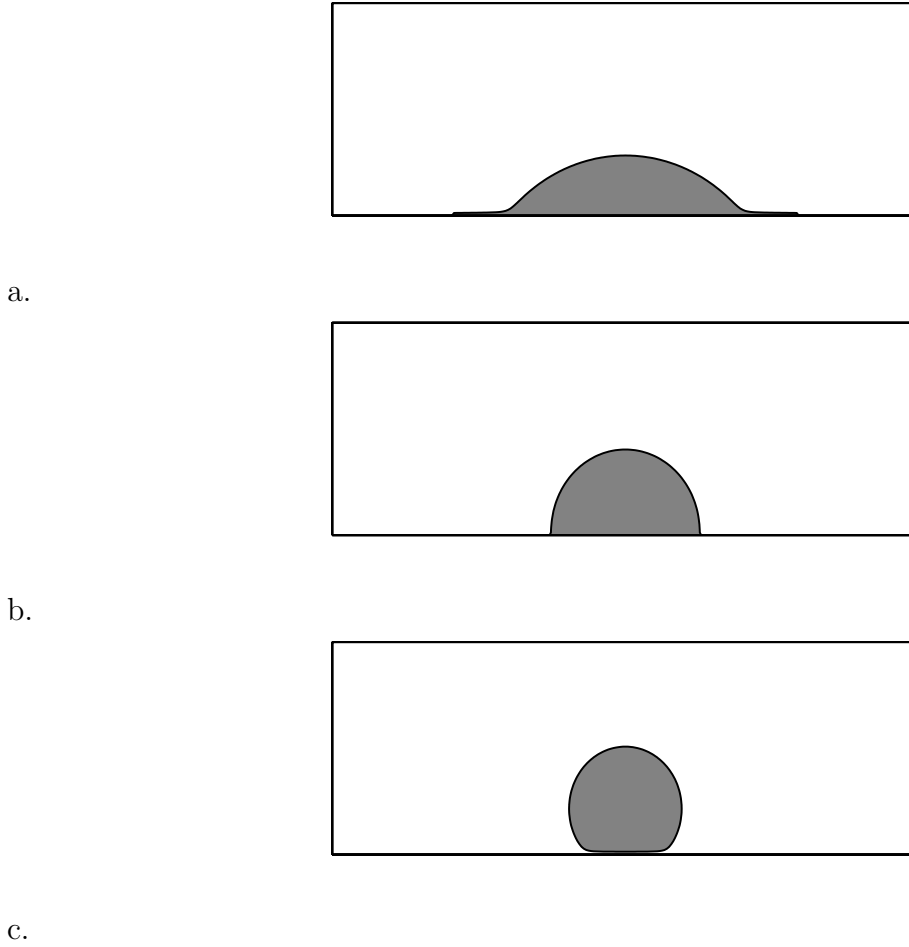


Figure 4.4: Droplets on a surface with a fraction order parameter of 0.5 compared to the dispersed phase (a), on a neutral surface (b) and on a surface with a fraction order parameter of 0.5 compared to the continuous phase (c). In the simulation box presented in these pictures only the bottom part with the droplet is shown (i.e. the total simulated box is larger).

same as the order parameter of the oil droplet) and for very hydrophilic surfaces (ϕ_{wall} almost the same as the order parameter of the water phase) it is very difficult to determine accurate values for the contact angle due to the (finite) dimensions of the box and therefore these values were not included.

Simulations of droplet formation in a T-junction

Comparison with experiments

Droplet formation was performed in a rectangular T-shaped microchannel junction. Figure 4.6 gives a schematic topview of the T-junction and a

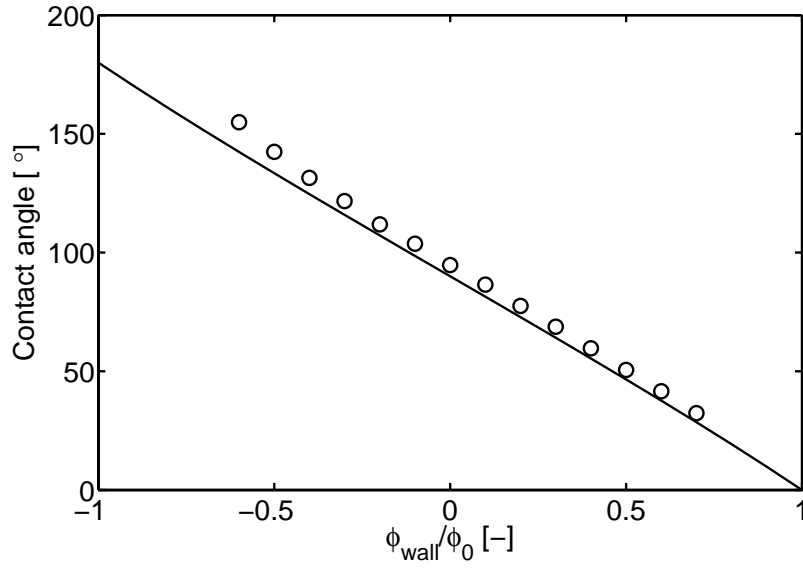
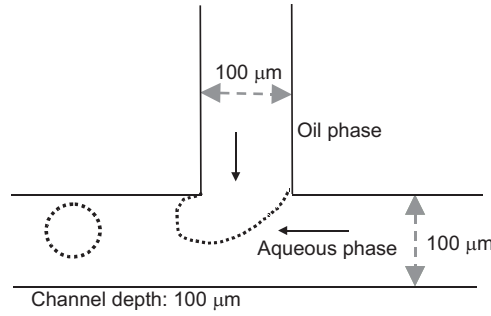


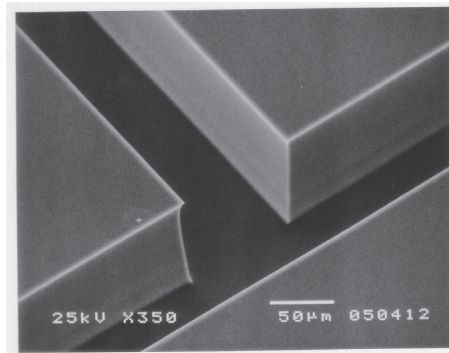
Figure 4.5: The contact angles as a function of the order parameter of the surface with the simulation data points (\circ) and the solid line for analytical theory.

SEM micrograph of the actual T-junction with its dimensions. The width and depth of both channels is $100\ \mu\text{m}$. Droplet formation experiments were performed with 1,6-hexanediol diacrylate as to-be-dispersed phase, and 2 wt.% polyvinyl alcohol aqueous solution as continuous phase. For a detailed description of the experimental procedure we refer to Nisisako *et al.* [37]. As to-be-dispersed phase, a solution with the same properties as 1,6-hexanediol diacrylate (viscosity: $6.71 \cdot 10^{-3}\ \text{Pa}\cdot\text{s}$, density: $1.02 \cdot 10^3\ \text{kg}\cdot\text{m}^{-3}$) has been modelled. As continuous phase, a solution of 2 wt.% polyvinyl alcohol aqueous solution (viscosity $1.95 \cdot 10^{-3}\ \text{Pa}\cdot\text{s}$, density $1.00 \cdot 10^3\ \text{kg}\cdot\text{m}^{-3}$) was modelled. The slight difference in density in the experimental solutions was neglected in the simulations and for both phases $1.00 \cdot 10^3\ \text{kg}\cdot\text{m}^{-3}$ was assumed. With this information and knowledge about the flow profile in a square channel, the capillary number and Reynolds numbers can be calculated. The capillary number was calculated using equation 4.30 with $\dot{\gamma}$ the average shear rate in the continuous phase channel, r the radius of the channel with to-be-dispersed phase, η the dynamic viscosity of the continuous phase and σ_{ow} the interfacial tension between the two fluids. The following definition was used for the Reynolds numbers in the two channels of the T-junction:

$$Re_{\text{channel}} = \frac{v_{\text{max}} \cdot D}{\nu}, \quad (4.34)$$



a.



b.

Figure 4.6: Schematic picture (a) and a SEM micrograph of the T-junction including dimensions (b).

with v_{max} the maximum velocity in the channel, D the diameter of the channel, and ν the kinematic viscosity of the fluid. Table 4.1 gives an overview of dimensionless numbers used in the simulations, which correspond to experimental conditions. In addition, we used the numerical dimensionless parameters $Ch^*=2$ and $Pe=10$. As a viscosity ratio, λ , we used 3.44, which is in accordance with the experimental fluid properties. We applied the same wetting boundary conditions for the channel walls as were measured in the experimental setup, which is a contact angle of an oil droplet on a surface in a water phase of 135° (quite hydrophilic). An interfacial tension of $5 \text{ mN}\cdot\text{m}^{-1}$ was used, which was measured with an automated drop shape tensiometer at short time scales. Simulations were done in a system containing $20 \times 200 \times 60$ lattice cells (i.e., one lattice cell corresponds with $5 \mu\text{m}$). The difference between simulations with this grid and a finer grid ($1 \text{ cell} = 2.5 \mu\text{m}$) was only 3%; we found this acceptable.

Table 4.1: Dimensionless numbers of lattice Boltzmann simulations corresponding to experimental conditions.

to-be-dispersed phase flow rate [ml·h ⁻¹]	v_{max} [m·s ⁻¹]	$Re_{channel}$ [—]		
0.2	0.0083	0.124		

continuous phase flow rate [ml·h ⁻¹]	v_{max} [m·s ⁻¹]	$Re_{channel}$ [—]	Ca [—]	
0.2	0.0083	0.43	0.0033	
0.4	0.0167	0.85	0.0065	
1	0.0417	2.14	0.016	
2	0.0833	4.27	0.033	
4	0.1667	8.55	0.065	

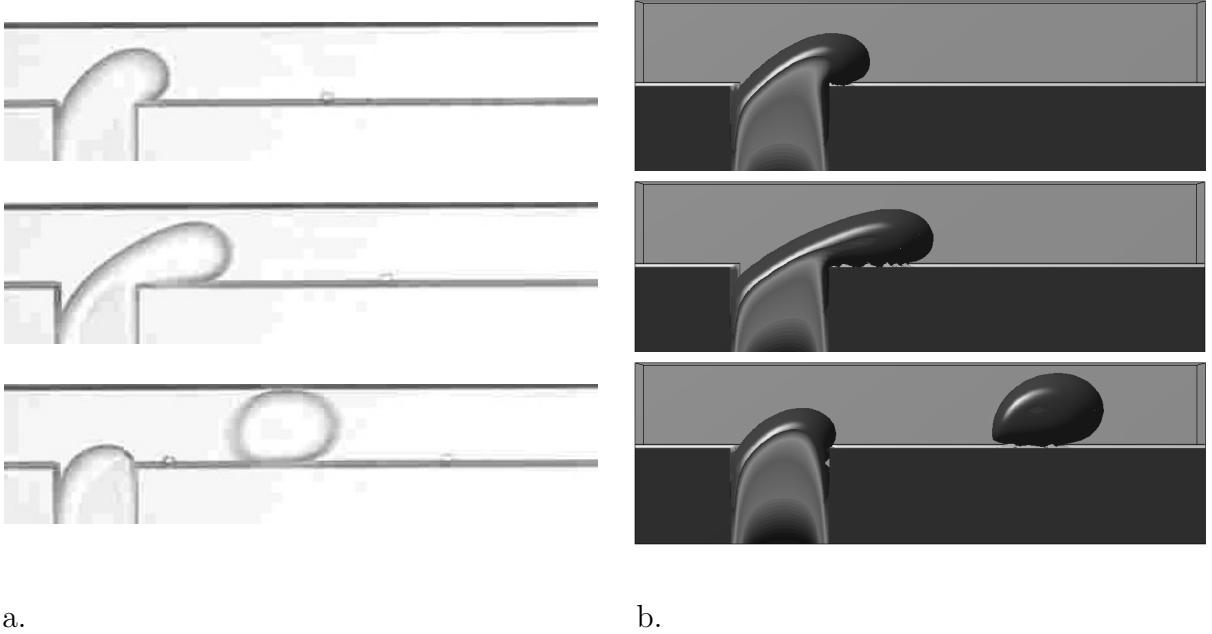


Figure 4.7: Snapshots of experiments (a) and simulations (b) of droplet detachment at a T-junction. The flow rate of the continuous phase is 2 ml·h⁻¹ and of the to-be-dispersed phase 0.2 ml·h⁻¹. The experimental pictures differ 2.5 ms in time (which corresponds with a strain of 4) and the simulation pictures correspond with a strain of 0, 5 and 10.

Figure 4.7 shows some snapshots of droplet formation experiments and of droplet formation simulations at a flow rate of the continuous phase of 2 ml·h⁻¹. The droplet deforms before detachment and the continuous phase intrudes into the pore. This intrusion of continuous phase stresses

the importance of contact line dynamics, which is thought to be essential for droplet detachment [38]. Both the shape of the droplets and the time interval (expressed as strain) between the different frames in figure 4.7 are comparable. The resulting diameter for a spherical droplet, d , was calculated from the droplet volume, V , as follows:

$$d = \left(\frac{6V}{\pi} \right)^{\frac{1}{3}}. \quad (4.35)$$

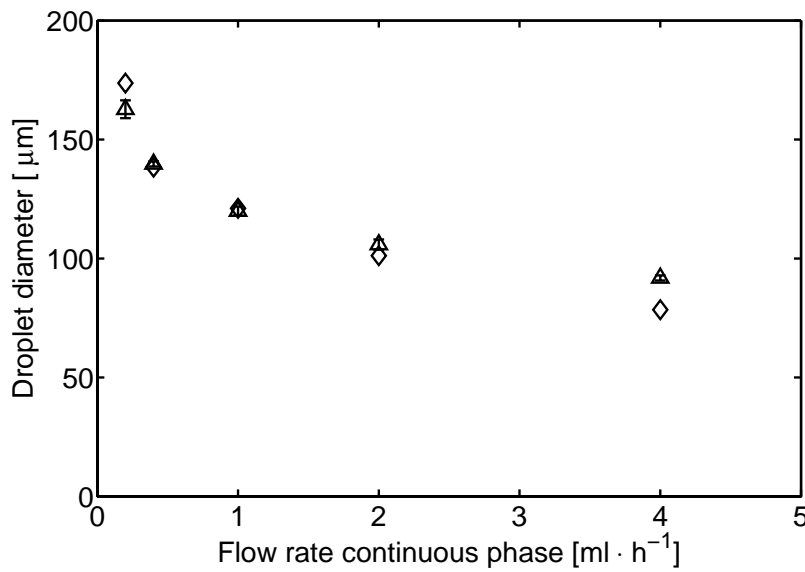


Figure 4.8: Droplet diameter as a function of the flow rate of the continuous phase for the experiments (\triangle) with standard deviation and for the simulations (\diamond), both with a contact angle of 135° .

Figure 4.8 gives the droplet diameters for both the experiments and the lattice Boltzmann simulations, for continuous phase flow rates between 0.2 and $4 \text{ ml} \cdot \text{h}^{-1}$. The simulation results are in fair agreement with the experimental results. At a low continuous phase flow rate of $0.2 \text{ ml} \cdot \text{h}^{-1}$ the simulations slightly overestimate the droplet diameter and at higher continuous phase flow rates the simulation results slightly underestimate the droplet diameter. The wetting conditions used for the simulations in figure 4.8 were based on a measured equilibrium contact angle of a droplet in equilibrium. Possibly, the behavior of a dynamic droplet with dynamic wetting conditions (with advancing and receding contact angles) is slightly different and this is investigated further.

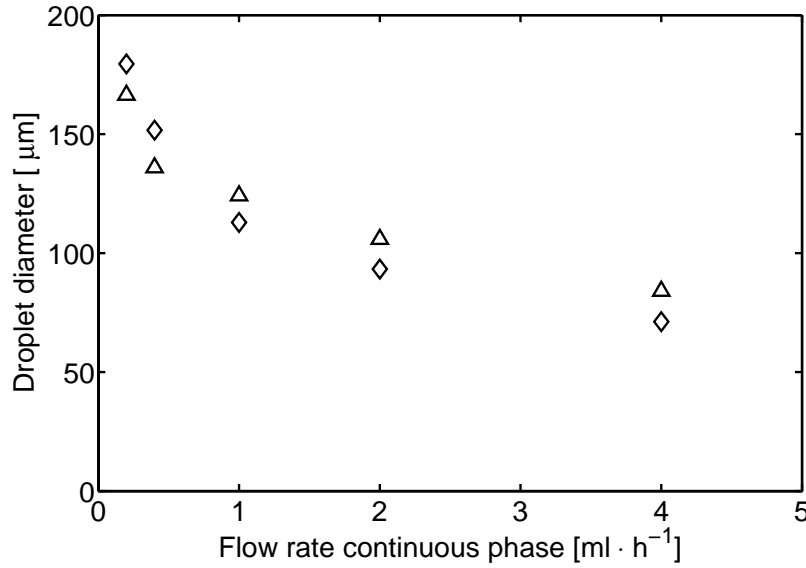


Figure 4.9: Simulation results of the droplet diameter as a function of the flow rate of the continuous phase for slightly hydrophilic (115°) wetting conditions of the channel (Δ) and for completely hydrophilic (180°) wetting conditions (\diamond).

Figure 4.9 shows the influence of the wetting conditions of the channel on the droplet size as a function of the continuous phase flow rate. The wetting conditions influence the droplet size, but not strongly. It is remarkable that at low continuous phase flow rates slightly more hydrophobic wetting conditions (115°) produce smaller droplets while at high continuous phase flow rates these wetting conditions produce larger droplets. This is in line with the experimental results. These findings could be an explanation for the deviations between the experimental and simulation results seen in figure 4.8. Assuming a somewhat more hydrophobic contact angle would improve the match with the experimental values. Possibly, the contact angle during these specific experiments may have been somewhat lower than was assumed for the simulations.

Influence of capillary number on droplet size

Having validated the code against benchmarks and experimental results, it is now possible to systematically study the influence of different parameters on the final droplet size. We did simulations with various interfacial tensions ($1\text{--}15 \text{ mN}\cdot\text{m}^{-1}$) and various continuous phase flow rates ($1\text{--}4 \text{ ml}\cdot\text{h}^{-1}$) as a function of the to-be-dispersed phase flow rate. Hydrophilic wetting

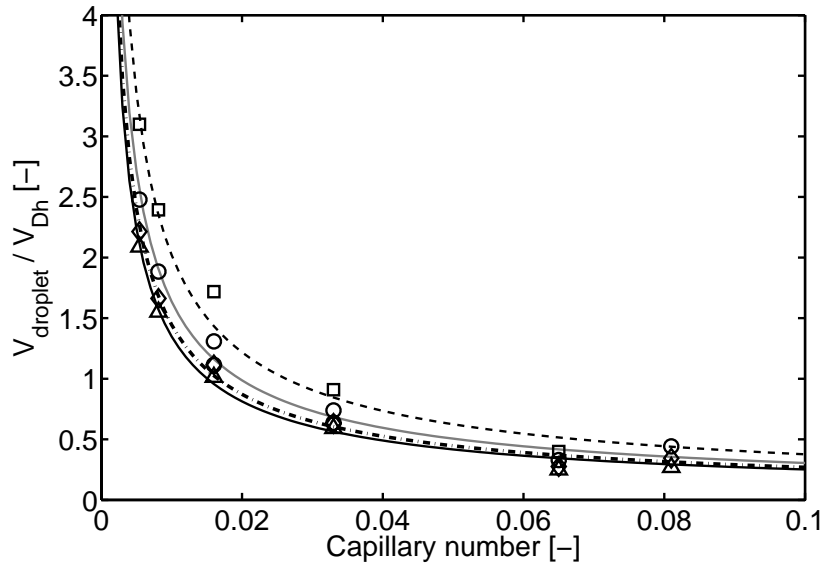


Figure 4.10: Simulation results and their fits of the dimensionless droplet volume, i.e. the droplet volume divided by the volume of a droplet with the hydraulic diameter ($D_h=100\ \mu\text{m}$) as diameter ($\frac{V_{\text{droplet}}}{V_{D_h}} = \frac{\frac{4}{3}\pi(\frac{D_d}{2})^3}{\frac{4}{3}\pi(\frac{D_h}{2})^3}$), as a function of the capillary number for to-be-dispersed phase flow rates of $0.05\ \text{ml}\cdot\text{h}^{-1}$ (\triangle , -), $0.1\ \text{ml}\cdot\text{h}^{-1}$ (\diamond , $\cdot - \cdot$), $0.2\ \text{ml}\cdot\text{h}^{-1}$ (\circ , grey -) and $0.4\ \text{ml}\cdot\text{h}^{-1}$ (\square , - -).

conditions ($\theta=180^\circ$) were applied to minimize dynamic contact angle effects, viscosity and geometry were the same as above. In a previous paper [39] we concluded that the final droplet volume in a T-shaped microchannel is a result of two stages of droplet growth, namely an expansion stage and a necking stage:

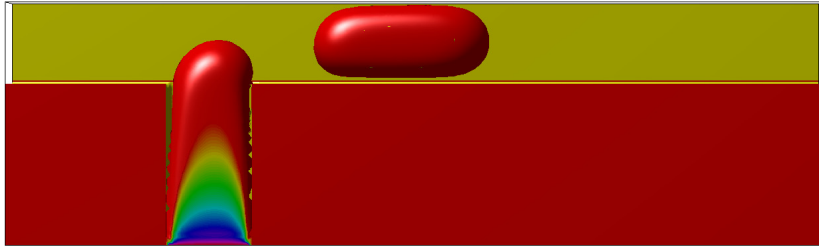
$$V = V_{\text{crit}} + t_{\text{neck}} \cdot \phi_d, \quad (4.36)$$

with $V_{\text{crit}} (= \phi_d \cdot t_{\text{crit}})$ the critical volume that represents the volume at which the drag force exerted on the droplet is just as large as the interfacial tension-based force that attaches the droplet to the pore mouth, determined by a force or torque balance, t_{neck} the time needed for necking, and ϕ_d the to-be-dispersed phase flow rate. V_{crit} is in fact the droplet volume that would be obtained when the droplet detachment process was very fast ($t_{\text{neck}} \rightarrow 0$), and only a force or torque balance is relevant. The value of V_{crit} depends, amongst others, on the interfacial tension and the shear stress caused by the continuous phase flow rate. Figure 4.10 shows the results of the simulations. The droplet volumes were made dimensionless by relating it to the volume of a droplet having a diameter equal to the

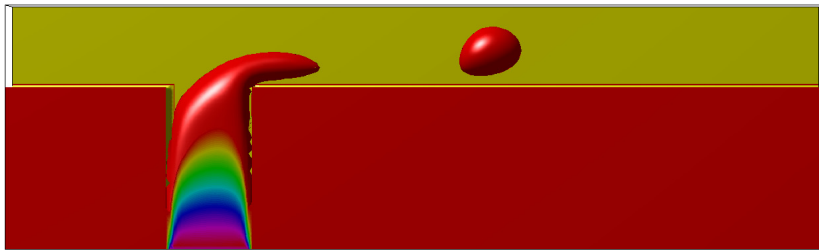
hydraulic diameter of the cross-flow channel. These dimensionless droplet volumes were plotted as a function of the capillary number. The droplet volume decreases as a function of the capillary number and the droplet size increases somewhat with increasing to-be-dispersed phase flow rate. The following equation:

$$V = V_{crit,ref} \cdot Ca^m + t_{neck,ref} \cdot Ca^n \cdot \phi_d, \quad (4.37)$$

with $V_{crit,ref}$ the critical volume at $Ca=1$ and $t_{neck,ref}$ the necking time at $Ca=1$ was used to fit all the data. It was found that the equation could be simplified to $m = n$ and for this a value of -0.75 was found, together with $V_{crit,ref} = 2.5 \cdot 10^{-5} \mu l$ and $t_{neck,ref} = 0.135$ ms. This means that V_{crit} scales with $Ca^{-0.75}$, which is a result of the specific force or torque balance in this specific geometry. For other geometries, like for droplet formation from a pore in a system in which the droplet is not distorted by channel walls, V_{crit} will scale with Ca^{-1} , assuming a torque balance model or with $Ca^{-\frac{3}{2}}$, assuming a force balance model [40]. Apparently, the effect of the constraining walls is such, that the dependence on shear rate and interfacial tension is slightly less.



a.



b.

Figure 4.11: Snapshots of a droplet just after detachment for $Ca=0.0054$ (a) and $Ca=0.081$ (b) for a to-be-dispersed phase flow rate of $0.05 \text{ ml} \cdot \text{h}^{-1}$.

Figure 4.11 shows droplets just after detachment at $Ca=0.0054$ and $Ca=0.081$ for a to-be-dispersed phase flow rate of $0.05 \text{ ml}\cdot\text{h}^{-1}$ (Δ in figure 4.10). For droplets with a diameter larger than the hydraulic diameter a slug is formed ($Ca=0.0054$), while for droplet volumes with a diameter smaller than the hydraulic diameter of the channel, the droplet can move freely in the channel ($Ca=0.081$). It is expected that at larger capillary numbers ($Ca>0.1$) the influence of the geometry of the channel decreases and there will be a transition to the regime that scales with Ca^{-1} (assuming a torque balance model) [11, 41].

In our geometry, not only V_{crit} , but also the necking time scales with $Ca^{-0.75}$; a higher shear rate causes a shorter necking time and a higher interfacial tension causes a longer necking time (table 4.2). As the critical volume is influenced in a similar fashion by these parameters, $(\frac{t_{neck}}{t_{total}})$ does not change.

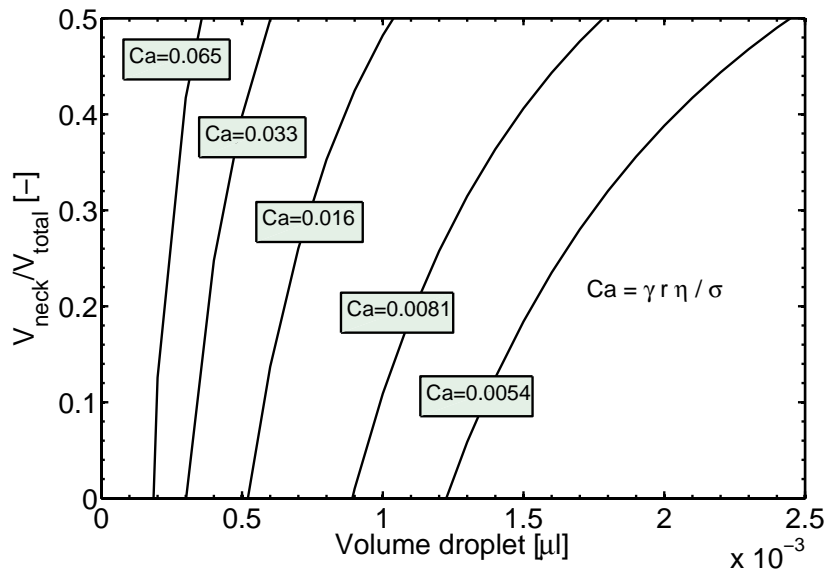


Figure 4.12: Necking fraction as a function of the final droplet volume for different capillary numbers.

The final droplet volume thus consists both of V_{crit} and a volume as a result of droplet growth during necking, V_{neck} , and a higher to-be-dispersed phase flow rate causes a higher V_{neck} . If the to-be-dispersed phase flow rate varies somewhat, it can be advisable to work in a regime where $V_{crit} \gg V_{neck}$ i.e. at a low to-be-dispersed phase flow rate. On the other hand, if it is more important to produce droplets fast, a higher to-be-dispersed

flow rate is desirable and V_{neck} can no longer be neglected. Figure 4.12 shows the contribution of V_{neck} to the final droplet volume, $(V_{neck}+V_{crit})$, as a function of the final droplet volume for different capillary numbers. The figure shows which conditions to choose for droplets with a certain size.

Table 4.2: Necking times (t_{neck}) and critical volumes (V_{crit}) corresponding to various continuous phase flow rates (ϕ_c) and various interfacial tensions (σ) and their capillary number (Ca).

ϕ_c [ml·h ⁻¹]	σ [mN·m ⁻¹]	Ca [—]	t_{neck} [ms]	V_{crit} [·10 ⁻⁴ μl]
1	1	0.081	0.86	1.6
1	5	0.016	2.8	5.1
1	10	0.0081	4.6	8.4
1	15	0.0054	6.2	11.3
2	5	0.033	1.7	3.1
4	5	0.065	1.0	1.8

Conclusion

Droplet formation was studied both in experiments and with lattice Boltzmann simulations. The flow profile and wetting properties showed good agreement with theoretical relations. Deformation of a droplet between two shearing plates shows that droplets break up at the correct critical capillary number (Ca=0.4).

Droplet detachment in a T-junction has been investigated both experimentally and theoretically and both the shape of the droplet and the final droplet size are comparable. This shows that lattice Boltzmann simulations are a valid tool to describe droplet detachment behaviour.

With the developed code a parameter study was performed. The results show that the droplet volume decreases as a function of the capillary number and increases with the to-be-dispersed phase flow rate. Both the critical volume and the volume increase during necking were found to scale with $Ca^{-\frac{3}{4}}$.

To obtain droplets with a certain size a combination of capillary number and to-be-dispersed phase flow rate should be chosen. For a higher capillary number and a higher to-be-dispersed phase flow rate, V_{neck} contributes considerably to the final droplet volume, whereas for a lower capillary number and a lower to-be-dispersed phase flow rate V_{neck} can be negligible.

Acknowledgement

This research was supported by the European Community, project QLRT-2000-01228 and by the HPC-Europa project RII3-CT-2003-506079. The authors thank Pieter Kroon for technical assistance, Peter Lammers from the High Performance Computing Centre in Stuttgart and Julia Yeomans and co-workers from Oxford University for valuable discussions.

Appendix A

The used coefficients in the equilibrium distributions are for D_3Q_{19} . The subscript 1 is used for the nearest ($i = 1..6$) vectors and the subscript 2 for the next nearest ($i = 7..18$) vectors:

$$A_1 + G_{1\alpha\beta}c_{1\alpha}c_{1\beta} = \frac{P_{\alpha\beta}\delta_{\alpha\beta}}{2c^2} - \frac{(P_{xx} + P_{yy} + P_{zz})}{9c^2}, \quad (4.38)$$

$$A_2 + G_{2\alpha\beta}c_{2\alpha}c_{2\beta} = \frac{(P_{xx} + P_{yy} + P_{zz})}{36c^2} + \frac{P_{\alpha\beta}c_{\alpha}c_{\beta}}{4c^4}, \quad (4.39)$$

$$B_1 = \frac{\rho}{6c^2}, \quad B_2 = \frac{\rho}{12c^2}, \quad (4.40)$$

$$C_1 = -\frac{\rho}{12c^2}, \quad C_2 = -\frac{\rho}{24c^2}, \quad (4.41)$$

$$D_1 = \frac{\rho}{4c^4}, \quad D_2 = \frac{\rho}{8c^4}, \quad (4.42)$$

$$H_1 = \frac{\Gamma\mu}{6c^2}, \quad H_2 = \frac{\Gamma\mu}{12c^2}, \quad (4.43)$$

$$K_1 = \frac{\phi}{6c^2}, \quad K_2 = \frac{\phi}{12c^2}, \quad (4.44)$$

$$J_1 = -\frac{\phi}{12c^2}, \quad J_2 = -\frac{\phi}{24c^2}, \quad (4.45)$$

$$Q_1 = \frac{\phi}{4c^4}, \quad Q_2 = \frac{\phi}{8c^4}. \quad (4.46)$$

References

1. D.J. McClements, R. Chanamai, Physicochemical properties of monodisperse oil-in-water emulsions, *J. Dispersion Sci. Technol.* 23, 1-3 (2002) 125.
2. T. Nakashima, M. Shimizu, M. Kukizaki, Membrane emulsification by microporous glass, *Key Eng. Mater.* 61&62 (1991) 113.
3. S. Sugiura, M. Nakajima, J. Tong, H. Nabetani, M. Seki, Preparation of monodispersed solid lipid microspheres using a microchannel emulsification technique, *J. Colloid Interface Sci.* 227 (2000) 95.
4. I. Kobayashi, M. Nakajima, K. Chun, Y. Kikuchi, H. Fujita, Silicon array of elongated through-holes for monodisperse emulsion droplets, *AIChE J.* 48, 8 (2002) 1639.
5. S.L. Anna, N. Bontoux, H.A. Stone, Formation of dispersions using "flow focusing" in microchannels, *Appl. Phys. Lett.* 82, 3 (2003) 364.
6. D.R. Link, S.L. Anna, D.A. Weitz, H.A. Stone, Geometrically mediated breakup of drops in microfluidic devices, *Phys. Rev. Lett.* 92, 5 (2004) 054503-1.
7. A.J. Abrahamse, A. van der Padt, R.M. Boom, W.B.C. de Heij, Process fundamentals of membrane emulsification: simulation with CFD, *AIChE J.* 47, 6 (2001) 1285.
8. M. Ohta, M. Yamamoto, M. Suzuki, Numerical analysis of a single drop formation process under pressure pulse condition, *Chem. Eng. Sci.* 50, 18 (1995) 2923.
9. I. Kobayashi, S. Mukataka, M. Nakajima, CFD simulation and analysis of emulsion droplet formation from straight-through microchannels, *Langmuir* 20 (2004) 9868.
10. M. Rayner, G. Trägårdh, C. Trägårdh, P. Dejmek, Using the surface evolver to model droplet formation processes in membrane emulsification, *J. Colloid Interface Sci.* 279 (2004) 175.
11. V. Cristini, Y.-C. Tan, Theory and numerical simulation of droplet dynamics in complex flows - a review, *Lab Chip* 4 (2004) 257.
12. D. Jacqmin, Calculation of two-phase Navier-Stokes flows using phase-field modeling, *J. Comp. Phys.* 155 (1999) 96.
13. M.R. Swift, E. Orlandini, W.R. Osborn, J.M. Yeomans, Lattice Boltzmann simulations of liquid-gas and binary fluid systems, *Phys. Rev. E* 54, 5 (1996) 5041.
14. A. Lamura, G. Gonella, J.M. Yeomans, Modeling the dynamics of amphiphilic fluids, *Int. J. Mod. Phys. C* 9, 8 (1998) 1469.
15. A. Lamura, G. Gonella, J.M. Yeomans, A lattice Boltzmann model of ternary fluid mixtures, *Europhys. Lett.* 45, 3 (99) 314.
16. A.C. Balazs, R. Verberg, C.M. Pooley, O. Kuksenok, Modeling the flow of complex fluids through heterogeneous channels, *Soft Matter* 1 (2005) 44.
17. X. Shan, H. Chen, Lattice Boltzmann model for simulating flows with multiple phases and components, *Phys. Rev. E* 47, 3 (1993) 1815.
18. B.R. Sehgal, R.R. Nourgaliev, T.N. Dinh, Numerical simulation of droplet deformation and break-up by lattice-Boltzmann method, *Prog. Nucl. Energy* 34, 4 (1999) 471.

19. Z.L. Yang, T.N. Dinh, R.R. Nourgaliev, B.R. Sehgal, Numerical investigation of bubble coalescence characteristics under nucleate boiling condition by a lattice-Boltzmann model, *Int. J. Therm. Sci.* 39 (2000) 1.
20. Q. Kang, D. Zhang, S. Chen, Displacement of a two-dimensional immiscible droplet in a channel, *Phys. Fluids* 14, 9 (2002) 3203.
21. X. He, G.D. Doolen, Thermodynamic foundations of kinetic theory and lattice Boltzmann models for multiphase flows, *J. Stat. Phys.* 107 (2002) 309.
22. M.R. Swift, W.R. Osborn, J.M. Yeomans, Lattice Boltzmann simulations of nonideal fluids, *Phys. Rev. Lett.* 75, 5 (1995) 830.
23. J.-C. Desplat, I. Pagonabarraga, P. Bladon, LUDWIG: A parallel Lattice-Boltzmann code for complex fluids, *Comput. Phys. Commun.* 134 (2001) 273.
24. O. Theissen, G. Gompper, Lattice-Boltzmann study of spontaneous emulsification, *Eur. Phys. J. B* 11 (1999) 91.
25. P. Yue, J.J. Feng, C. Liu, J. Shen, A diffuse-interface method for simulating two-phase flows of complex fluids, *J. Fluid Mech.* 515 (2004) 293.
26. C. Liu, J. Shen, A phase field model for the mixture of two incompressible fluids and its approximation by a Fourier-spectral method, *Physica D* 179 (2003) 211.
27. D. Iwahara, H. Shinto, M. Miyahara, K. Higashitani, Liquid drops on homogeneous and chemically heterogeneous surfaces: a two-dimensional lattice Boltzmann study, *Langmuir* 19 (2003) 9086.
28. J.W. Cahn, Critical point wetting, *J. Chem. Phys.* 66 (1977) 3667.
29. R.A. Jerry, E.B. Nauman, Phase transitions in thin films of a binary mixture, *Phys. Lett. A* 167 (1992) 198.
30. A.J. Briant, P. Papatzacos, J.M. Yeomans, Lattice Boltzmann simulations of contact line motion in a liquid-gas system, *Philos. Trans. R. Soc. London* 360 (2002) 485.
31. F.M. White, *Fluid Mechanics*, 2003, McGraw-Hill, New York.
32. J.F.L. Duval, H.P. van Leeuwen, J. Cecilia, J. Galceran, Rigorous analysis of reversible faradaic depolarization processes in the electrokinetics of the metal/electrolyte solution interface, *J. Phys. Chem. B* 107 (2003) 6782.
33. R. Chella, J. Vinals, Mixing of a two-phase fluid by cavity flow, *Phys. Rev. E* 53, 4 (1996) 3832.
34. G.I. Taylor, The viscosity of a fluid containing small drops of another fluid, *Proc. Roy. Soc. A* 138 (1932) 41.
35. G.I. Taylor, The formation of emulsions in definable fields of flow, *Proc. Roy. Soc. A* 146 (1934) 501.
36. J. Li, Y.Y. Renardy, M. Renardy, Numerical simulation of breakup of a viscous drop in simple shear flow through a volume-of-fluid method, *Phys. Fluids* 12, 2 (2000) 269.
37. T. Nisisako, T. Torii, T. Higuchi, Novel microreactors for functional polymer beads, *Chem. Eng. J.* 101 (2004) 23.

38. N.C. Christov, D.N. Ganchev, N.D. Vassileva, N.D. Denkov, K.D. Danov, P.A. Kralchevsky, Capillary mechanisms in membrane emulsification: oil-in-water emulsions stabilized by Tween 20 and milk proteins, *Colloids Surfaces A: Physicochem. Eng. Aspects* 209 (2002) 83.
39. S. van der Graaf, M.L.J. Steegmans, R.G.M. van der Sman, C.G.P.H. Schroën, R.M. Boom, Droplet formation in a T-shaped microchannel junction: a model system for membrane emulsification, *Colloids Surf. A: Physicochem. Eng. Aspects* 266 (2005) 106.
40. S.J. Peng, R.A. Williams, Controlled production of emulsions using a crossflow membrane. Part I: Droplet formation from a single pore, *Trans IChemE* 76 (1998) 894.
41. J.D. Tice, H. Song, A.D. Lyon, R.F. Ismagilov, Formation of droplets and mixing in multiphase microfluidics at low values of the reynolds and the capillary numbers, *Langmuir* 19 (2003) 9127.

Chapter 5

Diffuse interface model of surfactant adsorption onto flat and droplet interfaces

Abstract

For applications where emulsion droplet break up and surfactant adsorption are strongly coupled, a diffuse interface model is developed. The model is based on a free energy functional, partly adapted from the sharp interface model of Diamant and Andelman [1]. The model is implemented in a 2D lattice Boltzmann scheme, similar to existing micro-emulsion models, which are coupled to hydrodynamics. Contrary to these microemulsion models, we can describe realistic adsorption isotherms, such as the Langmuir isotherm. From the free energy functional, analytical expressions of equilibrium properties are derived, which compare reasonably with numerical results. Interfacial tension lowering scales with the logarithm of the area fraction of the interface unloaded with surfactant: $\Delta\sigma \sim \ln(1 - \psi_0)$. Furthermore, we show that adsorption kinetics are close to the classical relations of Ward and Tordai. Preliminary simulations of droplets in shear flow show promising results, with surfactants migrating to interfacial regions with highest curvature. We conclude that our diffuse interface model is very promising for apprehending above mentioned applications as membrane emulsification.

This chapter has been accepted for publication in *Rheologica Acta* as: R.G.M. van der Sman, S. van der Graaf, Diffuse interface model of surfactant adsorption onto flat and droplet interfaces.

Introduction

In this paper we present a diffuse interface model for surfactant adsorption onto the interface of two immiscible fluids, as occurs in emulsions of oil and water. Motivation behind this study is better understanding of this process, being of significant importance for making emulsions using the novel membranes or microdevices [2 – 6]. Despite numerous experimental work [7, 8], membrane emulsification is still a poorly understood process. Reason for this is the complex coupling to hydrodynamics, wetting and surfactant dynamics. A more feasible route for understanding is via numerical modelling [5, 9]. However these existing models only address oil-water systems without surfactants. Also from other research fields there exist yet no models which can address adsorption of soluble surfactants onto evolving droplets, which will eventually break off [10 – 15].

In this paper we present a diffuse interface model [16], implemented with the lattice Boltzmann model (see [17, 18] for general review), which is in principle capable of solving the problem of simulating membrane emulsification with surfactants. For describing surfactant adsorption we have transformed the free energy based, sharp interface model of Diamant and Andelman [1, 19], into a diffuse interface model. There already exist diffuse interface models for micro-emulsions [20 – 24], but they lack a realistic surfactant adsorption isotherm - in contrast to the model of Diamant and Andelman - which can model the Langmuir and Frumkin adsorption isotherms.

A diffuse interface model has the advantage that it can be coupled to hydrodynamics cf. [21, 24]. Like the well-known VOF method [11], a special field tracks the interface without the need of any remeshing of the grid. While the interface is artificially reconstructed every time step in the VOF method, the interface evolves according to chemical potential gradients in the diffuse interface method. The chemical potential is derived from a free energy functional, which includes squared gradient terms for describing the surface free energy in the spirit of van der Waals. Hence, as the diffuse interface method has a firm physical basis (in contrast to VOF), we think it is the most natural method to model surfactant adsorption onto (deforming and breaking) emulsion droplets.

In this paper we restrict the model to Langmuir adsorption, with equal solubility of the surfactant in both bulk phases. In a subsequent paper, we will introduce the extended model with Frumkin adsorption, and differen-

tial solubility of the surfactant in the two bulk phases. Furthermore, the current model is 2-dimensional, while we focus on comparison of analytical prediction and simulations. We first investigate the equilibrium properties of adsorbed surfactants on a planar interface and a circular interface of a droplet. Subsequently, we analyse the dynamics of surfactant adsorption on a planar interface. In conclusion we briefly investigate the surfactant adsorption on a droplet in linear shear flow, only to indicate the ability of the model to be coupled to hydrodynamics.

Surfactant adsorption model

The emulsion/surfactant system is described with two order parameters ϕ and ψ , indicating respectively the oil/water interface and the surfactant (volume fraction). The system evolves following a convection-diffusion equation, where diffusion of the two order parameters is driven by gradients in the chemical potential (μ_ϕ and μ_ψ). The density ρ and flow field ρu_α are described by the continuity equation and a generalised Navier-Stokes equation - which includes a Korteweg-DeVries stress tensor $P_{\alpha\beta}$ representing the effect of interfacial tension on the hydrodynamics. The chemical potential and the Korteweg-deVries stress tensor are derived from the free energy functional. Below we have listed the governing partial differential equations: (assuming the Einstein convention of summing over double indices):

$$\begin{aligned} \partial_t \phi + \partial_\alpha \phi u_\alpha &= M_\phi \partial_\alpha^2 \mu_\phi, \\ \partial_t \psi + \partial_\alpha \psi u_\alpha &= M_\psi \partial_\alpha^2 \mu_\psi, \\ \partial_t \rho + \partial_\alpha \rho u_\alpha &= 0, \\ \partial_t \rho u_\alpha + \partial_\beta \rho u_\alpha u_\beta &= -\partial_\beta P_{\alpha\beta} + \nu \partial_\alpha^2 \rho u_\alpha, \end{aligned} \tag{5.1}$$

with M_ϕ , M_ψ the mobilities of the two order parameters, and ν the kinematic viscosity of the fluid.

Our free energy functional can be decomposed in the following contributions:

$$F = F_{0,\phi} + F_{0,\psi} + F_{ex} + F_1, \tag{5.2}$$

with

$$\begin{aligned} F_{0,\phi} &= -\frac{A}{2}\phi^2 + \frac{B}{4}\phi^4 + \frac{\kappa}{2}(\partial_\alpha \phi)^2, \\ F_{0,\psi} &= \psi \ln \psi + (1 - \psi) \ln(1 - \psi), \end{aligned}$$

$$\begin{aligned} F_1 &= -\frac{1}{2}\epsilon\psi(\partial_\alpha\phi)^2, \\ F_{ex} &= \frac{1}{2}W\psi\phi^2. \end{aligned} \quad (5.3)$$

$F_{0,\phi}$ is the common double well free energy functional as used in Cahn-Hilliard theory of an immiscible binary fluid [16]. $F_{0,\psi}$ is the entropic part of free energy of mixing of the surfactant with the bulk phase, where we have normalized the surfactant order parameter ψ such that $\psi = 1$ if the interface is fully saturated with surfactant. F_1 is the surface free energy due to surfactant adsorption, F_{ex} is an enthalpic contribution introduced for numerical reasons, as is said to stabilize diffuse interface models of microemulsions [21]. F_1 is taken from the sharp interface model of Diamant and Andelman of surfactant adsorption, where we have replaced the delta-function $\delta(x)$ in their (surface) free energy functional with $(\partial_x\phi)^2$. In binary fluid models the order parameter field $\phi(x)$ describes a planar interface at $x = 0$ via the profile $\phi(x) = \phi_0 \tanh(x/\zeta)$ (with $\phi_0^2 = A/B$ and $\zeta^2 = 2\kappa/A$). Note that the squared gradient of the profile approximates the delta function.

Cf. [20, 24] we obtain the chemical potentials via variational derivatives of the free energy functional:

$$\begin{aligned} \mu_\phi &= -A\phi + B\phi^3 - \kappa\partial_\alpha^2\phi + W\psi\phi + \epsilon\psi\partial_\alpha^2\phi + \epsilon\partial_\alpha\psi\partial_\alpha\phi, \\ \mu_\psi &= \ln(\psi) - \ln(1 - \psi) + \frac{1}{2}W\phi^2 - \frac{1}{2}\epsilon(\partial_\alpha\phi)^2. \end{aligned}$$

The Korteweg-deVries pressure tensor is as follows [21]:

$$P_{\alpha\beta} = p_0\delta_{\alpha\beta} + q_{\alpha\beta}, \quad (5.4)$$

with p_0 the thermodynamic pressure:

$$p_0 = \phi\mu_\phi + \psi\mu_\psi - F, \quad (5.5)$$

and $q_{\alpha\beta}$ a contribution arising from Gibbs-Duhem relation:

$$\partial_\alpha P_{\alpha\beta} = (\phi\partial_\alpha\mu_\phi + \psi\partial_\alpha\mu_\psi)\delta_{\alpha\beta}. \quad (5.6)$$

Using the above we find:

$$\begin{aligned} p_0 &= -\frac{1}{2}A\phi^2 + \frac{3}{4}B\phi^4 - \frac{1}{2}\kappa(\partial_\alpha\phi)^2 - \kappa\phi\partial_\alpha^2\phi \\ &\quad - \ln(1 - \psi) + W\psi\phi^2 + \epsilon\phi\partial_\alpha\phi\partial_\alpha\psi + \epsilon\phi\psi\partial_\alpha^2\phi, \end{aligned} \quad (5.7)$$

$$q_{\alpha\beta} = (\kappa - \epsilon\psi)(\partial_\alpha\phi)(\partial_\beta\phi). \quad (5.8)$$

The diffuse interface model is implemented with a lattice Boltzmann model, using the D_2Q_9 model as used in [18, 21, 24]. The flow field, and the two order parameters are described by three particle distribution functions f_i , g_i and h_i , from which the following macroscopic fields are derived:

$$\sum_i f_i = \rho, \quad \sum_i c_{i,\alpha} f_i = \rho u_\alpha, \quad \sum_i g_i = \phi, \quad \sum_i h_i = \psi. \quad (5.9)$$

Here $c_{i,\alpha}$ is the cartesian component of the particle velocity. These particle distribution functions evolve on a square Bravais lattice, according to a discretisation of the Boltzmann equation, which is given for f_i :

$$f_i(\mathbf{x} + \mathbf{c}_i \Delta t, t + \Delta t) - f_i(\mathbf{x}, t) = -\omega_f [f_i(\mathbf{x}, t) - f_i^{eq}(\mathbf{x}, t)]. \quad (5.10)$$

Here f_i^{eq} is the equilibrium distribution - which approximates the Maxwell-Boltzmann distribution of an ideal gas in a simple lattice Boltzmann scheme for single phase fluid dynamics. In the free energy based LB schemes [18, 21, 24] the higher order moments of the equilibrium distribution are related to the chemical potentials and the stress tensor (with the lower order moments linked to the macroscopic fields as defined above):

$$\sum_i \tilde{c}_{i,\alpha} g_i^{eq} = 0, \quad \sum_i \tilde{c}_{i,\alpha} h_i^{eq} = 0, \quad (5.11)$$

$$\begin{aligned} \sum_i \tilde{c}_{i,\alpha} \tilde{c}_{i,\beta} f_i^{eq} &= P_{\alpha\beta}, \\ \sum_i \tilde{c}_{i,\alpha} \tilde{c}_{i,\beta} g_i^{eq} &= \Gamma_\phi \mu_\phi \delta_{\alpha\beta}, \\ \sum_i \tilde{c}_{i,\alpha} \tilde{c}_{i,\beta} h_i^{eq} &= \Gamma_\psi \mu_\psi \delta_{\alpha\beta}, \end{aligned} \quad (5.12)$$

with $\tilde{c}_{i,\alpha} = c_{i,\alpha} - u_\alpha$ the so-called peculiar velocity, which is a quantity much used in kinetic theory. $\delta_{\alpha\beta}$ is the Kronecker delta. The terms in the chemical potentials and stress tensor which include the gradient and Laplacian of the order parameters are computed with finite difference stencils cf. [18].

The transport coefficients are related to the relaxation parameters. The mobilities are equal to:

$$M_\phi = \Gamma_\phi (1/\omega_g - 1/2) \Delta t, \quad M_\psi = \Gamma_\psi (1/\omega_h - 1/2) \Delta t, \quad (5.13)$$

and the kinematic viscosity is equal to:

$$\nu = c_s^2(1/\omega_f - 1/2)\Delta t. \quad (5.14)$$

Apart for the different form of the free energy functional, our lattice Boltzmann model is identical as used in refs. [21, 24]. Hence, we refer the reader to these papers for more details on the lattice Boltzmann model.

Equilibrium properties

Analytical results

From the above free energy functional we can obtain analytical predictions for the equilibrium properties of surfactant adsorption. In the next paragraph analytical results are compared with numerical results.

The expression for the adsorption isotherm is obtained by the condition that the chemical potential, μ_b , of a bulk phase should be equal to the chemical potential at the (planar) interface. Assuming bulk surfactant concentration (volume fractions) $\psi_b \ll 1$, we have for the chemical potentials of the bulk phases:

$$\mu_{\psi,b} \approx \ln \psi_b + \frac{1}{2}W\phi_0^2. \quad (5.15)$$

Assuming that the sharpness of the diffuse interface is independent of the surfactant loading (thus $\phi(x) = \phi_0 \tanh(x/\zeta)$), the chemical potential at the interface is:

$$\mu_{\psi,0} = \ln(\psi_0) - \ln(1 - \psi_0) - \frac{1}{2}\epsilon\phi_0^2/\zeta^2. \quad (5.16)$$

Note that in the above equation we have used that $\partial_x\phi(x=0) = \phi_0/\zeta$.

In equilibrium holds $\mu_{\psi,b} = \mu_{\psi,0}$, and after substitution of the above expressions for the chemical potentials we obtain the Langmuir adsorption isotherm:

$$\begin{aligned} \psi_0 &= \frac{\psi_b}{\psi_b + \psi_c}, \\ \ln \psi_c &= -\frac{\epsilon\phi_0^2}{2\zeta^2} - \frac{1}{2}W\phi_0^2. \end{aligned} \quad (5.17)$$

Note, that ψ_0 is a dimensionless quantity, and attains the value $\psi_0 = 1$ if the surfactant is saturated (if $\psi_b \gg \psi_c$). Further, we note in case of $W = 0$ our expressions are equal to those in the model of Diamant and Andelman.

Also we obtain an analytical expression for the surfactant concentration profile by equating the chemical potential $\mu_\psi(x) = \mu_{\psi,b}$:

$$\psi(x) = \frac{\psi_{b,w}}{\psi_{c,w}(x) + \psi_{b,w}}, \quad (5.18)$$

with

$$\ln(\psi_{c,w}(x)) = -\frac{1}{2}\epsilon(\partial_x\phi(x))^2 + \frac{1}{2}W(\phi(x)^2 - \phi_0^2), \quad (5.19)$$

and $\phi(x) = \phi_0 \tanh(x/\zeta)$.

In sharp interface models the equation of state is obtained by integration of the Gibbs equation:

$$d\sigma = -\psi_0 d\mu_\psi. \quad (5.20)$$

As we deal with a diffuse interface, the excess amount of surfactant is to be obtained over integration over the diffuse interface [25]. We infer that the excess amount of surfactant is proportional to ψ_0 , and consequently that the interfacial tension lowering is proportional to that for a sharp interface: $d\sigma \sim -\psi_0 d\mu_{\psi,0}$. After substitution of Eq.(5.16) and integration we obtain the equation of state cf. [1]:

$$\sigma(\psi_0) - \sigma_0 \sim \ln(1 - \psi_0). \quad (5.21)$$

With $\sigma_0 = 4\kappa\phi_0^2/3\zeta$ the interfacial tension of the unloaded droplet.

Numerical analysis

We investigate the surfactant concentration profile for a planar interface. First simulations are performed with $\psi_c = 0.017$, $\phi_0 = 10$, $\kappa = \epsilon$, $Ch^* = \zeta/\Delta x = 3$ (grid Cahn number), $Ex = \epsilon/W\zeta^2 \approx 1$ and $\psi_b = \{10^{-4}, 10^{-3}, 10^{-2}\}$. Results are shown in figure 5.1, from which we observe that numerical results are in good agreement with the analytical predictions. In all cases the order parameter profile $\phi(x)$ follows the analytical prediction $\phi(x)/\phi_0 = \tanh(x/\zeta)$, and is thus independent of surfactant loading as we have assumed above. At low ψ_b there is a slight offset in the surfactant concentration at the interface ψ_0 , probably due to the discretisation error in estimation of the gradients and Laplacian via finite difference stencils.

Subsequently, we have analysed the validity of the Langmuir adsorption isotherm. $0.002 < \psi_c < 0.075$, $\eta = 0$, $\chi = 0$, $\phi_0 = 10$, $\epsilon = \kappa$, $Ch^* = 3$, and $Ex \approx 1$. Isotherms resulting from these simulations are shown in figure 5.2. Also shown are the analytical predictions of ψ_0 , using Eq.(5.17).

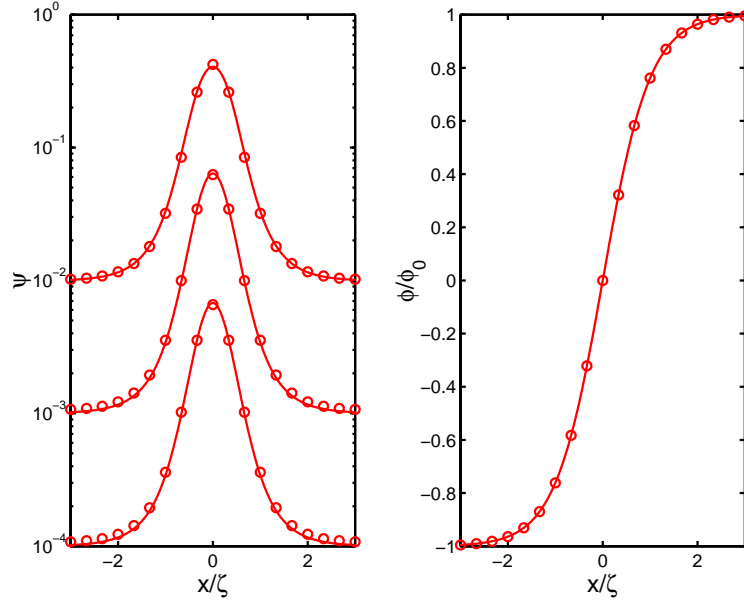


Figure 5.1: a) Profile of the surfactant concentration for a planar interface, located at $x = 0$, for various bulk concentrations $10^{-4} \leq \psi_b \leq 10^{-2}$. Parameter values are listed in the text. Numerical solutions are plotted as symbols and the solid line is the analytical prediction. b) Profile of the order parameter ϕ , according to surfactant adsorption model (symbols), compared to analytical prediction $\phi(x)/\phi_0 = \tanh(x/\zeta)$ (solid line).

One can observe that for high values of ψ_b and ψ_c the numerical values follow the analytical prediction reasonably well, but at lower levels of ψ_c the predictions are off. This is probably due to discretisation errors in the gradient of ϕ , or violation of the assumption $\psi_b \ll 1$ used above to derive the Langmuir isotherm.

Droplet phase

We investigate the lowering of the interfacial tension $\Delta\sigma$ due to surfactant adsorption on a droplet interface with radius R . At establishment of equilibrium we have computed $\Delta\sigma = \sigma - \sigma_0$, from σ_0 , the interfacial tension of the bare droplet:

$$\sigma_0 = \frac{4\kappa\phi_0^2}{3\zeta}, \quad (5.22)$$

and the droplet Laplace pressure:

$$\Delta p = \frac{\sigma}{R}. \quad (5.23)$$

Simulations are performed on a 2-D lattice $L_x/\Delta x = L_y/\Delta y = 64$, and radius $R = L_x/4$. We have chosen $\kappa = \epsilon$, $\zeta = 2$, and different values for ϕ_0 ,

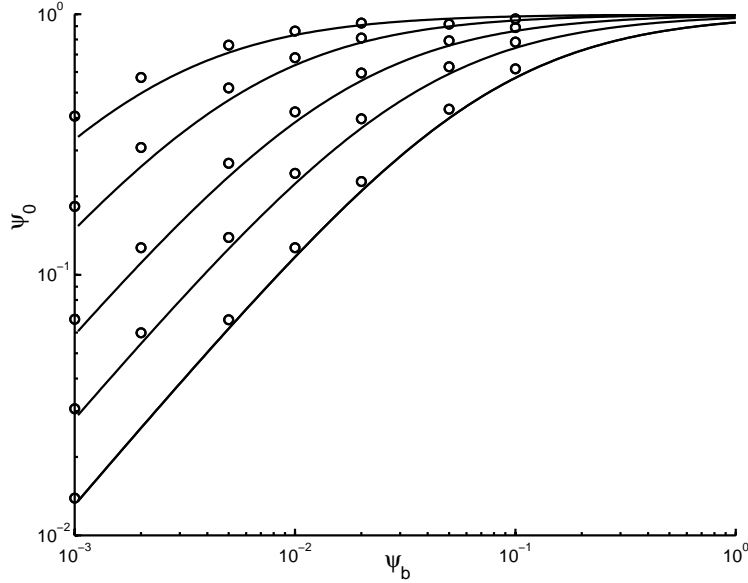


Figure 5.2: Adsorption isotherm, showing surfactant loading of a planar interface ψ_0 , as function of bulk concentration ψ_b for a range of values for $\psi_c = \{0.0020, 0.0056, 0.016, 0.035, 0.075\}$ (from top to bottom). Symbols represent numerical values, and solid lines are analytical predictions.

W , κ , and ψ_b . Initialisation is performed using the above analytical prediction of $\psi(r)$. The density profile is initialised such that the Laplace pressure of the droplet equals that of a droplet with a bare interface. From the resulting surfactant profile at equilibrium we have determined the surfactant loading of the interface ψ_0 . In figure 5.3 we have plotted the $\Delta\sigma$ versus $1 - \psi_0$ on a logarithmic scale. The three lines correspond with the following parameter sets: 1) $\sigma_0 = 6.4$ and $Ex = 1.9$, 2) $\sigma_0 = 14.4$ and $Ex = 0.5$, 3) $\sigma_0 = 24$ and $Ex = 0$. As one can observe for all parameter sets the interfacial lowering indeed follows the expected relation $\Delta\sigma \sim \ln(1 - \psi_0)$. However, the scaling clearly depends on Ex , which we yet can not explain theoretically. In case of $Ex = 0$ we have varied other parameters and have found that interfacial tension lowering only depends on ψ_0 . Observe that for parameter set 1) the relative lowering of the interfacial tension is maximally $\Delta\sigma/\sigma_0 < 0.5$, which is quite a realistic value.

Adsorption dynamics

We have investigated the dynamics of surfactant adsorption for a planar interface, using the classical Ward-Tordai problem [26], where one considers an interface in contact with a semi-infinite bulk phase, having initially a

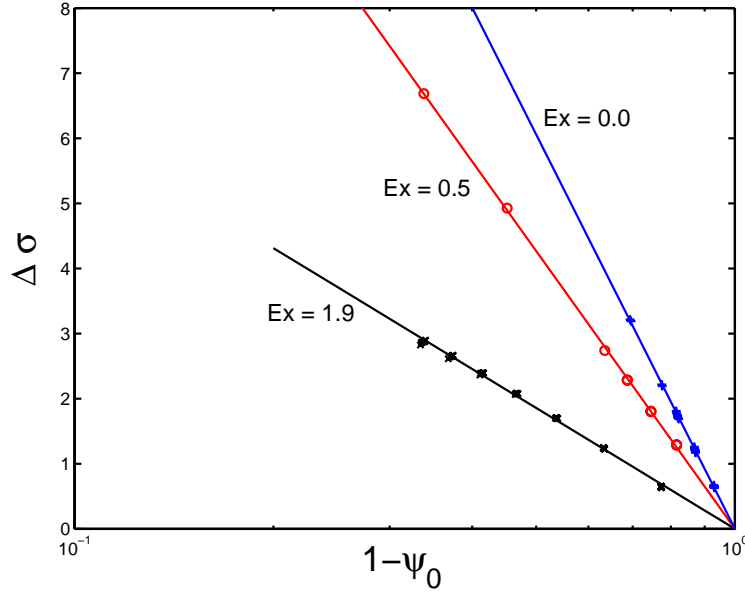
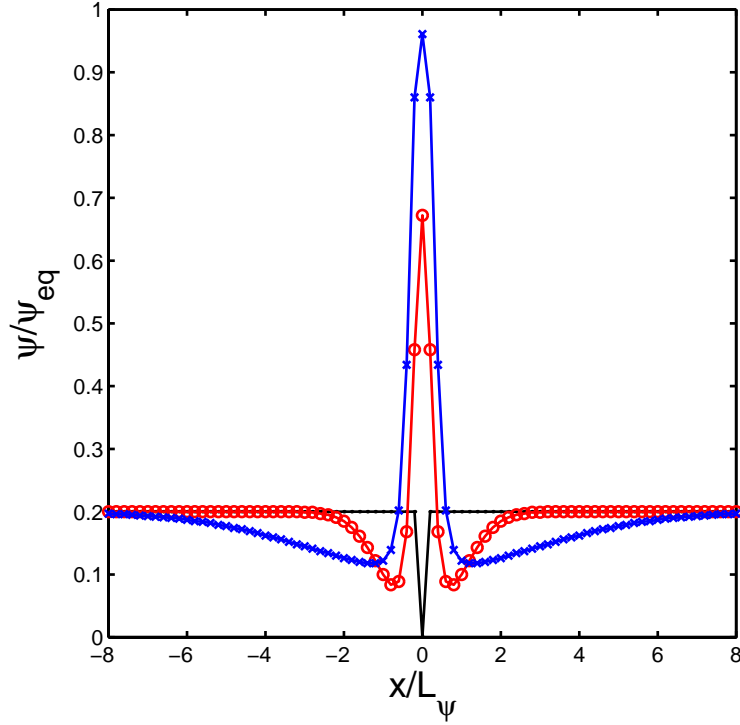


Figure 5.3: Interfacial tension lowering $\Delta\sigma$ as function of fraction of non-loaded interfacial area, $1 - \psi_0$. Parameter setting are mentioned in the main text. Numerical results are indicated with symbols, and the solid lines are linear regressions of the numerical data.

homogeneous surfactant concentration ψ_b , while the interface is depleted of surfactants $\psi_0(t = 0) = 0$. Surfactants will diffuse from the bulk phase to the interface. Hence, the surfactant concentration at the interface will rise, while depleting the bulk phase adjacent to the interface, the so-called sublayer. Soon the sublayer will be approximately in equilibrium with the interface, and the increase of the surfactant concentration at the interface will slow down, as the surfactants have to diffuse over longer distances in the bulk phase. Such behaviour of the surfactant profile is shown in figure 5.4, which is a result of our numerical analysis of the Ward-Tordai problem. For the Langmuir isotherm the Ward-Tordai can be solved analytically. We will compare our numerical results with approximations of the analytical predictions at short and long time scales.

We have investigated the Ward-Tordai problem numerically for a planar interface, in contact with oil and water bulk phases, having equal solubility of the surfactant and equal diffusivity of the surfactant D_ψ . In both bulk phases we assume Fickian diffusion. As in diffuse interface models the diffusive mass fluxes are formulated in gradients of the chemical potential ($j_\psi = -M_\psi \nabla \mu_\psi$), the surfactant mobility must be a function of ψ in order to obtain Fickian diffusion, cf.[22]: $M_\psi = D_\psi \psi(1 - \psi)$.

For a diffuse interface model of the Ward-Tordai problem of surfactant adsorption, there exists three length scales, for which there must be a


 Figure 5.4: Surfactant profile $\psi(x)$ at reduced times $\tau = 0, 0.5, 2.0$.

clear separation of scale. These scales are ζ , the thickness of the diffuse interface, L_ψ , the adsorption length, and L_x , the size of the simulation box. The classical definition of the adsorption length is $L_\psi/\Delta x = \psi_{eq}/\psi_b$ (assuming a sharp interface of thickness Δx). ψ_{eq} follows from the isotherm: $\psi_{eq} = \psi_b/(\psi_b + \psi_c)$. For a diffuse interface model the adsorption length is a factor 2-3 larger due to the finite width of the peak in the surfactant profile (see figure 5.4). The (classical) definition of the adsorption length is used to define the reduced time $\tau = tD_\psi/L_\psi^2$. Simulations are performed with $\zeta \ll L_\psi \ll L_x$, and no-flux boundary conditions at $x = \pm L_x/2$.

As said, we investigate the surfactant adsorption at short and long time scales, for which convenient approximations exist. For a sharp interface the surfactant adsorption at short times ($t \rightarrow 0$) in the Ward-Tordai problem follows:

$$\frac{\psi_0(\tau)}{\psi_{eq}} = \frac{2}{\sqrt{\pi}}\sqrt{\tau}. \quad (5.24)$$

The $\sqrt{\tau}$ behaviour holds for arbitrary bulk concentrations, and is independent of the type of adsorption isotherm.

Due to the finite width of the diffuse interface, we expect the surfactant adsorption in our model also to follow the $\sqrt{\tau}$ behaviour, but probably with

another proportionality constant. Henceforth, simulations are performed for $\psi_c = 0.0162$, $Ex \approx 0.1$, $\psi_b * 10^3 = \{1, 2, 5, 10\}$, $Ch^* = 3$, and $L_x/\Delta x = 400$. Results are shown in figure 5.5, and we view that all sorption curves $\psi(\tau)/\psi_{eq}$ for different ψ_b collapse to a single curve for short times $\tau < 0.02$:

$$\frac{\psi_0(\tau)}{\psi_{eq}} \approx \frac{5}{\sqrt{\pi}} \sqrt{\tau}. \quad (5.25)$$

This means that the adsorption length in the adsorption length for a diffuse interface is 0.4 times smaller than the adsorption length as defined for a sharp interface.

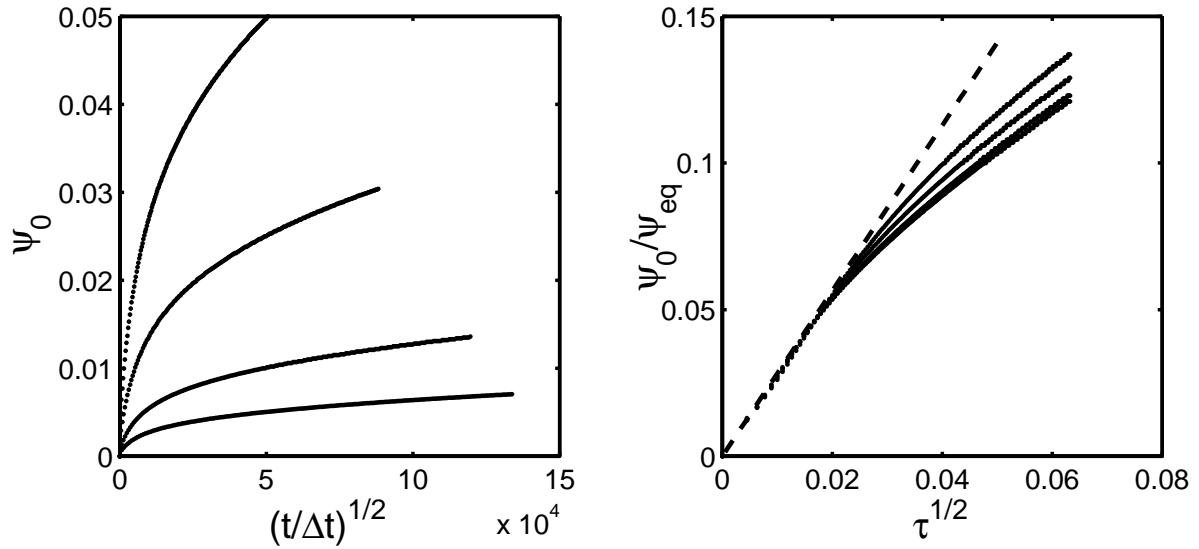


Figure 5.5: Evolution of surfactant loading of the interface at short time scale, a) in real time t and b) in reduced time τ . Dashed line shows the limiting behaviour at $\tau \rightarrow 0$. Values of ψ_b are listed in the text.

Surfactant adsorption at long times is shown in figure 5.6. Simulations are performed with the same parameter set as above, only the bulk concentrations are in the range of $\psi_b = \{0.05, 0.1, 0.2\}$, giving a small adsorption length in the order of $L_\psi \approx 20$, and Langmuir number of $La = \psi_b/\psi_c \approx \{3, 6, 12\}$. At long times the surfactant loading of the interface can be approximated with [27]:

$$\frac{\psi_0}{\psi_{eq}} = 1 - \frac{1}{\sqrt{(\pi\tau)} - La(1 - \sqrt{(\pi\tau)})}. \quad (5.26)$$

These approximations are drawn in figure 5.6 as dashed lines, and follow reasonably close our numerical results.

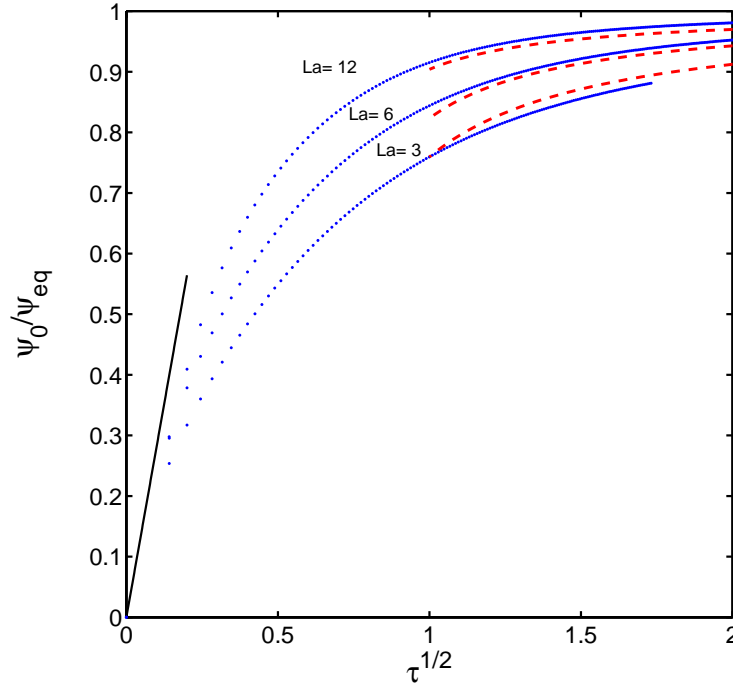


Figure 5.6: Evolution of surfactant loading of the interface in reduced time for Langmuir numbers $La = \psi_b/\psi_c \approx 3, 6, 12$. Dashed line shows the limiting behaviour at $\tau \rightarrow \infty$, and solid line the short time behaviour. Values of ψ_b are listed in the text.

At long times the adsorption is determined by the diffusion from distances $x \gg L_\psi$ to the subsurface layer, and therefore the finite width of the diffuse interface ζ does not play a role in the adsorption kinetics. At short times we have found that the finite size of the diffuse interface does effect the kinetics, leading to an apparent adsorption length of $L'_\psi = 0.4L_\psi$. The apparent adsorption length depends on ζ and also the initial surfactant loading of the interface at $t = 0$. For our simulations we have chosen to set $\psi(x) = 0$ for $x = 0$, and $\psi(x) = \psi_b$ for $x \neq 0$. An alternative initial condition is $\psi(x) = 0$ for $|x| < 2\zeta$, which probably will lead to a larger apparent adsorption length.

Surfactant adsorption on evolving droplets

To demonstrate that our diffuse interface model of surfactant adsorption can be coupled to hydrodynamics we have performed preliminary simulations of a surfactant laden drop in a uniform flow field and a linear shear

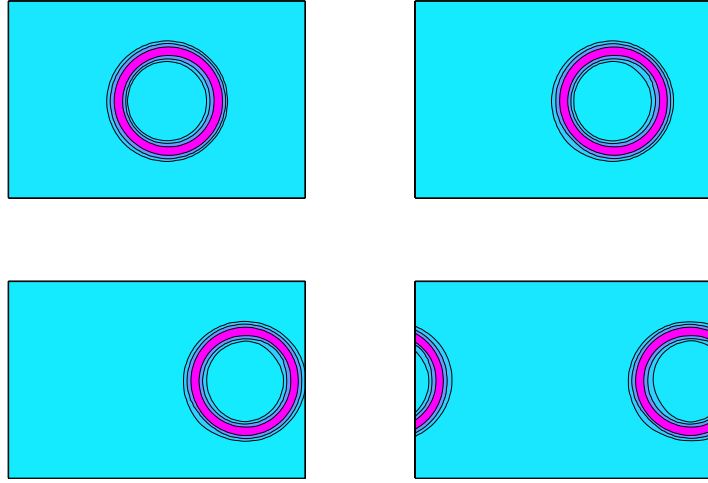


Figure 5.7: Contour plot of surfactant concentration of a surfactant laden droplet translating in a uniform flow field.

field. By simulating the drop in a uniform flow field, we investigate the Galilean invariance of a droplet in equilibrium with the bulk phases having a surfactant bulk concentration of ψ_b . By simulation of a deforming droplet we investigate whether the surfactant will diffuse over the interface of a deforming droplet.

Simulations are performed on a lattice of $L_x = 96\Delta x$ by $L_y = 64\Delta x$ lattice cells, with constant velocity boundary conditions at the top and bottom wall, and periodic boundary conditions at the side walls. The droplet has a radius of $R = 16\Delta x$, and is initially in equilibrium with the bulk phase. Furthermore the Courant number $Cr = u_{wall}\Delta t/\Delta x = 0.005$, the Peclet number $Pe = u_{wall}R/D_\psi = 533$, $\psi_c = 0.016$, $La \approx 1$, Reynolds number $Re = 0.3$.

Snapshots of the translating droplet in a uniform flow field are shown in figure 5.7. Here is depicted the contour plots of the surfactant concentration. The maximum surfactant concentration coincides with the droplet interface, and follows that while the droplet is translating in the flow field. However, if the Peclet number becomes a magnitude lower, the surfactant is not able to follow the motion of the droplet, and shows unphysical aggregation at the droplet interface.

By reversing the velocity of the top plate, we simulate the droplet in a shear field. Simulation is performed for a capillary number of $Ca =$

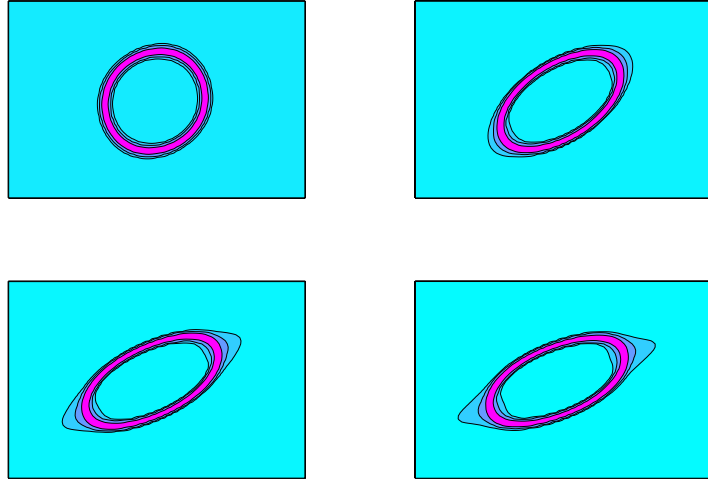


Figure 5.8: Contour plot of surfactant concentration of a surfactant laden droplet deforming in linear shear field.

$\gamma R\mu/\sigma_0 = 0.1$ with $\gamma = 2u_{wall}/L_y$ the shear rate, μ the dynamic viscosity of continuous phase, and σ_0 the interfacial tension of a bare interface.

Snapshots of the droplet in shear flow are shown in figure 5.8. Observe that the surfactant has migrated slightly to the regions with highest curvature, as one should expect [14, 28]. We have found that stability of the scheme is subtle, and needs more careful investigation of the wide set of numerical parameters in the model.

Conclusions

We have developed a diffuse interface model for surfactant adsorption onto the interface of an evolving droplet. In contrast to diffuse interface models of micro-emulsions our model exhibits realistic adsorption isotherms, namely the Langmuir isotherm.

For the equilibrium we have derived analytical expressions, which are in reasonable agreement with our numerical results. Differences arise due to discretisation errors in the finite difference approximations of the gradients and Laplacian of the order parameters ϕ and ψ . We expect accuracy to improve if wider stencils are used for these finite differences, cf. [29]. Lowering of interfacial tension σ of a droplet due to surfactant adsorption follows the correct theoretical behaviour of $\Delta\sigma \sim \ln(1 - \psi_0)$.

The dynamics of surfactant adsorption of the diffuse interface model simulating the classical Ward-Tordai problem is very similar to the dynamics for a sharp interface model. At short times we have found that the surfactant loading follows $\sqrt{(\tau)}$ behaviour. However, correct initial conditions are to be used to obtain the same proportionality factor. At long times the surfactant adsorption does follow quite closely the approximation, which holds for sharp interface models.

Via brief simulations of a surfactant laden drop in a (shear) flow field, we have shown that our diffuse interface model can be coupled to hydrodynamics. Upon deformation of the droplet, the surfactants diffuse to the part of the droplet interface with highest curvature.

We view that our model holds great potential in addressing problems where hydrodynamics and surfactant adsorption are strongly coupled (e.g. membrane emulsification) and especially problems involving droplet break up - which is modelled with much ease in diffuse interface models [10].

Mind that our model is yet limited to 2-D, non-ionic surfactants, with bulk concentrations below the critical micelle concentration (CMC). Extension to 3-D is straightforward for diffuse interface lattice Boltzmann models [29]. The other extensions do not present a problem in principle, as ideas for studies as [1, 30] can also be implemented straightforwardly.

Acknowledgements

We thank Gerhard Gompper and Reinhardt Miller for fruitful discussions.

References

1. H. Diamant, D. Andelman, Kinetics of surfactant adsorption at fluid/fluid interfaces: non-ionic surfactants, *Europhys. Lett.* 34, 8 (1996) 575.
2. S. Sugiura, M. Nakajima, T. Oda, M. Satake, M. Seki, Effect of interfacial tension on the dynamic behavior of droplet formation during microchannel emulsification, *J. Colloid Interface Sci.* 269 (2004) 178.
3. V. Schröder, O. Behrend, H. Schubert, Effect of dynamic interfacial tension on the emulsification process using microporous, ceramic membranes, *J. Colloid Interface Sci.* 202, 2 (1998) 334.
4. N.C. Christov, D.N. Ganchev, N.D. Vassileva, N.D. Denkov, K.D. Danov, P.A. Kralchevsky, Capillary mechanisms in membrane emulsification: oil-in-water emulsions stabilized by Tween 20 and milk proteins, *Colloids Surfaces A: Physicochem. Eng. Aspects* 209 (2002) 83.
5. A.J. Abrahamse, A. van der Padt, R.M. Boom, W.B.C. de Heij, Process fundamentals of membrane emulsification: simulation with CFD, *AIChE J.* 47 6 (2001) 1285.
6. S. van der Graaf, C.G.P.H. Schroën, R.G.M. van der Sman, R.M. Boom, Influence of dynamic interfacial tension on droplet formation during membrane emulsification, *J. Colloid Interface Sci.* 277, 2 (2004) 456.
7. M. Rayner, G. Trägårdh, Membrane emulsification modelling: how can we get from characterisation to design?, *Desalination* 145 (2002) 165.
8. A.J. Gijsbertsen-Abrahamse, A. van der Padt, R.M. Boom, Status of cross-flow membrane emulsification and outlook for industrial application, *J. Membr. Sci.* 230 (2004) 149.
9. I. Kobayashi, S. Mukataka, M. Nakajima, CFD simulation and analysis of emulsion droplet formation from straight-through microchannels, *Langmuir* 20 (2004) 9868.
10. D. Jacqmin, Calculation of two-phase Navier-Stokes flows using phase-field modeling, *J. Comp. Phys.* 155 (1999) 96.
11. J. Li, Y. Renardy, M. Renardy, Numerical simulation of breakup of a viscous drop in simple shear flow through a volume-of-fluid method, *Phys. Fluids* 12 (2000) 269.
12. C.D. Eggleton, and K. Stebe, An adsorption-desorption-controlled surfactant on a deforming droplet, *J. Colloid Interface Sci.* 208 (1998) 68.
13. H. Wong, D. Rumschitzki, C. Maldarelli, Maragoni effects on the motion of an expanding or contracting bubble pinned at a submerged tube tip, *J. Fluid Mech.* 379 (1999) 279.
14. C. Pozrikidis, Interfacial Dynamics for Stokes flow, *J. Comput. Phys.* 169 (2001) 250.
15. H. Zhou, V. Cristini, J. Lowengrub, C.W. Macosko, Numerical simulation of drop breakup and coalescence with soluble surfactant in 3D, *74th Annual Meeting Soc. Rheology* (2002).
16. D.M. Anderson, G.B. McFadden, A.A. Wheeler, Diffuse interface methods in fluid mechanics, *Annu. Rev. Fluid Mech.* 30 (1998) 139.

17. S. Chen, G.D. Doolen, Lattice Boltzmann method for fluid flows, *Ann. Rev. Fluid Mech.* 30 (1998) 329.
18. M.R. Swift, E. Orlandini, W.R. Osborn, J.M. Yeomans, Lattice Boltzmann simulations of liquid-gas and binary fluid mixtures, *Phys. Rev. E* 54, 5 (1995) 5041.
19. H. Diamant, G. Ariel, D. Andelman, Kinetics of surfactant adsorption: the free energy approach, *Colloids Surfaces A: Physicochem. Eng. Aspects* 183-185 (2001) 259.
20. M. Laradji, H. Guo, M. Grant, M.J. Zuckermann, The effect of surfactants on the dynamics of phase separation, *J. Phys.: Condensed Matter* 4 (1992) 6715.
21. O. Theissen, G. Gompper, Lattice Boltzmann study of spontaneous emulsification, *Eur. Phys. J. B* 11 (1999) 91.
22. E.B. Nauman, D.Q. He, Non-linear diffusion and phase separation, *Chem. Eng. Sci.* 56 (2001) 1999.
23. A.P. Russo, E.B. Nauman, Modeling the effect of compatibilizers in the coarsening of ternary polymer blends with core-shell morphology, *J. Polymer Sci. B* 96 (2000) 1301.
24. A. Lamura, G. Gonella, J.M. Yeomans, A Lattice Boltzmann model of ternary fluid mixtures, *Europhys. Lett.* 45,3 (1999) 314.
25. G.B. McFadden, A.A. Wheeler, On the Gibbs adsorption equation and diffuse interface models, *Proc. R. Soc. Lond. A* 458 (2002) 1129.
26. R. Miller, P. Joos, V.B. Fainerman, Dynamic surface and interfacial tensions of surfactant and polymer solutions, *Adv. Colloid Interface Sci.* 49 (1994) 249.
27. K.J. Mysels, Diffusion controlled adsorption on a plane: non-ideal isotherms, *Colloids Surf.* 16 (1985) 21.
28. H.A. Stone, Dynamics of drop deformation and breakup in viscous fluids, *Ann. Rev. Fluid Mech.* 26 (1994) 65.
29. J.C. Desplat, I. Pagonabarraga, P. Bladon, LUDWIG: A parallel Lattice-Boltzmann code for complex fluids, *Comput. Phys. Comm.* 134, 3 (2001) 273.
30. Y.C. Liao, O.A. Basaran, E.J. Franses, Micellar dissolution and diffusion effects on adsorption dynamics of surfactants, *AIChE J.* 49, 12 (2003) 3229.

Chapter 6

Preparation of double emulsions with membrane emulsification

Abstract

Double emulsions have potential for the production of low calorie food products, encapsulation of medicines and other high value products. The main issue is the difficulty to efficiently produce double emulsions in a well controlled manner due to their shear sensitivity. In membrane emulsification only mild shear stresses are applied and it is therefore expected that this process is very suitable for the production of double emulsions. In this review an overview is given of the state of the art; the advantages and disadvantages of membrane emulsification in relation to the production of stable double emulsions are summarized and compared. Finally an outlook on further research in this field is given.

This chapter has been published as: S. van der Graaf, C.G.P.H. Schroën, R.M. Boom, Preparation of double emulsions by membrane emulsification - a review, *Journal of Membrane Science* 251 (2005) 7-15.

Introduction

Double emulsions have promising applications in the food industry (low calorie products, improved sensoric characteristics, taste-masking), cosmetic industry (easily spreadable creams with encapsulated ingredients in both water and oil phase), pharmaceutical industry (drug delivery systems) and other fields like agriculture and the production of multicompartiment microspheres. Although a certain measure of 'controlled instability' is desired in some cases, such as for a drug delivery system, in general the stability of double emulsions is low and poorly controllable and therefore a main problem with regard to shelf life of a product. The instability usually leads to a significant part of the internal phase being lost already during the production of the double emulsion.

The first paper on double emulsions dates back eighty years (Seifriz, 1925 [1]), but there are still many challenges left for effective production of *stable* double emulsions. Control of shear forces is one of the main issues, that may be within reach of a relatively new production method: membrane emulsification.

In this review we briefly touch upon the production of single emulsions in order to introduce some basic concepts, but mainly focus on the production of double emulsions. Various emulsification methods such as rotor stator systems, high pressure homogenizers and obviously membrane emulsification and other membrane-based methods are discussed and compared. The role of surfactants is highlighted after which application areas of double emulsions are discussed. The paper rounds off with an outlook on the future of various aspects related to membrane emulsification and membrane-based techniques.

Single emulsions

Emulsions are dispersed, multiphase systems consisting of at least two insoluble liquids [2]. The dispersed phase is present in the form of droplets in a continuous phase. Depending on the emulsification process, the diameter of the droplets lies between 0.1 μm and 0.1 mm. Emulsions of this kind are thermodynamically unstable, which means that there is a tendency to reduce the interface (as a result of a relatively high interfacial tension), causing the droplets to coalesce and therewith decreasing the total amount of interface.

Double emulsions

A double emulsion is an emulsion in an emulsion. Two main types of double emulsions can be distinguished: water-in-oil-in-water (W/O/W) emulsions, in which a W/O emulsion is dispersed as droplets in an aqueous phase, and oil-in-water-in-oil (O/W/O) emulsions, in which an O/W emulsion is dispersed in an oil phase. W/O/W emulsions are more common than O/W/O emulsions. Double emulsions contain more interface and are even more thermodynamically unstable than single emulsions.

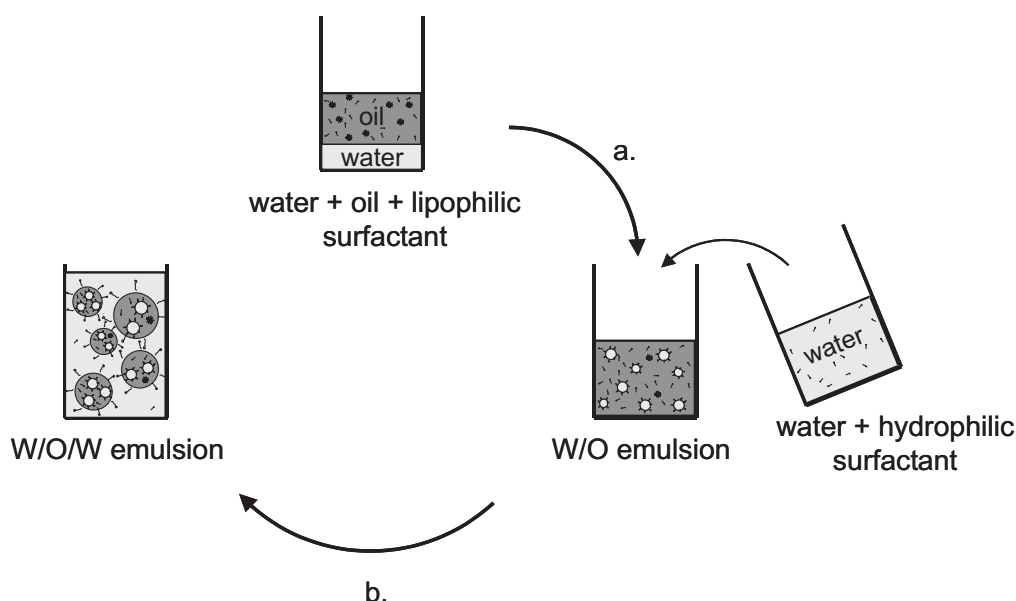


Figure 6.1: Preparation of a W/O/W double emulsion in two steps: a high shear emulsification step with lipophilic surfactants for the W/O emulsion (a) and a low shear emulsification step with hydrophilic surfactants for the W/O/W emulsion (b).

Usually double emulsions are prepared in a two-step emulsification process (see figure 6.1) using two surfactants; a hydrophobic one designed to stabilize the interface of the W/O internal emulsion and a hydrophilic one for the external interface of the oil globules (for W/O/W emulsions). The primary W/O emulsion is prepared under high-shear conditions to obtain small droplets while the secondary emulsification step is carried out with less shear to avoid rupture of the internal droplets [3]. In conventional emulsification processes high shear stresses are needed to decrease the droplet size and droplet size distribution of the coarse emulsion. However, external flow (shear) causes internal streaming in the droplets, which increases the frequency of collision (and thus coalescence) of internal

droplets with the outer water phase [4]. Besides, elongation of the droplets increases the interface available for release of internal droplets. Therefore, the release rate of internal droplets is dependent on the applied shear stress [5] and only moderate shear can be used for the production of double emulsions if a reasonable percentage of internal phase is required. This is the reason why double emulsions are in general polydisperse.

Florence and Whitehill [6] described four possible mechanisms for instability of W/O/W emulsions. These four mechanisms are (1) coalescence of the internal aqueous droplets; (2) coalescence of the oil drops; (3) rupture of the oil film separating the internal and external aqueous phases; and (4) passage of water (and water-soluble material, e.g. a drug) to and from internal droplets through the oil layer. This last point is subdivided into two possible mechanisms: via reverse micellar transport and by diffusion across areas where the oil layer is very thin [3]. All these mechanisms are known to occur, both during preparation of double emulsions and during storage. They influence the size distributions of the internal and outer droplets, which are important characteristics for double emulsions and the stability thereof. Further, double emulsions are often characterized by the entrapment yield of a certain compound in the inner droplet phase and the stability in time.

Table 6.1: Some examples of successful formulations used for the production of double emulsions ($W_1/O/W_2$) with membranes.

W_1	% W_1	O	W_2
no additives	30 vol.%	soybean oil 0.5% PC 0.5% PGCR	1% LPC [18] 5% glucose
no additives	10 vol.%	oleic acid 3 wt% TGPR	3 wt % Tween 20 [35]
no additives	5&10 wt%	rape seed oil 10 wt% PGPR	1-3 wt% Tween 80 [36]
tris-HCl buffer	10 vol.%	decane, ethyl oleate MCT, 5% Cr-310	tris-HCl buffer [37] (1% PGML)
5 wt% D(+) glucose	10-30 vol.%	soybean oil 5 wt% PGPR	0.5 wt% Tween 80 [39] 5 wt% D(+) glucose sodium alginate

An enormous amount of formulations for double emulsions is known in literature with various types of oil, different fractions of phases and different sorts of surfactants in varying concentrations (see table 6.1). Combinations of surfactants in the outer water phase have a beneficial effect on stability

and polymeric surfactants are very suitable emulsifiers (and stabilizers) for double emulsions, because they can protect double emulsions against coalescence by making them resistant to shear [3]. In general it can be stated that the formulation of double emulsions greatly influences the stability and droplet size, and this should be considered in conjunction with the choice of the preparation method.

Emulsification methods

General

The most important conventional emulsification devices are stirring apparatuses, rotor-stator systems and high-pressure homogenizers [2]. Stirrers are the earliest type of equipment that has been used for emulsification. The dispersed phase is broken up by the shear stresses of the turbulence. The energy consumption is usually large.

In rotor-stator systems, such as tooth-disc high speed homogenizers and colloid mills, a high shear is generated between a rotor and a stationary smooth, roughened or grooved surface. Also here turbulence is the primary cause of fluid disruption leading to the formation of droplets.

In high-pressure homogenizer systems the emulsion mixture is passed through a narrow orifice. This process may be assisted with use of ultrasound or electrical fields. Pressures in the range $5.0 \cdot 10^6$ - $3.5 \cdot 10^7$ Pa are common. In this process, emulsification is caused by turbulence and cavitation effects; the energy dissipation is high.

A few problems may be associated with these existing methods of production [7]. First, the droplet size and droplet size distribution cannot (easily) be controlled. Secondly, reproducibility is often poor and the quality of the product can vary per batch on the same manufacture scale. Scale-up is therefore a common difficulty.

For the production of double emulsions, it is important not to use high shear stresses to prevent disruption of the internal emulsions and coalescence with the external phase. Using conventional methods, this is not really feasible; only large droplets and a wide size distribution are obtained under low-shear conditions, leading to unstable products with unsatisfactory properties.

Membrane emulsification

Membrane emulsification [8] is a relatively new method for the production of emulsions that has received increasing attention over the last 15 years. The technique is attractive given the low energy consumption, the better control of droplet size and droplet size distribution and especially the mildness of the process.

For membrane emulsification (at least) two methods of operation are used, cross-flow membrane emulsification and pre-mix membrane emulsification [9]. In the latter method of operation, first a coarse pre-mix is made which is subsequently pushed through a membrane. Upon passage of the coarse droplets through the membrane they break up into finer droplets. The resulting droplet size distribution is slightly wider than those obtained with cross-flow membrane emulsification [9], though still narrower than obtained with conventional processes and higher fluxes can be obtained. We will here focus on cross-flow membrane emulsification (and use the term membrane emulsification for simplicity), we will discuss pre-mix membrane emulsification later.

In (cross-flow) membrane emulsification the to-be-dispersed phase is pressed through a microporous membrane while the continuous phase flows along the membrane surface. Droplets grow at pores and detach at a certain size, which is determined by the balance between the forces acting on the droplet [10, 11]. The main forces are the drag force and the interfacial tension force. With pores that are not cylindrical, another force is important, and can be even dominant in some cases. This is the force resulting from deformation of the to-be-dispersed phase at the pore. Intrusion of continuous phase into the pore can facilitate this deformation. A droplet growing from a non-cylindrical pore will form a droplet radius that is larger than the internal smallest radius in the pore. This will result in a negative pressure difference due to the Laplace pressure between the to-be-dispersed phase in the pore and in the droplet that is being formed, which can lead to spontaneous snap-off of the droplet (as long as the flow velocity of the to-be-dispersed phase through the pore is not too high). When this force is dominant, one typically observes that the droplet size is independent from the cross-flow velocity of the continuous phase. This has been observed with SPG membranes [12], and is common with microchannel emulsification (see section 'Microchannel emulsification'). For both detachment mechanisms (i.e. resulting from cross-flow, or spontaneous snap-off) it is

of the utmost importance that the membrane is and remains wetted by the continuous phase for proper droplet formation and droplet detachment.

In literature, reviews are available on the production of single emulsions with membranes (Joscelyne and Trägårdh [13], Charcosset *et al.* [14]) and microstructured systems (Lambrich and Vladisavljevic [15]). Gijsbertsen-Abrahamse *et al.* [16] reviewed the current status of membrane emulsification and gave an outlook for industrial application.

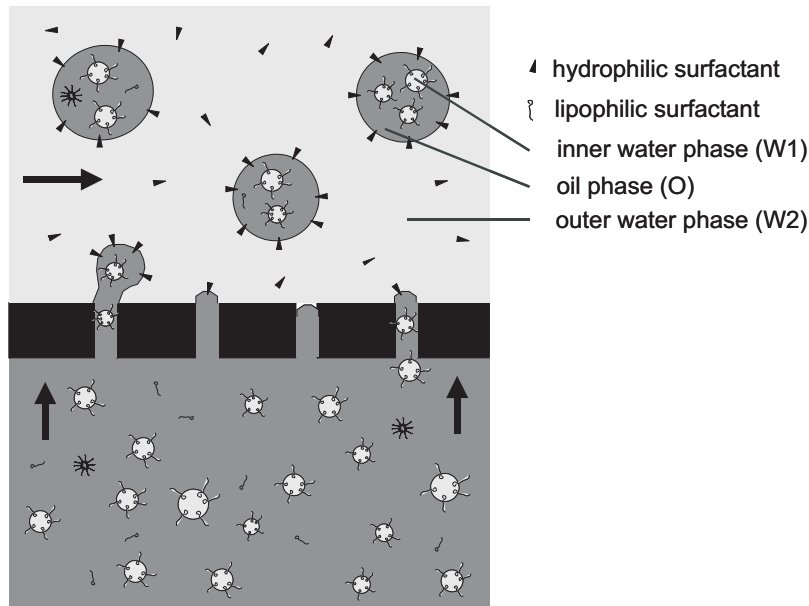


Figure 6.2: Schematic drawing of the production of a double emulsion ($W_1/O/W_2$) by membrane emulsification with a simple emulsion as dispersed phase. The arrows represent the direction of the fluid flow.

If a single emulsion (e.g. W/O) is used as the to-be-dispersed phase, also double emulsions (e.g. $W/O/W$) can be produced by this method (see figure 6.2). The primary emulsion may be produced by means of a conventional method or also by membrane emulsification. The mild conditions of membrane emulsification are especially useful for the second emulsification step in order to prevent rupture of the double emulsion droplets, which might even lead to inversion into a single O/W emulsion. In contrary to conventional emulsification methods, it becomes possible to produce small and monodisperse droplets without using high shear stresses that cause escape of the internal droplets.

A notable disadvantage of membrane emulsification is the low flux of the dispersed phase [14] caused by the low hydraulic permeability of most of the membranes used. However, the flux of dispersed phase could be

increased by using a membrane with a low hydraulic resistance [16]. New developments in nano and microengineering make it possible to produce membranes, so-called microsieves, with these desired properties [17].

Cross-flow membrane emulsification with SPG membranes

Mine *et al.* [18] were the first to report that it is possible to produce double emulsions (W/O/W) by membrane emulsification with Shirasu Porous Glass (SPG) membranes. They used a microfluidizer for the first W/O emulsion and SPG membranes for the second emulsification step. They found that the membrane has to be hydrophilic and needs to have an average pore size of at least twice the diameter of the primary water droplets of the W/O emulsion, otherwise these droplets will be rejected by the membrane. Preferably, the concentration of internal water droplets for W/O/W emulsions should be between 30 and 50%, however, Okochi and Nakano [19] also obtained good results with a lower fraction. For pharmaceutical or cosmetic applications natural emulsifiers, like phospholipids, are preferable. In the work of Mine *et al.* [18] it was shown that membrane emulsification is a reliable method for preparing W/O/W emulsions with these surfactants.

Okochi and Nakano [19] compared two W/O/W emulsions containing water soluble drugs, which were prepared by either membrane emulsification with SPG membranes (for the second emulsification step) or a (traditional) two-stage stirring emulsification method. Double emulsions prepared by membrane emulsification showed a smaller standard deviation of the mean particle size and a slightly lower viscosity. Also, the entrapment efficiency for membrane emulsification was somewhat higher. This makes the method with the SPG membranes especially useful for low molecular weight drugs, which normally give a relatively low entrapment efficiency. Drug release from the emulsion prepared by membrane emulsification was slower, which may be due to the more homogeneous particles and the sharper size distribution that make the emulsions more stable. Higashi *et al.* [20 – 23] published the first, very promising results for clinical studies of this new drug delivery system based on membrane emulsification with SPG membranes. A disadvantage of membrane emulsification compared to conventional methods is that it is very time consuming due to the low fluxes involved, which might be a problem if the stability of entrapped drugs is low [24].

Janardhanan *et al.* [25] investigated the yield of W/O/W emulsions produced by either ultra-turrax or membrane emulsification with SPG membranes for the second emulsification step. The results showed that stable emulsions with high yields ($\geq 90\%$) could be obtained with polyglycerol polyricinoleate (PGPR) as hydrophobic surfactant with both emulsification methods. W/O/W emulsions produced with Span 80 as hydrophobic surfactant showed considerably lower yields.

Ma *et al.* [26] prepared uniformly sized polystyrene-polyacrylamide composite microspheres from a W/O/W emulsion prepared with SPG membranes in the second emulsification step. It was found that the spherical polyacrylamide microdomains (the former inner aqueous phase) were distributed inside and on the surface of a composite particle. The number of polyacrylamide microdomains on the surface was controllable by varying the amount of cross-linking agent added to the oil phase.

Other reported applications and studies with SPG membranes include oral drug delivery of insulin encapsulated in W/O/W emulsions [27], leakage of irinotecan hydrochloride (which shows marked anti-tumor effects) from W/O/W emulsions [28], preparation of a solid microcarrier from W/O/W emulsions [29], influence of surfactants on leakage of anthocyanin from W/O/W emulsions [30] and the preparation of S/O/W emulsions as drug microcarriers (with solid particles under 500 nm) by dehydrating the W/O emulsion and using pre-mix emulsification with SPG membranes to make the S/O/W particles [31].

Only one peer-reviewed paper is known to us in which double emulsions were successfully prepared by membrane emulsification for both emulsification steps. Nakashima *et al.* [32] reported application of double membrane emulsification, which means the preparation of a W/O emulsion using a hydrophobic membrane and completion of the W/O/W emulsion using a hydrophilic membrane.

Microchannel emulsification

Microchannel emulsification [33] is a novel method for producing monodisperse emulsions; even more monodisperse than usually obtained with membrane emulsification. Micromachining technology was used to manufacture small, non-cylindrical microchannels in a silicon plate. Droplets are produced by forcing the to-be-dispersed phase through the microchannels. Microchannel emulsification exploits the interfacial tension (σ_{ow}), a large

force on micrometer scale, as the driving force for droplet formation [34]. The to-be-dispersed phase is forced to assume a distorted (elongated) disk-like shape on the terrace in the microchannel. This distorted shape has a higher interfacial area with at least one radius of curvature smaller than a spherical shape in the well with radius R_d , resulting in different Laplace pressures (Δp_1 on the terrace and Δp_2 in the well) and spontaneous droplet formation:

$$\Delta p_1 = \sigma_{ow} \left(\frac{1}{R_1} + \frac{1}{R_2} \right) \approx \frac{\sigma_{ow}}{R_1} \quad (R_2 \gg R_1), \quad (6.1)$$

$$\Delta p_2 = 2 \frac{\sigma_{ow}}{R_d}. \quad (6.2)$$

If $\Delta p_1 = \frac{\sigma_{ow}}{R_1} > \Delta p_2 = 2 \frac{\sigma_{ow}}{R_d}$, thus $R_1 < \frac{1}{2} R_d$, spontaneous snap-off may occur. One sees that, as long as σ_{ow} can be regarded as a constant, only the geometry determines the droplet size. The droplets are formed without shear by continuous phase flow, which makes this method interesting for the production of double emulsions.

Kawakatsu *et al.* [35] were the firsts to produce W/O/W emulsions by microchannel emulsification using W/O emulsions prepared by homogenization as feed emulsions. They also produced solid-in-oil-in-water (S/O/W) pectin microcapsules by gelation of the internal water phase, the pectin solution, using a calcium solution containing Tween 20 as an external phase.

Lambrich *et al.* [36] successfully produced W/O/W emulsions with microchannel emulsification containing 5 and 10% internal water phase and varied the outer surfactant concentration (0.5-4% (w/w) Tween 80). They used a high pressure homogenizer to make the primary emulsion. Other than with cross-flow or pre-mix membrane emulsification, there exists a pronounced upper limit to the maximum throughput velocity. At higher throughput velocities, the to-be-dispersed emulsion is supplied faster than the droplet can detach, thus leading to large, polydisperse droplets that do not detach spontaneously. A higher surfactant concentration in the outer water phase gave a lower maximum throughput velocity (critical velocity). This corresponds with the theory that the driving force is stonger at low surfactant concentrations and thus high dynamic interfacial tension. Coalescence between the inner water phase and the outer water phase was found to be minimal.

Sugiura *et al.* [37] also prepared W/O/W emulsions by two-step emulsification employing microchannel emulsification as the second step. They

used a homogenizer for the first emulsification step because of the low production rate of microchannel emulsification. Sugiura *et al.* fluoreometrically investigated the entrapment yield of the produced W/O/W emulsions. No leakage was observed during the microchannel emulsification process, even internal droplets larger than the channels could penetrate through the channels without disruption. An entrapment yield of 91% was found.

A disadvantage of microchannel emulsification for practical applications is its inherent low production rate. Usually, less than $1 \cdot 10^{-6} \text{ m}^3 \cdot \text{h}^{-1}$ of dispersed phase can be prepared per microchannel plate (this corresponds with $1 \cdot 10^{-2} \text{ m}^3 \cdot \text{m}^{-2} \cdot \text{h}^{-1}$ for a microchannel plate of 1 cm^2). According to Sugiura *et al.* [37], microchannel emulsification could still be scaled up by a factor 10^3 to 10^4 by using a larger microchannel plate, straight-through microchannels [38] and multiple microchannel plates.

Pre-mix membrane emulsification

Vladisavljevic *et al.* [39] produced W/O/W emulsions using multi-stage pre-mix membrane emulsification with SPG membranes. Better results with regard to particle size distribution were obtained using several (2-4) passes at moderate pressures instead of a single pass at high pressures. Relatively high (transmembrane) fluxes, in the range of $1.8\text{-}37 \text{ m}^3 \cdot \text{m}^{-2} \cdot \text{h}^{-1}$, were obtained.

Shima *et al.* [40] introduced this method to produce a W/O/W emulsion with a membrane. They first prepared a coarse W/O/W emulsion using conventional rotor/stator homogenization. The coarse W/O/W emulsion was passed through a cellulose acetate membrane to reduce the diameter of the oil droplets. This represents a form of pre-mix membrane emulsification of double emulsions (see figure 6.3). An important advantage of pre-mix membrane emulsification is that high fluxes can be obtained. During the second step of the preparation process of the coarse double emulsion, outer water phase became enclosed in the oil droplets. Observations revealed that this former outer water phase (W_2^*) was released to the outer water solution (W_2) from the interior of the oil droplets during the filtration step, while the inner water phase (W_1) hardly leaked into the outer water phase (W_2) solution. The reason is that the included outer water phase (W_2^*) solution wets the hydrophilic membrane quite well, because it contains hydrophilic surfactant, therewith facilitating exclusion of this phase from the oil droplets. The internal phase (W_1), in contrast, is well stabilised

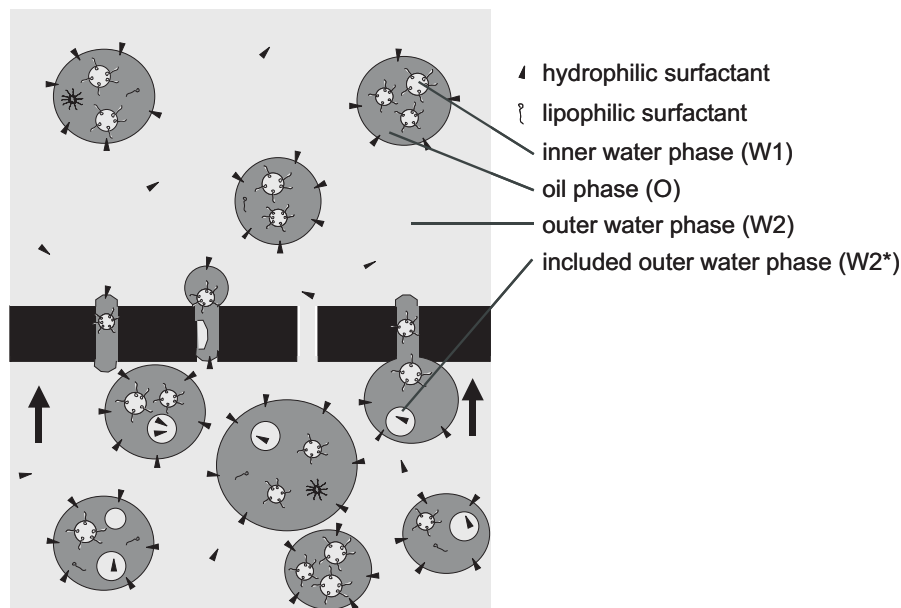


Figure 6.3: Schematic drawing of pre-mix membrane emulsification with a coarse double emulsion as dispersed phase. The arrows represent the direction of the fluid flow.

by the (lipophilic) surfactant system, and therefore will not coalesce easily with the external phase, or wet the pore walls. Observations also suggest that the droplets of the included outer water phase (W_2^*) are larger than the pore diameter.

Kawashima *et al.* [41] and Hino *et al.* [42] extruded a W/O/W emulsion, which was made in a conventional way, through polycarbonate membranes with pores of 3 or 8 μm in diameter. The membrane caused phase inversion and a semisolid W/O emulsion was formed with smaller aqueous droplets than the original emulsion after the first emulsification step. This fine and highly viscous W/O emulsion could easily be redispersed into a hydrophilic surfactant containing aqueous solution. The droplet size of the redispersed emulsion was smaller and more homogeneous than the original W/O/W emulsion. These effects were more pronounced when the pore size was small. The membrane materials and ratio of hydrophilic versus hydrophobic surfactants influenced this process. Extrusion of a W/O/W emulsion with a hydrophobic membrane resulted in a W/O emulsion, while extrusion with a hydrophilic membrane resulted in an O/W emulsion. It is thought that during extrusion of the W/O/W emulsion through a hydrophobic membrane, lamellar structures were formed and at the outlet of the pores reverse micelles would be formed. These reversed micelles

would coalesce and a W/O emulsion would be formed. For certain ratios of hydrophilic and hydrophobic surfactants phase inversion did not occur, which may explain why Shima *et al.* [40] did not observe phase inversion.

Table 6.2: Characteristics of cross-flow membrane emulsification (XME), pre-mix membrane emulsification (PME) and microchannel emulsification (MC).

	<i>XME</i>	<i>PME</i>	<i>MC</i>
Main mechanism	drag with continuous phase	confinement into branching and joining pores	interfacial tension; droplet deformation
Reported flux ¹ ($\text{l}\cdot\text{m}^{-2}\cdot\text{h}^{-1}$)	O/W:2-40 [13] W/O:2·10 ² -2·10 ³ [13] W/O/W:1.67·10 ⁻³ [19] ²	1·10 ³ -1.5·10 ⁴ [9] 1.8·10 ³ -3.7·10 ⁴ [39]	< 10 [37] 65 [38]
Membranes	SPG [8, 18, 19, 25, 26]	SPG [31] cellulose acetate [40] (polycarbonate [41]) ³	MC plate [35 – 37]
Internal phase primary emulsion	30-50 % [18], 20 % [24]	30 % [40], 10-30% [39]	10% [35, 37], 5, 10% [36]
Entrapment efficiency	high	> 90 % [40]	91 % [37]
Fouling	moderate; surface fouling	severe; membrane depth fouling	limited; fouling inside channel

Polycarbonate membranes were also used for the extrusion of multi-lamellar vesicles to produce liposomes with a defined size and homogeneous size distribution [43]. The liposomes were sequentially passed through membranes with pore diameters of 3.0, 1.0, 0.8, 0.6, 0.4 and 0.2 μm resulting in vesicles with a mean size approaching that of the polycarbonate membrane with the smallest pores (0.27 μm).

To summarize, table 6.2 gives an overview of the characteristics of the different emulsification methods for producing double emulsions with membranes and microstructures classified into the 3 main categories: cross-flow membrane emulsification, pre-mix membrane emulsification and microchannel emulsification.

Influence of surfactants

The type and concentration of surfactants affects the production process as well as the long term stability of double emulsions. Emulsion formation

¹Given for emulsification in general (not specific for double emulsions), only for XME given as a function of different emulsion types.

²In $\text{l}\cdot\text{h}^{-1}$, membrane surface area unknown.

³W/O/W emulsion was inverted to a W/O emulsion.

in cross-flow and pre-mix membrane emulsification is facilitated when the Laplace pressure is lowered by surfactants and the stability is improved because surfactants help to prevent coalescence. A surfactant with a low hydrophilic-lipophilic balance (HLB) is better soluble in oil and normally forms W/O emulsions, a surfactant with a high HLB dissolves in water and forms O/W emulsions. Therefore, double emulsions contain (at least) two surfactants of which one is lipophilic (low HLB) and one is hydrophilic (high HLB). The interaction of these two surfactants determine the stability of the double emulsion. Florence and Whitehill [6] showed that it is possible to deliberately use the knowledge about the behaviour of different surfactants to produce 3 types of W/O/W emulsions, type A with oil droplets containing one large internal droplet, type B containing several small internal drops and type C containing large numbers of internal droplets.

Kawakatsu *et al.* [35] found that W/O/W emulsions could not be produced with microchannel emulsification if Span 20 or Span 80 are used as lipophilic surfactant due to the low stability of the primary W/O emulsions. W/O/W emulsions could be produced with tetraglycerol polyricinoleate (TGPR) as lipophilic surfactant, however, the concentration of TGPR affected the stability of the internal water droplets and the oil droplets containing the water droplets. At a high TGPR concentration (5 wt%), the internal water phase was stable, but oil droplets containing water droplets had a tendency to coalesce.

A high concentration of hydrophobic surfactant in the oil phase and a low concentration of hydrophilic surfactant in the outer water phase have a beneficial effect on stability [3]. A high concentration of hydrophilic surfactant leads to rupturing of the oil film and helps to release inner water droplets [44, 45]. Kawashima *et al.* [41] found that a high concentration of hydrophilic surfactant in the outer water phase leads to a lower entrapment capacity in the emulsion. On the other hand, a relatively high concentration of surfactant in the outer water phase is needed for the production of monodisperse small droplets by membrane emulsification [46, 47]. This example nicely illustrates the complexity of optimization of surfactants and surfactant concentrations for the production of double emulsions by means of membrane emulsification. Apart from stability and production issues, it is often desirable to minimise the use of surfactants (e.g. in foods), because they are usually costly and not very healthy or have an unhealthy image.

Applications of double emulsions produced by membrane emulsification

The main application so far of double emulsions produced by membrane emulsification is as a drug delivery system [32]. For example, most anticancer drugs are used as emulsions because they are water-soluble. In the form of an emulsion it is possible to control release rates of medicine and suppress strong side effects of the drug. However, a single emulsion cannot be used since W/O emulsions generally have such a high viscosity that infusion of emulsions to arteries/capillaries via catheters is difficult if not impossible. Also O/W emulsions are not an option because they do not encapsulate the drug [42]. But W/O/W emulsion systems are suitable drug carriers because of the encapsulation of the drug in the internal water phase and the low viscosity due to the external water phase. For the application of W/O/W emulsions as drug delivery systems it is important to prepare a very stable W/O/W emulsion in which countless submicron water droplets are encapsulated. Preparation of such an emulsion starts with the production of a submicron W/O emulsion containing the drug in the dispersed water phase, using a hydrophobic membrane. Then, the W/O/W emulsion is made with the W/O emulsion as dispersed phase, using a hydrophilic membrane. The advantage of this method is that a medically safe emulsion can be prepared since the precise design of the emulsion particle is possible.

Higashi *et al.* [20 – 23] prepared such a new drug delivery system for treating hepatocellular carcinoma (HCC) using W/O/W emulsions made by membrane emulsification in the second emulsification step (W/O emulsion was made by sonification). The emulsions were prepared with iodinated poppy-seed oil (IPSO). The emulsion accumulates in the small vessels in the tumor when injected to the liver via the hepatic artery. The inner water phase contained water soluble epirubicin (drug). By the use of different glass membranes of an appropriate pore size it is possible to produce W/O/W emulsions with IPSO droplets in a range of 1 to 70 μm . Separation or breakdown of the emulsion did not occur for at least 40 days. Clinical studies [23] showed that the size of IPSO microdroplets influenced the anti-tumor effect of the therapy: very small droplets passed through the tumor, while very large droplets did not reach the tumor. This confirms the importance of a controlled droplet size, which was not feasible before the membrane emulsification technique was developed.

Toorisaka *et al.* [48] developed a S/O/W emulsion for oral administration of insulin. Surfactant-coated insulin was dispersed in the oil by ultrasonication, this dispersion was mixed with the outer water phase with a homogenizer and finally, the S/O/W emulsion thus obtained was adjusted to a constant particle size by passage through a SPG membrane. The S/O/W emulsion showed hypoglycemic activity for a long period after oral administration to rats. The authors expect that the S/O/W emulsions will become widely used in the treatment of diabetes.

Nakajima *et al.* [49] specifically refer to membrane emulsification as a method to make functional ethanol-in-oil-in-water (E/O/W) emulsions. These E/O/W emulsions are suitable to encapsulate functional components that have a low solubility with respect to water and oil but are soluble in ethanol. An example is taxol which is an anticancerous terpenoid.

Another possible application of double emulsions is in the food industry. Preliminary studies have been performed in the field of entrapment of a flavour component in a release system [50]. Sensitive food materials and flavours can be encapsulated in W/O/W emulsions. Sensory tests have indicated that there is a significant taste difference between W/O/W emulsions and O/W emulsions containing the same ingredients, and that there is a delayed release of flavour in double emulsions.

Conclusions and Outlook

Several papers show that it is possible to produce double W/O/W emulsions by means of membrane emulsification (as the second emulsification step). Especially the production of emulsions with SPG membranes showed promising results. In the medical field, this method even made it possible to develop a new drug delivery system for the treatment of liver cancer. No studies are known in which O/W/O emulsions were prepared by membrane emulsification.

However, there are also some drawbacks. It takes much more time to produce double emulsions by membrane emulsification than by conventional means, because the flux of the dispersed phase through the membrane is fairly low. Optimization of the formulation can increase the dispersed phase flux somewhat, however, this is not enough to make the method much more attractive. The use of a new type of membranes with a low resistance for permeation (e.g. microsieves) may help to increase the dispersed phase flux by orders of magnitude. For microchannel emulsifica-

tion, the flux is even lower than with SPG membranes. However, scaling up this process (e.g. through straight-through microchannels) seems possible. Another possible option to increase the flux is pre-mix membrane emulsification with double emulsions, which was recently introduced by Shima and should be investigated further. However, it is expected that this method is more sensitive to fouling, especially when proteins are incorporated in the formulation.

The fact that membrane emulsification is time consuming, especially if a thick emulsion is required, is one of the reasons why membrane emulsification is not (widely) used as the first emulsification step in the production of double emulsions. It is expected that using membrane emulsification also for the first emulsification step will increase the stability of the produced emulsion even further, due to a smaller droplet size distribution of the inner droplets. Moreover, it may then be possible to design double emulsions with specific inner and outer diameters.

Currently, only for the production of very high value products like drug delivery systems, the production of double emulsions with membrane emulsification is feasible. Therefore, future research should focus on increasing the flux of the to-be-dispersed phase (e.g. by optimization of the type of membrane), while maintaining the advantageous conditions of membrane emulsification. Further elucidation of the different possible mechanisms of droplet formation and homogenization with membranes will enable optimization of the process. Increasing the dispersed phase flux is still a challenge. But we expect that as soon as this challenge is met, membrane emulsification will also become attractive for (large scale) production of double emulsions for certain food and cosmetic products, especially those products that benefit most from a uniform droplet size and/or a mild production process.

Acknowledgement

This research was supported by the European Community, project QLRT-2000-01228.

Abbreviations

CR-310	tetraglycerin-condensed ricinoleic acid ester
E/O/W	ethanol-in-oil-in-water
HCC	hepatocellular carcinoma
HLB	hydrophilic-lipophilic balance
IPSO	iodinated poppy-seed oil
LPC	lysophosphatidylcholine
MCT	medium-chain triglyceride
PC	phosphatidylcholine
O/W	oil-in-water
O/W/O	oil-in-water-in-oil
PGCR	polyglycerol esters of polycondensed ricinoleic acid
PGML	pentaglycerin monolaurate
PGPR	polyglycerol polyricinoleate
S/O/W	solid-in-oil-in-water
SPG	Shirasu Porous Glass
TGPR	tetraglycerol polyricinoleate
W/O	water-in-oil
W/O/W	water-in-oil-in-water

References

1. W. Seifriz, Studies in emulsions. III Double reversal of oil emulsions occasioned by the same electrolyte, *J. Phys. Chem.* 29 (1925) 738.
2. H. Schubert, H. Armbruster, Principles of formation and stability of emulsions, *Int. Chem. Eng.* 32 (1992) 14.
3. N. Garti, C. Bisperink, Double emulsions: progress and applications, *Curr. Opin. Colloid Interface Sci.* 3 (1998) 657.
4. J.K. Klahn, J.J.M. Janssen, G.E.J. Vaessen, R. de Swart, W.G.M. Agterof, On the escape process during phase inversion of an emulsion, *Colloids Surfaces A: Physicochem. Eng. Aspects* 210 (2002) 167.
5. V. Muguet, M. Seiller, G. Barratt, D. Clausse, J.P. Marty, J.L. Grossiord, W/O/W multiple emulsions submitted to a linear shear flow: correlation between fragmentation and release, *J. Colloid Interface Sci.* 218 (1999) 335.
6. A.T. Florence, D. Whitehill, Some features of breakdown in water-in-oil-in-water multiple emulsions, *J. Colloid Interface Sci.* 79, 1 (1981) 243.
7. R.A. Williams, S.J. Peng, D.A. Wheeler, N.C. Morley, D. Taylor, M. Whalley, D.W. Houldsworth, Controlled production of emulsions using a crossflow membrane. Part 2: Industrial Scale Manufacture, *Trans. Int. Chem. Eng.* 76 Part A (1998) 902.
8. T. Nakashima, M. Shimizu, M. Kukizaki, Membrane emulsification by microporous glass, *Key Eng. Mater.* 61&62 (1991) 513.
9. K. Suzuki, I. Fujiki, Y. Hagura, Preparation of corn oil/water and water/corn oil emulsions using PTFE membranes, *Food Sci. Technol. Int. Tokyo* 4, 2 (1998) 164.
10. V. Schröder, O. Behrend, H. Schubert, Effect of dynamic interfacial tension on the emulsification process using microporous, ceramic membranes, *J. Colloid Interface Sci.* 202 (1998) 334.
11. M. Rayner, G. Trägårdh, Membrane emulsification modelling: how can we get from characterisation to design?, *Desalination* 145 (2002) 165.
12. M. Yasuno, M. Nakajima, S. Iwamoto, T. Maruyama, S. Sugiura, I. Kobayashi, A. Shono, K. Satoh, Visualization and characterization of SPG membrane emulsification, *J. Membr. Sci.* 210 (2002) 29.
13. S.M. Joscellyne, G. Trägårdh, Membrane emulsification - a literature review, *J. Membr. Sci.* 169 (2000) 107.
14. C. Charcosset, I. Limayem, H. Fessi, Review. The membrane emulsification process - a review, *J. Chem. Technol. Biotechnol.* 79 (2004) 209.
15. U. Lambrich, G.T. Vladisavljevic, Emulgieren mit mikrostrukturierten Systemen, *Chem.-Ing.-Tech.* 76, 4 (2004) 376.
16. A.J. Gijsbertsen-Abrahamse, A. van der Padt, R.M. Boom, Status of cross-flow membrane emulsification and outlook for industrial application, *J. Membr. Sci.* 230 (2004) 149.
17. C.J.M. van Rijn, Nano and Micro Engineered Membrane Technology, 2004, Elsevier Science, Amsterdam.

18. Y. Mine, M. Shimizu, T. Nakashima, Preparation and stabilization of simple and multiple emulsions using a microporous glass membrane, *Colloids Surfaces B: Biointerfaces* 6 (1996) 261.
19. H. Okochi, M. Nakano, Comparative Study of two preparation methods of W/O/W emulsions: stirring and membrane emulsification, *Chem. Pharm. Bull.* 45, 8 (1997) 1323.
20. S. Higashi, K. Iwata, S. Tamura, Arterial-injection chemotherapy for hepatocellular carcinoma using monodispersed poppy-seed oil microdroplets containing fine aqueous vesicles of epirubicin, *Cancer* 75 (1995) 1245.
21. S. Higashi, Y. Maeda, M. Kai, T. Kitamura, H. Tsubouchi, S. Tamura, T. Setoguchi, A case of hepatocellular carcinoma effectively treated with epirubicin aqueous vesicles in monodispersed iodized poppy-seed oil microdroplets, *Hepato-Gastroenterology* 43 (1996) 1427.
22. S. Higashi, T. Setoguchi, Hepatic arterial injection chemotherapy for hepatocellular carcinoma with epirubicin aqueous solution as numerous vesicles in iodinated poppy-seed oil microdroplets: clinical application of water-in-oil-in-water emulsion prepared using a membrane emulsification technique, *Adv. Drug Delivery Rev.* 45 (2000) 57.
23. S. Higashi, N. Tabata, K.-H. Kondo, Y. Maeda, M. Shimizu, T. Nakashima, T. Setoguchi, Size of lipid microdroplets effects results of hepatic arterial chemotherapy with an anticancer agent in water-in-oil-in-water emulsion to hepatocellular carcinoma, *J. Pharmacol. Exp. Ther.* 289, 2 (1999) 816.
24. H. Okochi, M. Nakano, Review. Preparation and evaluation of W/O/W type emulsions containing vancomycin, *Adv. Drug Delivery Rev.* 45 (2000) 5.
25. J. Janardhanan, A.J. Mawson, L. Ferreira, Factors influencing the yield stability of W/O/W emulsions, *Proceedings ICEF 9*, 2004, Montpellier.
26. G.-H. Ma, H. Sone, S. Omi, Preparation of uniform-sized polystyrene-polyacrylamide composite microspheres from a W/O/W emulsion by membrane emulsification technique and subsequent suspension polymerization, *Macromolecules* 37 (2004) 2954.
27. H. Ono, K. Yamasaki, S. Kashiwagi, K. Arimori, S. Matsuda, M. Shimizu, New approach for oral insulin preparation with emulsion as drug carrier, *Proceedings of the 36th SPG Forum Miyazaki*, 2001, 31.
28. T. Yoneyama, M. Saito, T. Nakashima, Leakage of irinotecan hydrochloride from W/O/W emulsion carrier and hydrolysis, *Proceedings of the 36th SPG Forum Miyazaki*, 2001, 54.
29. M. Kukizaki, M. Shimizu, T. Nakashima, Preparation of W/O/W emulsion using hardened oil and suppression of leakage of encapsulated material, *Proceedings of the 36th SPG Forum Miyazaki*, 2001, 58.
30. K. Fukui, K. Matsugano, M. Shimizu, S. Matsuda, Preparation of anthocyanin-encapsulated emulsion and suppression of anthocyanin leakage, *Proceedings of the 36th SPG Forum Miyazaki*, 2001, 66.
31. M. Shimizu, S. Matsuda, T. Nakashima, Preparation of S/O/W emulsion by dehydrating W/O emulsion to develop DDS medicine, *Proceedings of the 36th SPG Forum Miyazaki*, 2001, 70.

32. T. Nakashima, M. Shimizu, M. Kukizaki, Particle control of emulsions by membrane emulsification and its applications, *Adv. Drug Delivery Rev.* 45 (2000) 47.
33. T. Kawakatsu, Y. Kikuchi, M. Nakajima, Regular-sized cell creation in microchannel emulsification by visual microprocessing method, *J. Am. Oil Chem. Soc.* 74, 3 (1997) 317.
34. S. Sugiura, M. Nakajima, S. Iwamoto, M. Seki, Interfacial tension driven monodispersed droplet formation from microfabricated channel array, *Langmuir* 17 (2001) 5562.
35. T. Kawakatsu, G. Trägårdh, C. Trägårdh, Production of W/O/W emulsions and S/O/W pectin microcapsules by microchannel emulsification, *Colloids Surfaces A: Physicochem. Eng. Aspects* 189 (2001) 257.
36. U. Lambrich, S. van der Graaf, K.S. Dekkers, R.M. Boom, H. Schubert, Production of double emulsions using microchannel emulsification, *Proceedings ICEF 9*, 2004, Montpellier.
37. S. Sugiura, M. Nakajima, K. Yamamoto, S. Iwamoto, T. Oda, M. Satake, M. Seki, Preparation characteristics of water-in-oil-in-water multiple emulsions using microchannel emulsification, *J. Colloid Interface Sci.* 270 (2004) 221.
38. I. Kobayashi, M. Nakajima, K. Chun, Y. Kikuchi, H. Fujita, Silicon array of elongated through-holes for monodisperse emulsion droplets, *AIChE J.* 48, 8 (2002) 1639.
39. G.T. Vladisavljevic, M. Shimizu, T. Nakashima, Preparation of monodisperse multiple emulsions at high production rates by multi-stage premix membrane emulsification, *J. Membr. Sci.* 244, 1-2 (2004) 97.
40. M. Shima, Y. Kobayashi, T. Fujii, M. Tanaka, Y. Kimura, S. Adachi, R. Matsuno, Preparation of fine W/O/W emulsion through membrane filtration of coarse W/O/W emulsion and disappearance of the inclusion of outer phase solution, *Food Hydrocolloids* 18 (2004) 61.
41. Y. Kawashima, T. Hino, H. Takeuchi, T. Niwa, K. Horibe, Shear-induced phase inversion and size control of water/oil/water emulsion droplets with porous membrane, *J. Colloid Interface Sci.* 145, 2 (1991) 512.
42. T. Hino, Y. Kawashima, S. Shimabayashi, Basic study for stabilization of w/o/w emulsion and its application to transcatheter arterial embolization therapy, *Adv. Drug Delivery Rev.* 45 (2000) 27.
43. F. Olson, C.A. Hunt, F.C. Szoka, W.J. Vail, D. Papahadjopoulos, Preparation of liposomes of defined size distribution by extrusion through polycarbonate membranes, *Biochim. Biophys. Acta* 557 (1979) 9.
44. K. Pays, J. Giermanska-Kahn, B. Pouligny, J. Bibette, F. Leal-Calderon, Coalescence in surfactant-stabilized double emulsions, *Langmuir* 17 (2001) 7758.
45. M.-F. Ficheux, L. Bonakdar, F. Leal-Calderon, J. Bibette, Some stability criteria for double emulsions, *Langmuir* 14 (1998) 2702.
46. S. van der Graaf, C.G.P.H. Schroën, R.G.M. van der Sman, R.M. Boom, Influence of dynamic interfacial tension on droplet formation during membrane emulsification, *J. Colloid Interface Sci.* 277, 2 (2004) 456.

47. N.C. Christov, D.N. Ganchev, N.D. Vassileva, N.D. Denkov, K.D. Danov, P.A. Kralchevsky, Capillary mechanisms in membrane emulsification: oil-in-water emulsions stabilized by Tween 20 and milk proteins, *Colloids Surfaces A: Physicochem. Eng. Aspects* 209 (2002) 83.
48. E. Toorisaka, H. Ono, K. Arimori, N. Kamiya, M. Goto, Hypoglycemic effect of surfactant-coated insulin solubilized in a novel solid-in-oil-in-water (S/O/W) emulsion, *Int. J. Pharm.* 252 (2003) 271.
49. M. Nakajima, H. Nabetani, S. Ichikawa, Q.Y. Xu, Functional emulsions, United States Patent, US 6538019, 2003.
50. M. Rayner, B. Bergenståhl, L. Massarelli, G. Trägårdh, Double emulsions prepared by membrane emulsification: stability and entrapment degree in a flavour release system, abstract Food Colloids 2004 Conference, Harrogate.

Chapter 7

Discussion

Introduction

In the previous chapters, various aspects that play a role during cross-flow membrane emulsification were discussed. The size of the formed droplets depends on various parameters: the properties of the membrane, the process conditions and the properties of the ingredients (see figure 1.2, Chapter 1). In this thesis we mostly focussed on the influence of the interfacial tension (which is determined by the ingredient properties) on the final droplet size in cross-flow membrane emulsification.

Although the cross-flow technique is an interesting option for emulsification, it is not the only one. For example, microchannel emulsification and pre-mix emulsification are both techniques that could become important for industrial (large scale) applications. Microchannel emulsification is a novel method for producing monodisperse emulsions in which droplets are produced by forcing the to-be-dispersed phase through the microchannels. The to-be-dispersed phase is forced to assume a distorted flat shape on the terrace in the microchannel resulting in a higher Laplace pressure and a driving force for spontaneous droplet formation. In pre-mix membrane emulsification, first a coarse pre-mix is made which is subsequently pushed through a membrane. Upon passage of the coarse droplets through the membrane they break up into finer droplets. A schematic picture of the three techniques is given in figure 1.1 in Chapter 1.

In this discussion, general trends and new insights and their effects on the detachment process and droplet size for all three membrane emulsification methods are discussed. Besides this, the future prospect of these techniques for industrial production purposes is discussed.

Interfacial tension and droplet diameter

The size of droplets formed with cross-flow membrane emulsification is determined by a complex interplay between forces and dynamic effects. Detachment of a droplet begins when it has reached a critical volume, at which the drag forces exerted by the cross-flow balance the interfacial tension force keeping the droplet connected to the pore mouth. From that moment, the dynamic necking process begins, which contributes to the resulting total droplet volume as well (Chapters 3, 4). In general, low interfacial tensions lead to small droplets, while high interfacial tensions lead to large droplets (Chapters 2, 3, 4, [1] [2]).

While for cross-flow membrane emulsification a high interfacial tension delays droplet detachment and thus leads to larger droplets, for microchannel emulsification faster droplet formation and detachment can be obtained at a high interfacial tension, however, the size of the droplets is usually not influenced. Thus, the effect of the dynamic interfacial tension in cross-flow membrane emulsification and microchannel emulsification seems reverse. In general, for microchannel emulsification [3] the driving force for droplet detachment is the difference in Laplace pressures between the terrace and the well, which is determined by the design of the microchannel [4]. Sugiura *et al.* [5] and Lambrich *et al.* [6] found experimentally that higher interfacial tensions caused faster droplet detachment, which is in agreement with the findings of Kobayashi and Nakajima [7]. They also found that droplets could be formed without surfactants, which was also reported by Sugiura *et al.* [8], however, the resulting droplets were not stable against coalescence.

In pre-mix membrane emulsification [9][10] droplet break up is expected to occur already in or even before pre-mix droplets enter the pores of the membrane. Many different break up mechanisms operate at the same time [11]. The direct influence of interfacial tension on droplet break up is still poorly understood.

Although many effects are related to interfacial tension effects it is often difficult to assess its actual value in case of the presence of surfactants. For a constant relative expansion rate it is possible to measure the dynamic interfacial tension with an overflowing cylinder [12], albeit only at low expansion rates. For such a situation with a constant relative expansion rate a model can be used [13] which describes the difference between the static interfacial tension and the dynamic interfacial tension. However, during

droplet formation the relative expansion rate varies in time and is too high to measure reliably, therefore we do not know the value of the interfacial tension in time very accurately. Secondly, there is flow over the interface of the droplet, resulting in a redistribution of the surfactant in time. The effects of this are still largely unknown. At the moment, only estimations based on other measurements (as in Chapter 2) and mass transfer calculations of surfactant molecules to an expanding oil-water interface [14] can give information about the interfacial tension just before detachment. In the near future, new developments in the field of interfacial tension measurement instruments [15] may overcome this problem and it may become possible to measure the interfacial tension of a water-oil interface at high expansion rates. This would open possibilities to directly link the measured interfacial tension values to the droplet formation process.

Influence of necking time

For cross-flow membrane emulsification the droplet formation process consists of an expansion and a necking stage (Chapters 3 and 4). Until recently, much research on cross-flow membrane emulsification was focussed on the expansion stage by investigation of the relevant forces [1], while the necking stage was neglected. However, the necking stage contributes substantially to the final droplet volume (Chapter 4). Xu *et al.* [16] found that an increase in the to-be-dispersed phase flow rate resulted in larger droplet sizes, which could be explained by a detachment process needing time (= necking). Cramer *et al.* [17] studied droplet formation in a co-flowing system and found that the necking process is accelerated at higher velocities of the continuous phase. In Chapter 4 we reported on the same phenomenon. Based on lattice Boltzmann simulations that could predict experimental results very well, we were able to quantify the contribution of the necking process. This can be considerable, depending on the flow rates used.

It is interesting to consider whether also in microchannel emulsification with spontaneous droplet formation and in pre-mix membrane emulsification with various break up mechanisms a necking or detachment stage contributes to the final droplet size and whether this necking process can be accelerated. Acceleration of the (spontaneous) necking process will allow higher to-be-dispersed phase flow rates. Sugiura *et al.* [5] studied the influence of surfactant concentration on the detachment time for microchannel

emulsification. They found that at lower surfactant concentrations and thus higher interfacial tensions the detachment time decreased and that at higher flow rates monodisperse droplets could be obtained. Kobayashi *et al.* [18] found that above a threshold value for the dynamic viscosity, the droplet size increases as a function of the dynamic viscosity for systems containing surfactant (SDS), while there is no increase in systems without surfactants. This could point to a decrease in the dynamic interfacial tension that promotes the expansion of the oil phase and prevents the cutoff of the neck, possibly resulting in a longer necking time and thus larger droplets.

Intrusion of water phase

It is not always possible to clearly distinguish between the two different detachment mechanisms (caused by a cross-flow or a Laplace pressure difference). An example is droplet detachment from SPG membranes. Both Christov *et al.* [2] and Yasuno *et al.* [19] microscopically studied droplet detachment from a SPG membrane without cross-flow. They found two regimes of droplet detachment: in one regime (A) small monodisperse droplets are produced and in the other regime (B) large polydisperse droplets are formed, which sometimes resulted in bimodal size distributions. The fact that in regime A small monodisperse droplets are formed without a cross-flow suggests that also with SPG membranes spontaneous droplet formation is possible, caused by intrusion of the water phase.

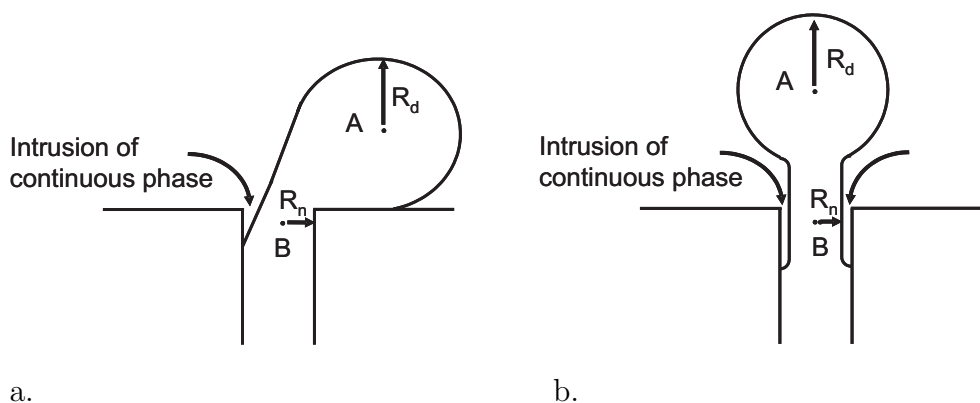


Figure 7.1: Intrusion of water phase for cross-flow membrane emulsification (a) and for spontaneous (microchannel) emulsification (b).

It is expected that intrusion of water is critical for (spontaneous) detachment, see figure 7.1. Our hypothesis is that if water has intruded into

the pore, the pressure at location B ($\Delta p_{neck} = \frac{\sigma}{R_n}$) is similar to location A ($\Delta p_{drop} = \frac{2\sigma}{R_d}$). Thus, when $\frac{1}{R_n} > \frac{2}{R_d}$ or $R_n < \frac{1}{2}R_d$, the conditions for spontaneous detachment have been created, in principle regardless of the shape of the pore. However, the shape of the pore can facilitate or inhibit intrusion of water.

Kobayashi *et al.* [20] found that slit shaped pores in straight-through microchannel emulsification, a scaled up system for microchannel emulsification, produce monodisperse emulsions while circular straight-through microchannels produce polydisperse emulsion droplets. Both the shape of the channel (or pore), e.g. presence of a terrace [8], and the wetting conditions [21] are important for intrusion of the water phase. They also modelled droplet detachment from a microchannel with CFD and found that sufficient space for water at the channel exit had to be present for the necking process inside the microchannel and subsequent detachment [22]. Both the CFD and experimental results [23] showed that a slot aspect ratio of at least 3-3.5 resulted in spontaneous droplet formation. A slightly lower aspect ratio (2.7) gave a bimodal size distribution, caused by both spontaneous and non-spontaneous detachment. This could also explain the results presented in Chapter 2 that showed large droplets from microsieves, probably due to the absence of spontaneous break up.

For intrusion of the water phase, it is important that the membrane or microchannel is preferentially wetted by the water phase. This implies that certain surfactants disqualify because they change the wettability of the pore or microchannel wall. As an example, cationic surfactants and proteins below their iso-electric point are not suited for microchannel emulsification because they turn the microchannel hydrophobic [21] [24] [25] and therewith prevent intrusion of the water phase.

A drawback of spontaneous droplet detachment in e.g. microchannel emulsification is that there is a clear upper limit to the flow rate per pore. Water intrudes slowly into the pore. A higher to-be-dispersed phase flux results in non-spontaneous droplet formation and thus polydisperse droplets. Accelerating water intrusion into the pore and therewith accelerating the necking process may be the key to faster (spontaneous) droplet formation.

Applying a cross-flow results in a drag force and may be a route to accelerate intrusion of continuous phase into the pore from one side. A limited number of studies [26] [27] show that intrusion occurs in cross-flow systems. Lattice Boltzmann modelling of 2 dimensional droplet deformation from a slot [28] showed that the wetting properties inside the pore determine wa-

ter intrusion and therewith droplet detachment. Also in Chapter 3 and 4 intrusion of the water phase into the pore was reported. To obtain a high flux, a membrane with a low hydraulic resistance is desirable, this means a thin membrane like a microsieve. However, for intrusion of water phase in the pore (also in a slit shaped pore) and subsequent necking and detachment from the pore, we have the impression that the membrane should not be too thin because a certain intrusion depth is required. Another way to increase the flux is using pre-mix membrane emulsification. In pre-mix membrane emulsification the presence of a cross-flow is not required for droplet detachment [10]. Probably, detachment of droplets is facilitated by the water phase that is already present in the pre-mix.

Consequences for industrial production

An important question is whether membrane emulsification is interesting for large-scale production of emulsions in industry (see figure 7.2). One advantage is the low energy requirement, especially for producing emulsions with a low dispersed phase fraction. However, for most applications a considerable dispersed phase fraction is required. The energy savings become less in that case, but are still relevant. Another advantage of membrane emulsification is the control of droplet size and droplet size distribution. Compared to conventional techniques, membrane emulsification renders no small sub-micron droplets, and therefore, less interface is present. The (moderate) shear forces required for cross-flow membrane emulsification are not required in microchannel emulsification and therewith an additional advantage could be gained. In that case, microchannels have to be placed in parallel [29] in order to achieve an industrially relevant flux. This is expected to be an important field for future research.

In practice, various demands will be placed on emulsification processes such as:

1. minimal use of surfactants,
2. high production rates at low membrane areas,
3. little or no shear,
4. small emulsion droplets with a narrow droplet size distribution.

Demand 1, 2 and 3 have to be met if a certain amount of emulsion has to be produced in an economic fashion, which is relevant for bulk products. The most economic way to produce emulsions with membranes is

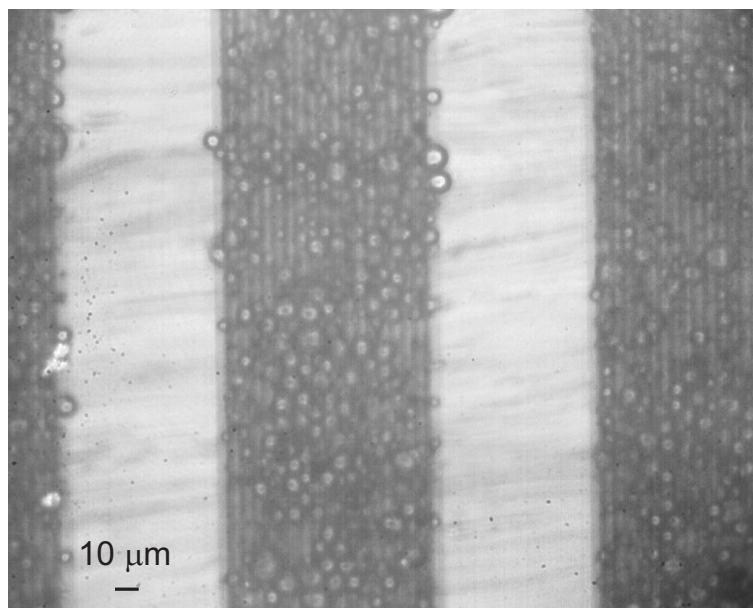


Figure 7.2: Droplet formation from an (industrial) high porosity microsieve, see also [30].

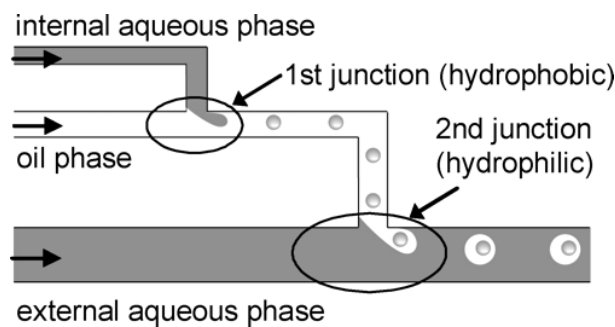
applying a high to-be-dispersed phase flow rate and a high cross-flow at a low surfactant concentration, which should be sufficiently high to prevent coalescence. Just below the jetting regime, the droplet size distribution is expected to be somewhat broader than at a lower to-be-dispersed phase flux, but probably still more monodisperse than with conventional methods. Another option to obtain a relatively large flux is using pre-mix membrane emulsification. Future research should thus focus on producing droplets close to the desired size at a high production rate.

Point 3 and 4 imply an increase of the quality of the emulsion and are therefore most important for the production of (very) high added value products. A membrane or microstructure designed to facilitate droplet detachment (e.g. by water intrusion) should be used. For a very monodisperse emulsion, a lower to-be-dispersed phase flow rate is inevitable, either with cross-flow membrane emulsification systems or with spontaneous detachment in microchannel emulsification and other microstructures. The intruding water phase will bring foulants like proteins in the channel. Especially sharp corners, which are crucial for microchannel emulsification, will be prone to fouling. Whether emulsification with spontaneous droplet detachment will become feasible for the industry, depends on the developments in parallelisation of the system and the prevention of fouling, for example by modification of the surface.

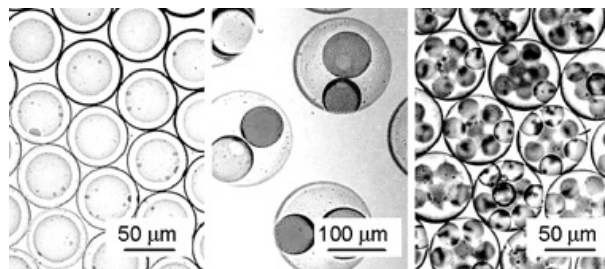
New developments: design of particles

Recent developments in microtechnology and lithographic techniques make it possible to prepare particles with specific microfluidic devices. Nisisako and co-workers [31][32][33] made a device in which bicolored droplets could be formed. They also designed double emulsions (diameter $\pm 100\ \mu\text{m}$) with a controlled number of internal droplets, which may have different compositions, by serially connecting hydrophobic and hydrophilic microchannels and applying different flow rates (see figure 7.3). Also Utada *et al.* [34] developed a device for the production of double emulsions. Yi *et al.* [35] made a microfluidic device for the production of uniform colloidal assemblies. For an overview of various types of emulsions and microparticles that can be produced with membrane emulsification and microsystems we refer to Vladisavljevic and Williams [36].

At this moment, these particles can only be produced at very small production rates and the development of "large scale" microfluidic devices by parallelization is expected to give this field of research a boost.



a.



b.

Figure 7.3: Schematic diagram of the formation of a W/O/W double emulsion (a) and stable W/O/W emulsions with a controlled number of internal droplets ($n=1,2$ and 8) (b), from [32] [33].

New developments: simulation techniques

Although membrane emulsification has been modelled by several groups with different modelling techniques like the Surface Evolver [37], CFX [26] and CFD-ACE+ [22], all simulations till now were done with a constant interfacial tension. Still, these simulations give valuable information for understanding the process of droplet formation and droplet detachment. For example, Rayner [37] found a general relationship between pore shape, contact angle and droplet size. For an extensive review about simulation methods of droplet dynamics in general, we refer to Cristini and Tan [38].

A first attempt to incorporate dynamic interfacial tension in a lattice Boltzmann code was presented in Chapter 5. Contrary to other lattice Boltzmann literature with a surfactant phase [39] [40], this code is suitable for modelling (macro-)emulsions instead of micro-emulsions. Future research in this field should focus on the implementation of models for dynamic interfacial tension in extensive three-dimensional lattice Boltzmann models and other (commercial) packages. One of the features of the lattice Boltzmann approach is that the system has a solid, thermodynamic approach to interactions between all components. Thus, it is possible to directly translate simulation parameter values to thermodynamic parameters of the experimental components used (including surfactant). Ultimately, one could tune the type and concentration of surfactant by introducing specific (experimentally known) parameters such as HLB value and diffusion coefficient and herewith limit the amount of experiments necessary for the membrane emulsification process and product (droplet or microparticle) design considerably.

Concluding remarks

In this thesis, the influence of dynamic interfacial tension on the droplet formation process in model systems for cross-flow membrane emulsification has been evaluated. Both experimentally and by means of simulations, the effect of the necking time in relation to the interfacial tension was found to be of importance, which has implications for the design of the emulsification process. These new insights will facilitate large scale production of emulsions and also the development of highly specified emulsions and particles.

References

1. V. Schröder, O. Behrend, H. Schubert, Effect of dynamic interfacial tension on the emulsification process using microporous, ceramic membranes, *J. Colloid Interface Sci.* 202 (1998) 334.
2. N.C. Christov, D.N. Ganchev, N.D. Vassileva, N.D. Denkov, K.D. Danov, P.A. Kralchevsky, Capillary mechanisms in membrane emulsification: oil-in-water emulsions stabilized by Tween 20 and milk proteins, *Colloids Surf. A: Physicochem. Eng. Aspects* 209 (2002) 83.
3. S. Sugiura, M. Nakajima, S. Iwamoto, M. Seki, Interfacial tension driven monodispersed droplet formation from microfabricated channel array, *Langmuir* 17 (2001) 5562.
4. S. Sugiura, M. Nakajima, M. Seki, Prediction of droplet diameter for microchannel emulsification, *Langmuir* 18 (2002) 3854.
5. S. Sugiura, M. Nakajima, T. Oda, M. Satake, M. Seki, Effect of interfacial tension on the dynamic behavior of droplet formation during microchannel emulsification, *J. Colloid Interface Sci.* 269 (2004) 178.
6. U. Lambrich, S. van der Graaf, K.S. Dekkers, R.M. Boom, H. Schubert, Production of double emulsions using microchannel emulsification, *Proceedings ICEF 9*, 2004, Montpellier.
7. I. Kobayashi, M. Nakajima, Effect of emulsifiers on the preparation of food-grade oil-in-water emulsions using a straight-through extrusion filter, *Eur. J. Lipid Sci. Technol.* 104 (2002) 720.
8. S. Sugiura, M. Nakajima, J. Tong, H. Nabetani, M. Seki, Preparation of monodispersed solid lipid microspheres using a microchannel emulsification technique, *J. Colloid Interface Sci.* 227 (2000) 95.
9. K. Suzuki, I. Fujiki, Y. Hagura, Preparation of corn oil/water and water/corn oil emulsions using PTFE membranes, *Food Sci. Technol. Int. Tokyo* 4, 2 (1998) 164.
10. G.T. Vladislavjevic, M. Shimizu, T. Nakashima, Preparation of monodisperse multiple emulsions at high production rates by multi-stage premix membrane emulsification, *J. Membr. Sci.* 244, 1-2 (2004) 97.
11. E.A. van der Zwan, C.G.P.H. Schroën, K.C. van Dijke, R.M. Boom, Visualization of droplet break-up in pre-mix membrane emulsification using microfluidic devices, *Colloids Surf. A: Physicochem. Eng. Aspects*, submitted (2005).
12. D.J.M. Bergink-Martens, *Interface dilatation. The overflowing cylinder technique*, Ph.D. thesis, Wageningen University, 1993.
13. F. van Voorst Vader, Th.F. Erkens, M. van den Tempel, Measurement of dilatational surface properties, *Trans. Faraday Soc.* 60 (1964) 1170.
14. M. Rayner, G. Trägårdh, C. Trägårdh, The impact of mass transfer and interfacial expansion rate on droplet size in membrane emulsification processes, *Colloids Surf. A: Physicochem. Eng. Aspects* 266, 1-3 (2005) 1.
15. www.sinterface.com
16. J.H. Xu, G.S. Luo, G.G. Chen, J.D. Wang, Experimental and theoretical approaches on droplet formation from a micrometer screen hole, *J. Membr. Sci.* 266 (2005) 121.

17. C. Cramer, P. Fischer, E.J. Windhab, Drop formation in a co-flowing ambient fluid, *Chem. Eng. Sci.* 59 (2004) 3045.
18. I. Kobayashi, S. Mukataka, M. Nakajima, Effects of type and physical properties of oil phase on oil-in-water emulsion droplet formation in straight-through microchannel emulsification, experimental and CFD studies, *Langmuir* 21 (2005) 5722.
19. M. Yasuno, M. Nakajima, S. Iwamoto, T. Maruyama, S. Sugiura, I. Kobayashi, A. Shono, K. Satoh, Visualization and characterization of SPG membrane emulsification, *J. Membr. Sci.* 210 (2002) 29.
20. I. Kobayashi, M. Nakajima, K. Chun, Y. Kikuchi, H. Fujita, Silicon array of elongated through-holes for monodisperse emulsion droplets, *AIChE J.* 48, 8 (2002) 1639.
21. I. Kobayashi, M. Nakajima, S. Mukataka, Preparation characteristics of oil-in-water emulsions using differently charged surfactants in straight-through microchannel emulsification, *Colloids Surf. A: Physicochem. Eng. Aspects* 229 (2003) 33.
22. I. Kobayashi, S. Mukataka, M. Nakajima, CFD simulation and analysis of emulsion droplet formation from straight-through microchannels, *Langmuir* 20 (2004) 9868.
23. I. Kobayashi, S. Mukataka, M. Nakajima, Effect of slot aspect ratio on droplet formation from silicon straight-through microchannels, *J. Colloid Interface Sci.* 279 (2004) 277.
24. J. Tong, M. Nakajima, H. Nabetani, Y. Kikuchi, Surfactant effect on production of monodispersed microspheres by microchannel emulsification method, *J. Surfactants Detergents* 3, 3 (2000) 285.
25. M. Saito, L.-J. Yin, I. Kobayashi, M. Nakajima, Preparation characteristics of monodispersed oil-in-water emulsions with large particles stabilized by proteins in straight-through microchannel emulsification, *Food Hydrocolloids* 19 (2005) 745.
26. A.J. Abrahamse, A. van der Padt, R.M. Boom, W.B.C. de Heij, Process fundamentals of membrane emulsification: simulation with CFD, *AIChE J.* 47, 6 (2001) 1285.
27. T. Nisisako, T. Torii, T. Higuchi, Droplet formation in a microchannel network, *Lab Chip* 2, 1 (2002) 24.
28. S. van der Graaf, R.G.M. van der Sman, R.M. Boom, Modeling of droplet formation processes relevant to membrane emulsification, *Proceedings AIChE annual meeting 2003*, 563e, San Francisco, 2003.
29. S. Matthias, F. Müller, Asymmetric pores in a silicon membrane acting as massively parallel brownian ratchets, *Nature* 424 (2003) 53.
30. C.J.M. van Rijn, Nano and Micro Engineered Membrane Technology, 2004, Elsevier Science, Amsterdam.
31. T. Nisisako, T. Torii, T. Higuchi, Novel microreactors for functional polymer beads, *Chem. Eng. J.* 101 (2004) 23.
32. S. Okushima, T. Nisisako, T. Torii, T. Higuchi, Controlled production of monodisperse double emulsions by two-step droplets breakup in microfluidic devices, *Langmuir* 20 (2004) 9905.
33. T. Nisisako, S. Okushima, T. Torii, Controlled formulation of monodisperse double emulsions in a multiple-phase microfluidic system, *Soft Matter* 1 (2005) 23.

34. A.S. Utada, E. Lorenceau, D.R. Link, P.D. Kaplan, H.A. Stone, D.A. Weitz, Monodisperse double emulsions generated from a microcapillary device, *Science* 308 (2005) 537.
35. G.-R. Yi, T. Thorsen, V.N. Manoharan, M.-J. Hwang, S.-J. Jeon, D.J. Pine, S.R. Quake, S.-M. Yang, Generation of uniform colloidal assemblies in soft microfluidic devices, *Adv. Mater.* 15, 15 (2003) 1300.
36. G.T. Vladisavljevic, R.A. Williams, Recent developments in manufacturing emulsions and particulate products using membranes, *Adv. Colloid Interface Sci.* 113 (2005) 1.
37. M. Rayner, Membrane emulsification: modelling interfacial and geometric effects on droplet size, Ph.D. thesis, Lund University, 2005.
38. V. Cristini, Y.-C. Tan, Theory and numerical simulation of droplet dynamics in complex flows - a review, *Lab Chip* 4 (2004) 257.
39. O. Theissen, G. Gompper, D.M. Kroll, Lattice-Boltzmann model of amphiphilic systems, *Europhys. Lett.* 42, 4 (1998) 419.
40. A. Lamura, G. Gonnella, J.M. Yeomans, A lattice Boltzmann model of ternary fluid mixtures, *Europhys. Lett.* 45, 3 (1999) 314.

Summary

Emulsions are mixtures of water and oil. Because water and oil are not miscible, one phase is dispersed as droplets in the other phase and surfactants are added to stabilize the oil-water interface of the droplets. In this way, an oil-in-water (O/W) emulsion or a water-in-oil (W/O) emulsion can be formed. Examples of emulsions in the food industry are mayonnaise, butter, milk and spreads. Emulsions are also used in for example the pharmaceutical, cosmetic, and chemical industry, in products like medicines, cosmetic creams, and paints.

To produce an emulsion the two liquid phases have to be mixed. Conventional methods to do this are mixers, rotor-stator systems and high-pressure homogenizers. A relatively new way to produce emulsions is cross-flow membrane emulsification. In this method the to-be-dispersed phase (e.g. oil) is pressed through a membrane and droplets are formed at the other side of the membrane, where they are detached by the cross-flowing continuous phase (e.g. water). An advantage of this new method is the use of process conditions that require less energy than the conventional methods. Another advantage is that all the formed droplets have the same size when the correct conditions are taken. The size of the formed droplets depends on the properties of the membrane, the process conditions and the properties of the ingredients. All these parameters, which sometimes also influence each other, determine the droplet formation process and the final droplet size. This thesis describes experiments (Chapter 2 and 3) and simulations (Chapter 4 and 5) that were performed with model systems.

Chapter 2 describes experiments that were performed with microsieves with a single circular pore of $4.8\text{ }\mu\text{m}$. The process of droplet formation was studied with the help of a microscope connected to a high speed camera. Results show that smaller droplets are formed at high surfactant concentrations and therefore low interfacial tension. The interfacial tension just before detachment can be estimated with the help of interfacial tension measurements at lower relative expansion rates. At higher transmembrane

pressures larger droplets are formed as a result of the higher interfacial tension and the necking process, which is relatively slow.

Also Chapter 3 describes droplet formation experiments that were studied with a microscope connected to a high speed camera. For these experiments we used glass chips with a T-junction. Also in this model system, smaller droplets are formed at low interfacial tension. Besides this, the flow rate of the to-be-dispersed phase has an influence on the droplet size; a higher flow rate results in larger droplets. The droplet size can be described with a model that assumes that the final droplet size is determined by a volume as a result of both the force or torque balance and the necking process. For low surfactant concentrations the droplet size becomes independent of the surfactant concentration. This can be explained by the fact that the droplets are formed very fast and the surfactants have little time to diffuse to the interface, and also by the fact that the T-junction is very shallow; the surfactants can only adsorb at the edges of the droplet.

A model for numerical simulations has been developed, based on the lattice Boltzmann (LB) method. Subsequently, this model has been extended to model multiple phases based on a Ginzburg-Landau free energy functional. Droplet formation in a T-junction was modelled at various continuous phase flow rates. The size of the formed droplets were compared to experimental results. The sizes of the formed droplets in the experiments and the simulations are in good agreement. With the validated code, we performed a parameter study in which the flow rates of both phases and the interfacial tension have been varied. Results show that both the volume as a result of the force or torque balance and the volume as a result of the necking process scale with the capillary number to the power -0.75. Besides this, the flow rate of the to-be-dispersed phase influences the necking volume; a larger flow rate causes a larger volume during the necking process.

In Chapter 5 the free energy functional in the simulations is extended to describe the effect of the presence of surfactant, besides oil and water. Contrary to many models in literature that are only suitable to model the adsorption behaviour of surfactants in micro-emulsions, this model can also describe Langmuir adsorption at interfaces of (macro-)emulsions. Analytical equations for the concentration profile of surfactants at a planar interface were derived from the free energy functional and the numerical results agree well with these analytical equations. One can describe the decrease in interfacial tension as a function of the loading of the interface.

The adsorption rate was compared with the analytical solution by Ward and Tordai. The solutions of the simulations match with the analytical solution on all time scales.

In Chapter 6 the production of double emulsions with membranes is reviewed. Double emulsions are emulsions in emulsions. One can distinguish both water-in-oil-in-water (W/O/W) and oil-in-water-in-oil (O/W/O) emulsions. Because in conventional emulsification methods high shear rates are applied, these are not suitable for the production of double emulsions. The high shear rates used in the preparation of the external droplets would disrupt the internal droplets, resulting in their coalescence with the external phase. Membrane emulsification, however, is a milder process and is therefore a suitable technique for the preparation of double emulsions. Three different methods are distinguished in literature: cross-flow membrane emulsification, microchannel emulsification and pre-mix membrane emulsification. The most important application of double emulsions prepared by membrane emulsification so far, is their use for targetted release of intravenous medicines.

Finally, in Chapter 7 the process of droplet formation and the influence of interfacial tension effects are discussed. The newly acquired insights show that the intrusion of the continuous phase into the pore is very important for the break up process, and the necking process has a significant influence on the final droplet size. Membrane emulsification can be an interesting method for industrial applications, especially for the production of high value products. New developments in microtechnology make it possible to prepare very well-defined double and more complex emulsions and other microparticles for specific applications.

Samenvatting

Emulsies zijn mengsels van water en olie. Omdat water en olie niet zomaar mengbaar zijn is de ene fase in kleine druppeltjes verdeeld in de andere fase en worden oppervlakte-actieve stoffen toegevoegd om het olie-watergrensvlak van de druppels te stabiliseren. Op deze manier ontstaat een water-in-olie (W/O) emulsie of een olie-in-water (O/W) emulsie. Voorbeelden van emulsies in de levensmiddelenindustrie zijn mayonaise, boter, melk en spreads. Ook in andere industrieën zoals de farmaceutische, cosmetische en chemische industrie komen emulsies voor in bijvoorbeeld medicijnen, crèmes en verf.

Om een emulsie te maken moeten de twee vloeistoffen met elkaar worden gemengd. Traditionale apparaten die hiervoor worden gebruikt zijn mixers, rotor-stator systemen en hoge-druk homogenisatoren. Een relatief nieuwe manier om emulsies te maken is langsstroommembraanemulgeren. Bij deze methode wordt de te dispergeren fase (bv. olie) door een membraan geperst en worden druppels gevormd aan de andere zijde van het membraan in de continue fase (bv. water), die langsstroomt en op deze manier de druppels laat afbreken. Een voordeel van deze nieuwe productiewijze is dat het productieproces mild is en er minder energie nodig is om de emulsie te maken. Een ander voordeel is dat onder de juiste omstandigheden de gevormde druppels allemaal even groot zijn. De grootte van de gevormde druppels is afhankelijk van de eigenschappen van het membraan, de procesomstandigheden en de eigenschappen van de gebruikte ingrediënten. Al deze factoren, die soms ook elkaar beïnvloeden, bepalen het druppelvormingsproces en de uiteindelijke druppelgrootte. Dit proefschrift beschrijft experimenten (Hoofdstuk 2 en 3) en simulaties (Hoofdstuk 4 en 5) die zijn uitgevoerd met modelsystemen voor membranen met één porie.

Hoofdstuk 2 beschrijft experimenten die zijn uitgevoerd met microtechnologisch gefabriceerde membranen met een enkele cirkelvormige porie van $4.8\ \mu\text{m}$. Het proces van druppelvorming is bestudeerd met behulp van een microscoop verbonden met een hoge-snelheidscamera. Resultaten

laten zien dat kleinere druppels worden gevormd bij hoge concentraties oppervlakte-actieve stoffen en dus lagere grensvlakspanning. De grensvlakspanning net voordat de druppel afbreekt kan worden geschat met behulp van grensvlakspanningsmetingen die gedaan zijn bij lagere expansiesnelheden. Bij een hogere transmembraandruk worden grotere druppels gevormd ten gevolge van de hogere grensvlakspanning en de tijd die nodig is voor het nekkingsproces.

Ook Hoofdstuk 3 beschrijft druppelvormingsexperimenten die zijn bestudeerd met een microscoop verbonden met een hoge-snelheidscamera. Dit keer is er gebruik gemaakt van glascups met een T-splitsing. Ook in dit modelsysteem worden kleinere druppels gevormd bij een lagere grensvlakspanning. Daarnaast heeft het debiet van de te dispergeren fase invloed op de druppelgrootte; een groter debiet resulteert in grotere druppels. De druppelgrootte kan worden beschreven met een model waarin wordt aangenomen dat de uiteindelijke druppelgrootte wordt bepaald door een bijdrage aan het volume ten gevolge van zowel een krachten- of momentbalans als het nekkingsproces. Bij lage concentraties oppervlakte-actieve stoffen wordt de druppelgrootte onafhankelijk van de concentratie oppervlakte-actieve stoffen. Dit komt enerzijds doordat de druppels heel snel worden gevormd en de oppervlakte-actieve stoffen weinig tijd hebben om naar het grensvlak te diffunderen en anderzijds doordat de T-splitsing erg ondiep is en de oppervlakte-actieve stoffen alleen aan de rand van de druppel kunnen adsorberen.

Een model voor numerieke simulaties is ontwikkeld, gebaseerd op de lattice Boltzmann (LB) methode. Dit model is vervolgens uitgebreid om meerdere fasen te modelleren aan de hand van een Ginzburg-Landau vrije-energiefunctionaal. Druppelvorming in een T-splitsing is gesimuleerd bij verschillende debieten van de continue fase. De druppeldiameters zijn vergeleken met experimentele resultaten. De grootte van de druppels in de experimenten en in de simulaties komen goed met elkaar overeen. Met de code is vervolgens een parameterstudie uitgevoerd waarbij de debieten van beide fasen en de grensvlakspanning zijn gevarieerd. Resultaten laten zien dat zowel het volume ten gevolge van de krachten- of momentbalans als het volume ten gevolge van het nekkingsproces schalen met het capillair getal tot de macht $-0,75$. Daarnaast beïnvloedt het debiet van de te dispergeren fase het volume ten gevolge van nekking; een groter debiet zorgt voor een groter volume tijdens het nekkingsproces.

In Hoofdstuk 5 wordt de vrije-energiefunctionaal in de simulaties uitge-

breid om de aanwezigheid van oppervlakte-actieve stoffen te modelleren, naast olie en water. In tegenstelling tot veel modellen in de literatuur, die alleen geschikt zijn voor het modelleren van adsorptiegedrag van oppervlakte-actieve stoffen bij micro-emulsies, kan dit model Langmuiradsorptie beschrijven aan grensvlakken zoals bij (macro-)emulsies. Van deze vrije-energiefunctionaal zijn analytische vergelijkingen voor het concentratieprofiel van oppervlakte-actieve stoffen in evenwicht aan een vlak grensvlak afgeleid en de numerieke resultaten komen overeen met deze analytische vergelijkingen. Het is tevens mogelijk om het verlagen van de grensvlakspanning als functie van de belading van het grensvlak te beschrijven. De adsorptiesnelheid is vergeleken met de analytische oplossing die door Ward en Tordai is opgesteld. Op alle tijdschalen komen de resultaten van de simulaties overeen met de analytische oplossing.

In Hoofdstuk 6 wordt de productie van dubbele emulsies met behulp van membranen geëvalueerd. Dubbele emulsies zijn emulsies in emulsies. Er bestaan zowel water-in-olie-in-water (W/O/W) als olie-in-water-in-olie (O/W/O) emulsies. Conventionele emulgeerprocessen zijn niet geschikt voor het produceren van dubbele emulsies, omdat hierbij hoge afschuifspanningen worden gebruikt en de vorming van de externe druppels de interne druppels zou laten coalesceren met de externe fase. Membraanemulgeren is echter een milder proces en is daarom een geschikte techniek voor de productie van dubbele emulsies. Drie vormen van membraanemulgeren kunnen in de literatuur worden onderscheiden: langsstroommembraanemulgeren, microkanaalemulgeren en pre-mixmembraanemulgeren. De belangrijkste toepassing van dubbele emulsies die gemaakt zijn met membraanemulgeren tot nu toe is voor het gebruik van intraveneuze medicijnen voor gecontroleerde medicijnafgifte.

Tenslotte wordt in Hoofdstuk 7 het proces van druppelvorming en de invloed van de grensvlakspanning bediscussieerd. Volgens de nieuw verworven inzichten is de indringing van continue fase in de porie van groot belang voor het opbreekproces en heeft het nekkingsproces een redelijk grote invloed op de uiteindelijke druppelgrootte. Voor de industrie kan membraanemulgeren een interessante methode zijn, zeker voor de productie van producten met een hoge toegevoegde waarde. Nieuwe ontwikkelingen in de microtechnologie maken het mogelijk om goed gedefinieerde dubbele en complexere emulsies en andere microdeeltjes voor specifieke toepassingen te vervaardigen.

Nawoord

Het proefschrift is af! Hier ben ik natuurlijk erg blij mee en tegelijkertijd is het jammer dat een leuke tijd bij proceskunde is afgelopen. Gedurende de 4 jaar aiotijd heb ik met veel mensen samengewerkt, gelachen, koffiegedronken en geborreld. Daarom wil ik een aantal mensen bedanken.

Ten eerste wil ik mijn begeleiders noemen voor hun niet geringe bijdrage aan het onderzoek. Remko, bedankt voor de motiverende werkbесprekingen en je stroom aan ideeën voor nieuwe experimenten. Karin, naast je wezenlijke bijdrage aan het onderzoek vond ik het vooral prettig dat ik altijd even aan kon kloppen voor advies. Ruud, bedankt voor de kennis-making met lattice Boltzmann simulaties en het bijbrengen van de nodige programmeerkennis. Jullie hebben er alledrie aan bijgedragen dat de artikelen een stuk leesbaarder zijn geworden, mijn promotie nauwelijks is uitgelopen en het proefschrift zowel experimentele, theoretische als numerieke elementen bevat. Heel erg bedankt!

Pieter en Olivier wil ik bedanken voor onderhoud aan het computer-cluster, Jos voor ondersteuning op het lab, Gerrit voor het oplossen van computerproblemen en Joyce en Hedy voor de secretariële ondersteuning. Ook wil ik Hans en Jan van de werkplaats bedanken voor het maken van verschillende membraanmodules en Boudewijn voor zijn hulp bij de microscopie-experimenten.

Further I would like to thank all the partners of the European project for the nice collaboration, and also Aquamarijn for the supply of microsieves and Jo Janssen for the good coordination. I want to thank Takasi Nisisako for his contribution to chapter 4 and the nice Dutch-Japanese collaboration, Kristina Lodaite for the pleasant collaboration on droplet formation experiments with microsieves and Julia Yeomans and colleagues for learning me the multiphase code. I would also like to thank Peter Lammers and Rainer Keller from HLRS for learning me how to parallelize the lattice Boltzmann code during my two-month stay in Stuttgart.

Afgelopen jaren heb ik een aantal studenten mogen begeleiden die ik wil

bedanken. Koen, je hebt je experimenteel werk in Karlsruhe uitgevoerd. Ik vond het leuk om op deze manier met jou en Uwe samen te werken. Tjalling, bedankt voor je werk aan het bestuderen van druppelvorming. Gilles, ik vond de NMR metingen aan dubbele emulsies heel interessant, jammer dat het met het membraanemulgeren minder lukte. Maartje, ik heb hoofdstuk 3 grotendeels aan jou te danken en vind het leuk dat je daarna mijn collega bent geworden.

Mijn kamergenoten hebben erg bijgedragen aan mijn werkplezier. Eerst waren dat Anneke die me goed op weg heeft geholpen, René die altijd in is voor een praatje en de altijd vrolijke en optimistische Mark. Jasper verving Anneke in het Europese project en wist zich als enige man een tijdje staande te houden in het nieuwe gezelschap samen met Marleen en Cynthia. Marleen, het was leuk om je Enschedese nuchterheid op de kamer te hebben en Cynthia, bedankt voor je gezelligheid en natuurlijk dat je paranimf wilt zijn.

Verder wil ik m'n membraanmaatjes Eduard, Gerben, Koen en Maartje bedanken voor de leuke tijd tijdens congressen. Gerben, wij zijn op dezelfde dag begonnen als aio en ik ben blij dat je nu mijn paranimf wilt zijn. Ook wil ik alle aio's bedanken voor de leuke tijd tijdens de aioreizen (en vakanties daarna!) naar Zuid-Afrika en Canada. Daarnaast waren er ook de gezellige borrels, etentjes, filmavondjes, labuitjes en feestjes die ervoor hebben gezorgd dat ik het afgelopen jaren erg naar mijn zin heb gehad.

Ook wil ik mijn oud-bestuursgenoten van het PNN (destijds LAIOO) bedanken voor het intensieve, maar vooral leuke bestuursjaar! Iedereen van Aqua wil ik bedanken voor de zeilweekenden en borrels, mijn oud-huisgenoten op de Hoogstraat voor een relaxed thuisfront gedurende de eerste 3 aiojaren en natuurlijk mijn jaarclub voor de gezellige etentjes en nodige afleiding.

Mijn ouders wil ik bedanken dat ze me altijd hebben gestimuleerd om te gaan studeren. En tenslotte wil ik Geert bedanken. Je hebt altijd het vertrouwen in mij behad dat het wel goed zou komen met dit proefschrift. Ik hoop dat we samen nog een mooie tijd tegemoet gaan!

Sandra

List of publications

S. van der Graaf, T. Nisisako, C.G.P.H. Schroën, R.G.M. van der Sman, R.M. Boom, Lattice Boltzmann simulations of droplet formation in a T-shaped microchannel, submitted 2005.

R.G.M. van der Sman, **S. van der Graaf**, Diffuse interface model of surfactant adsorption onto flat and droplet interfaces, accepted for publication in *Rheologica Acta*.

S. van der Graaf, M.L.J. Steegmans, R.G.M. van der Sman, C.G.P.H. Schroën, R.M. Boom, Droplet formation in a T-shaped microchannel junction: a model system for membrane emulsification, *Colloids and Surfaces A: Physicochemical and Engineering Aspects* 266 (2005) 106-116.

S. van der Graaf, C.G.P.H. Schroën, R.M. Boom, Preparation of double emulsions by membrane emulsification - a review, *Journal of Membrane Science* 251 (2005) 7-15.

S. van der Graaf, C.G.P.H. Schroën, R.G.M. van der Sman, R.M. Boom, Influence of dynamic interfacial tension on droplet formation during membrane emulsification, *Journal of Colloid and Interface Science* 277 (2004) 456-463.

Conference proceedings

U. Lambrich, **S. van der Graaf**, K.S. Dekkers, R.M. Boom, H. Schubert, Production of double emulsions using microchannel emulsification, *Proceedings ICEF 9*, 364, Montpellier, 2004.

S. van der Graaf, R.G.M. van der Sman, R.M. Boom, Modeling of droplet formation processes relevant to membrane emulsification, *Proceedings AIChE annual meeting 2003*, 563e, San Francisco, 2003.

R.G.M. van der Sman, **S. van der Graaf**, A.J. Gijsbertsen-Abrahamse, 2-D droplet deformation and breakup with Lattice Boltzmann model, In: *Computational Methods in Multiphase flow 2*, Eds. A.A. Mammoli and C.A. Brebbia, WIT press, Southampton, p. 333-342, 2003.

Overview of training activities

Discipline specific activities

Courses

- Computational Fluid Dynamics for Chemical Engineers (OSPT) 2001
- Emulsification Techniques (University of Karlsruhe) 2002
- A Unified Approach to Mass Transfer (OSPT) 2002
- Understanding Molecular Simulations (OSPT/UvA) 2003
- Numerical Methods in Chemical Engineering (OSPT) 2004
- European Membrane Society Summerschool 2004
- Parallel Programming Workshop (University of Stuttgart) 2004
- Han-sur-Lesse Winterschool on Physical Chemistry 2005

Meetings and visits

- Two weeks visit to Theoretical Physics, University of Oxford, England 2002
- 1st, 2nd, 3rd and 5th Netherlands Process technology Symposium (NPS) 2001 (Lunteren), 2002 (Zeist), 2003 and 2005 (Veldhoven)
- American Institute of Chemical Engineering (AIChE) Annual Meeting, San Francisco, USA 2003
- Network Young Membranes 6 and 7, 2004 (Hamburg, Germany), 2005 (Enschede)
- Euromembrane Conference, Hamburg, Germany 2004
- Two months High Performance Computing (HPC-Europa) visit to the High Performance Computing Center (HLRS) Stuttgart, Germany 2004

- 6th Liquid Matter Conference, Utrecht 2005
- 19th Conference of the European Colloid and Interface Society (ECIS), Geilo, Norway 2005

General courses

- PhD introduction week (VLAG) 2001
- Teaching and supervising students (OWU) 2002
- Scientific Writing (CENTA) 2002
- Discussion Techniques (OWU) 2005
- Career Perspectives (WGS) 2005

Optional activities

- PhD study tour Process Engineering South Africa 2002
- European Council of Doctoral Candidates and Young Researchers (Eurodoc) Conference, Soest 2003
- Brainstorm week Process Engineering 2003
- PhD study tour Process Engineering Canada 2004

Curriculum Vitae

Sandra van der Graaf werd op 6 november 1977 te Lekkerkerk geboren. In 1996 behaalde zij haar gymnasiumdiploma aan het Krimpenerwaard College te Krimpen aan den IJssel. In januari 1997 begon ze aan de studie Moleculaire Wetenschappen aan Wageningen Universiteit en specialiseerde zich in de fysisch-chemische richting. Afstudeervakken werden afgelegd bij Fysische Chemie en Kolloïdkunde en bij Levensmiddelenproceskunde. Stage liep ze bij Bayer AG, corporate research, afdeling grensvlakfysica, in Leverkusen (Duitsland). Tijdens haar studie ontving ze 2 studiebeurzen van de Vereniging van de Nederlandse Chemische Industrie (VNCI) voor goede studieresultaten en in juni 2001 studeerde ze met lof af. Van september 2001 tot november 2005 was ze werkzaam als promovendus bij de sectie Proceskunde van Wageningen Universiteit. Van juni 2002 tot juli 2003 zat ze tevens als secretaris in het bestuur van het Landelijke AIO/OIO Overleg (LAIOO, thans PNN). Het promotie-onderzoek maakte deel uit van het Europese project 'Towards Highly Advanced Membrane Emulsification Systems'. De resultaten van het onderzoek staan beschreven in dit proefschrift. Vanaf half november 2005 is ze via United Technical Solutions werkzaam bij ASML in Veldhoven.